

AD-A142 675

A NEW OPTICAL TECHNIQUE FOR RAPID DETERMINATION OF  
CREEP AND FATIGUE THRE. (U) JOHNS HOPKINS UNIV  
BALTIMORE MD W N SHARPE APR 84 AFWAL-TR-84-4028

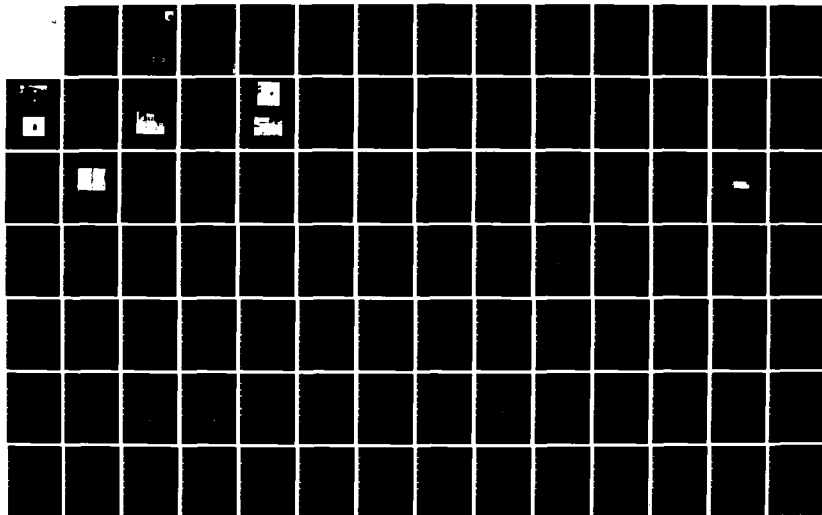
1/2

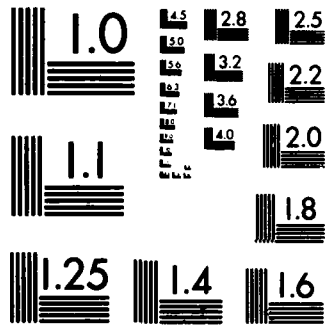
UNCLASSIFIED

F33655-81-K-5014

F/G 20/11

NL





MICROCOPY RESOLUTION TEST CHART  
NATIONAL BUREAU OF STANDARDS-1963-A



A NEW OPTICAL TECHNIQUE FOR RAPID DETERMINATION OF  
CREEP AND FATIGUE THRESHOLDS AT HIGH TEMPERATURE

The Johns Hopkins University  
Baltimore, MD 21218

April 1984

Final Report for Period January 1981 through January 1984

Approved for public release; distribution unlimited.

AD-A142 675

DTIC FILE COPY

DTIC  
ELECTE  
S JUL 05 1984 D  
E

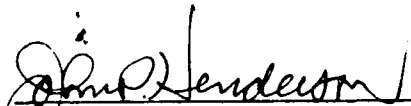
MATERIALS LABORATORY  
AIR FORCE WRIGHT AERONAUTICAL LABORATORIES  
AIR FORCE SYSTEMS COMMAND  
WRIGHT-PATTERSON AIR FORCE BASE, OHIO 45433


NOTICE

When Government drawings, specifications, or other data are used for any purpose other than in connection with a definitely related Government procurement operation, the United States Government thereby incurs no responsibility nor any obligation whatsoever; and the fact that the government may have formulated, furnished, or in any way supplied the said drawings, specifications, or other data, is not to be regarded by implication or otherwise as in any manner licensing the holder or any other person or corporation, or conveying any rights or permission to manufacture use, or sell any patented invention that may in any way be related thereto.

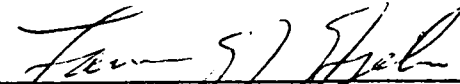
This report has been reviewed by the Office of Public Affairs (ASD/PA) and is releasable to the National Technical Information Service (NTIS). At NTIS, it will be available to the general public, including foreign nations.

This technical report has been reviewed and is approved for publication.

  
\_\_\_\_\_  
JOHN P. HENDERSON, Chief  
Metals Behavior Branch  
Metals and Ceramics Division

  
\_\_\_\_\_  
GORDON R. ATKINS  
Materials Engineer  
Metals Behavior Branch

FOR THE COMMANDER

  
\_\_\_\_\_  
LAWRENCE N. HELM, Asst Chief  
Metals and Ceramics Division  
Materials Laboratory

"If your address has changed, if you wish to be removed from our mailing list, or if the addressee is no longer employed by your organization please notify AFWAL/MLLN, W-PAFB, OH 45433 to help us maintain a current mailing list".

Copies of this report should not be returned unless return is required by security considerations, contractual obligations, or notice on a specific document.

## REPORT DOCUMENTATION PAGE

1a. REPORT SECURITY CLASSIFICATION Unclassified		1b. RESTRICTIVE MARKINGS	
2a. SECURITY CLASSIFICATION AUTHORITY		3. DISTRIBUTION/AVAILABILITY OF REPORT Approved for public release; distribution unlimited	
2b. DECLASSIFICATION/DOWNGRADING SCHEDULE			
4. PERFORMING ORGANIZATION REPORT NUMBER(S)		5. MONITORING ORGANIZATION REPORT NUMBER(S) AFWAL-TR-84-4028	
6a. NAME OF PERFORMING ORGANIZATION Johns Hopkins Univ. Baltimore, MD 21218	6b. OFFICE SYMBOL (If applicable)	7a. NAME OF MONITORING ORGANIZATION Materials Laboratory (AFWAL/MLIN) Air Force Wright Aeronautical Labs.	
6c. ADDRESS (City, State and ZIP Code)		7b. ADDRESS (City, State and ZIP Code) Wright-Patterson Air Force Base, Ohio 45433	
8a. NAME OF FUNDING/SPONSORING ORGANIZATION	8b. OFFICE SYMBOL (If applicable)	9. PROCUREMENT INSTRUMENT IDENTIFICATION NUMBER F33615-81-K-5014	
8c. ADDRESS (City, State and ZIP Code)		10. SOURCE OF FUNDING NOS.	
		PROGRAM ELEMENT NO. ILIR	PROJECT NO. 01
		TASK NO. 39	WORK UNIT NO.
11. TITLE (Include Security Classification) A New Optical Technique for Rapid Determination of Creep and Fatigue Thresholds at High Temperature			
12. PERSONAL AUTHOR(S) William N. Sharpe, Jr.			
13a. TYPE OF REPORT Final	13b. TIME COVERED FROM Jan. 81 to Jan. 84	14. DATE OF REPORT (Yr., Mo., Day) April 13, 1984	15. PAGE COUNT 105
16. SUPPLEMENTARY NOTATION			
17. COSATI CODES		18. SUBJECT TERMS (Continue on reverse if necessary and identify by block number)	
FIELD	GROUP	SUB. GR.	
19. ABSTRACT (Continue on reverse if necessary and identify by block number) A laser-based interferometric displacement gage was used to measure crack opening displacements very near the tips of fatigue precracks. The test material was Inconel 718 and the temperature 650C. Creep and fatigue cracking thresholds were determined in times as short as one-half hour and found to be approximately 11 MPa-m <sup>2</sup> in both cases. Details of the measurement technique as well as of the displacements measured near the tip are given.			
20. DISTRIBUTION/AVAILABILITY OF ABSTRACT UNCLASSIFIED/UNLIMITED <input type="checkbox"/> SAME AS RPT. <input checked="" type="checkbox"/> OTIC USERS <input type="checkbox"/>		21. ABSTRACT SECURITY CLASSIFICATION Unclassified	
22a. NAME OF RESPONSIBLE INDIVIDUAL		22b. TELEPHONE NUMBER (Include Area Code)	22c. OFFICE SYMBOL

TABLE OF CONTENTS

SECTION	PAGE
I INTRODUCTION	1
II THE INTERFEROMETRIC STRAIN/DISPLACEMENT GAGE	4
III EXPERIMENTAL PROCEDURES	20
IV CREEP THRESHOLD MEASUREMENTS	23
V FATIGUE THRESHOLD MEASUREMENTS	39
VI COD MEASUREMENTS AWAY FROM TIP	62
VII CONCLUSIONS	74
APPENDIX A - CREEP TEST RESULTS	76
APPENDIX B - FATIGUE TEST RESULTS	94
REFERENCES	101

Accession For	
NTIS GRA&I	<input checked="" type="checkbox"/>
DTIC TAB	<input type="checkbox"/>
Unannounced	<input type="checkbox"/>
Justification	
By	
Distribution/	
Availability Codes	
Dist	Avail and/or Special
A-1	

ORIGINAL  
 COPY  
 INSPECTED

## LIST OF ILLUSTRATIONS

FIGURE		PAGE
1	Schematic of the ISDG	5
2	Indentations across a fatigue crack. The spacing is 100 micrometers.	6
3	A photograph of a fringe pattern.	6
4	Schematic of ISDG System	8
5	Overview of ISDG System	8
6	Closeup of scanning mirror and PMT	10
7	Overview of minicomputer system	10
8a	Sweep of entire fringe pattern	12
8b	Attenuated mirror sweep adjusted for test	12
9	Successive scans about selected fringe minimum	14
10	Listing of the displacement measuring subroutine.	15
11	A check of large displacement measurements.	19
12	A compact tension specimen in the special grips.	21
13	Loading schedule for creep tests.	24
14	Creep crack opening displacement for Test 21092.	26
15	Measured compliances for Test 21092.	27
16	Crack surface after four tests.	32
17	Average crack growth rate versus K.	35
18	Normalized crack opening displacement rate versus K.	37
19	Loading schedule for fatigue tests.	40
20	Crack opening displacement at minimum and maximum loads for Test 11083.	41
21	Selected load-displacement plots for Test 11083.	43
22	Reduced data for first cycle of Test 11083.	44
23	Crack growth rates for fatigue threshold tests.	47
24	Crack opening displacements at minimum and maximum loads for Test 08083.	48

FIGURE		PAGE
25	Information and data for Test 08083.	49
26	Crack opening displacements at minimum and maximum loads for Test 11083.	50
27	Information and data for Test 11083.	51
28	Creep crack opening displacement for Test 12083.	52
29	Information and data for Test 12083.	53
30	Crack opening displacement for Test 16003.	54
31	Information and data for Test 16003.	55
32	Crack opening displacement for Test 09083.	56
33	Information and data for Test 09083.	57
34	Crack opening displacement for Test 17083.	58
35	Information and data for Test 17083.	59
36	Schematic of crack for Tests 18123 and 19123.	63
37	Load-displacement plots at various positions behind the crack tip.	64
38	Load-displacement plots at two positions at 22C and 650C.	65
39	Crack opening displacement and their difference for Test 19123.	67
40	Single cycle load-displacement plots at various cycles for Test 19123.	68
41	Schematic of the cracks before and after Test 21123.	69
42	First and twentieth cycles of Test 21123.	70
43	Crack opening displacements measured 4.41 mm behind tip and their difference for Test 21123.	72
44	Load-displacements for selected single cycles of Test 21123.	73



LIST OF TABLES

TABLE		PAGE
1	Crack Lengths, Loads, and Creep Displacements for the Creep Tests	28
2	Calculated and Measured Compliances for the Creep Tests	29
3	First Compliances for the Creep Tests	31
4	Average Crack Lengths and Compliances for the Creep Tests	34
5	Crack Lengths, Loads, and Average Crack Growth for the Fatigue Tests	46
6	Compliances for the Fatigue Tests	46
7	Compliances Measured away from the Crack Tip	71
8	Initial and Final Compliances Measured away from the Crack Tip	74

## INTRODUCTION

The Retirement of a cracked part dictates that a component be inspected regularly and replaced if necessary. The inspection procedure and the criteria for deciding on replacement are important parts of this approach. This research is concerned with development techniques for determining crack growth behavior more readily and accurately. Such techniques will require more extensive material testing and the development of more reliable criteria for replacement.

The turbine disks of air-breathing jet engines are complicated components that operate in a severe environment. The many holes, fillets, turbine blade mounting locations, etc. are prime candidates for crack initiation. These components are expensive enough - both in material costs and in manufacturing costs - to warrant regular inspection. Furthermore, they are critical to the operation of an aircraft; a shattered disk means loss of the engine at least. So, if turbine disks are regularly inspected for cracks, the question of what should be done once a crack of a certain size is found must be answered. This requires knowledge, which is obtained by experiment, of the material behavior in the presence of cracks. This knowledge is also useful in designing the inspection program.

A turbine disk experiences steady, transient, and cyclic loads in operation. At constant cruise speed, the centrifugal loads on the disk are steady. During activities such as take-off, landing, or tactical maneuvers, the loads are transient. There are many low-level vibratory loads in normal operation, but, viewed on a longer time scale, the take-off and landing can be considered as a cyclic load of large magnitude and low frequency. It is clear then that one must examine the material behavior under both creep and fatigue loading.

If one is to study crack growth behavior, one must obviously measure crack lengths. Given that the environment of a turbine disk is approximately 650C in air, the measurement is more difficult. The time-honored approach is the travelling microscope. Bonath (1) used this technique at 730C on turbine disk material and reported a resolution of 0.03 mm (0.001 inch) for surface crack measurements.

The sophisticated technique of Bonath (2) uses holography to measure the crack opening displacement away from the crack tip at 120C. The crack growth is then inferred from this measurement. Resolution is not reported by him, but it

appears to be approximately 0.025 mm. A similar approach is also used by others such as Kaufman et al (3). They measured crack mouth displacement with position sensors located outside the heated region and connected to the specimen by extension rods. The relation between crack mouth displacement and crack length is obtained from experimental calibration. They do not report the resolution, but an optimistic estimate is 0.040 mm. The relative uncertainty of the calibration curve should be considered in describing this technique. These techniques measure an average crack length; the actual measuring is done far from the crack tip.

Another technique that measures average crack lengths is the electropotential method. Current passing through the uncracked portion of the specimen is a measure of the crack size. Examples of this are given by Landes and Begley (4) and Haigh (5). Landes and Begley report a resolution of 0.3 mm at 650 C, while Haigh's resolution is given as 0.1 mm at 550 C. This method has its output based on the physical location and shape of the crack tip, whereas the crack opening displacement techniques locate the crack by computation. Both approaches (except that by Hsu (2)) provide real-time continuous data that is easily recorded.

Donath (1) used a compliance technique in addition to the microscope measurements to determine crack length. He measured load-line displacement with linear variable differential transformers mounted outside the furnace and periodically lowered the load 15 to 25 per cent of the maximum value to record a compliance. Effective crack length was calculated from an elasticity-based analysis. The resolution of this method is not reported, but it appears from the plotted results to be on the order of 0.1 mm.

The work reported here is a study of a more sensitive crack opening displacement approach as it applies to both creep and fatigue. The laser-based interferometric strain/displacement gage (ISDG) has a short gage length and high sensitivity. The idea then is to measure crack opening displacement,  $v$ , which is related to the crack length, load, and location of the measurement position with respect to the crack tip,  $r, \theta$ , by:

$$v = \frac{K}{G} \sqrt{\frac{r}{2\pi}} \sin \frac{\theta}{2} \left[ \frac{2}{1+\nu} - \cos^2 \frac{\theta}{2} \right] \quad (1)$$

If the crack grows an increment  $\Delta r$  away from the measurement position, the relative changes in "a" and "b" are much smaller, so approximately:

Taking some typical values as used in this work,  $r = 100$  micrometers,  $v = 5$  micrometers then

The ISDG has a resolution of 0.02 micrometers, so one should be able to detect an increment of 0.8 micrometers. This reported research is a study of the capabilities of this approach under creep and fatigue conditions at 650 C.

This report is divided largely into three parts, - ISDG technique development, creep threshold studies, and fatigue threshold studies. The compact tension specimens were Inconel 718, and the test temperature was 650 C.

ISDG development was conducted in conjunction with another research project, "Benchmark Tests for Life Prediction", sponsored by NASA-Lewis. It was a joint effort between General Electric and Louisiana State University. That test program focussed on the measurement of cyclic plastic strain at the root of a notch in a specimen subjected to a tensile/compressive load spectrum. The results are reported in references 6 and 7; Mr. Mike Ward made a major contribution as part of his master's program. The Ph.D. thesis work of Dr. Mike Guillot (8) was also of major benefit to the ISDG development.

The second phase of the work was application of the ISDG to the determination of creep threshold values. Mr. J. J. Shen, a visiting scholar from the Peoples Republic of China assisted in that work which is reported in reference 9. The third phase involved determination of fatigue threshold values and includes the master's thesis research of Mr. J. J. Lee.

## THE INTERFEROMETRIC STRAIN/DISPLACEMENT GAGE

The interferometric strain/displacement gage (ISDG) in its most recent version is described in this section. There have been various applications of the ISDG over the years, and these are described in a summary fashion in reference 10. This part of the report is intended to serve as a primer on the ISDG.

Basics of the ISDG

A more complete discussion of the optical principles behind the ISDG is given in reference 11; only a short review is given here. Figure 1 is a schematic which will aid in the explanation.

Two square pyramidal indentations are pressed into the surface of the specimen with a Vicker's hardness tester. These indents are each small enough ( $\approx 25 \mu\text{m}$  on a side) that appreciable diffraction occurs when they are illuminated with visible radiation. If that radiation is coherent and monochromatic such as that from a laser, then the diffracted rays from the two indents overlap and form interference patterns in space. This is simply the Young's Two-Slit Interference demonstration from elementary optics except that it is in reflection, not transmission. The governing equation establishing the location of the fringes is

$$d \sin \theta = m\lambda, \quad m = 0, \pm 1, \pm 2 \dots \quad (4)$$

where "d" is the indent spacing,  $\theta$  is measured from the incident laser beam, and  $\lambda$  is the wave length of light. Figure 2 is a photograph of a pair of indentations across a fatigue crack. Figure 3 is a photograph of a fringe pattern; it is triangular in shape because the reflecting sides of the indents are triangular.

The underlying idea of the ISDG is that as "d" changes, the angle associated with a fringe of given order, m, also changes. That is, the fringes move in space, and this motion can be recorded and related to the relative displacement between indents. Four fringe patterns are formed in space, but only the two in a plane which includes the loading axis of the specimen are used. Motion of these two patterns can occur due to relative displacement or to rigid-body motion parallel to the loading axis (which is inevitable). However, if one averages the motion of the two fringe patterns and takes fringe motion toward the incident

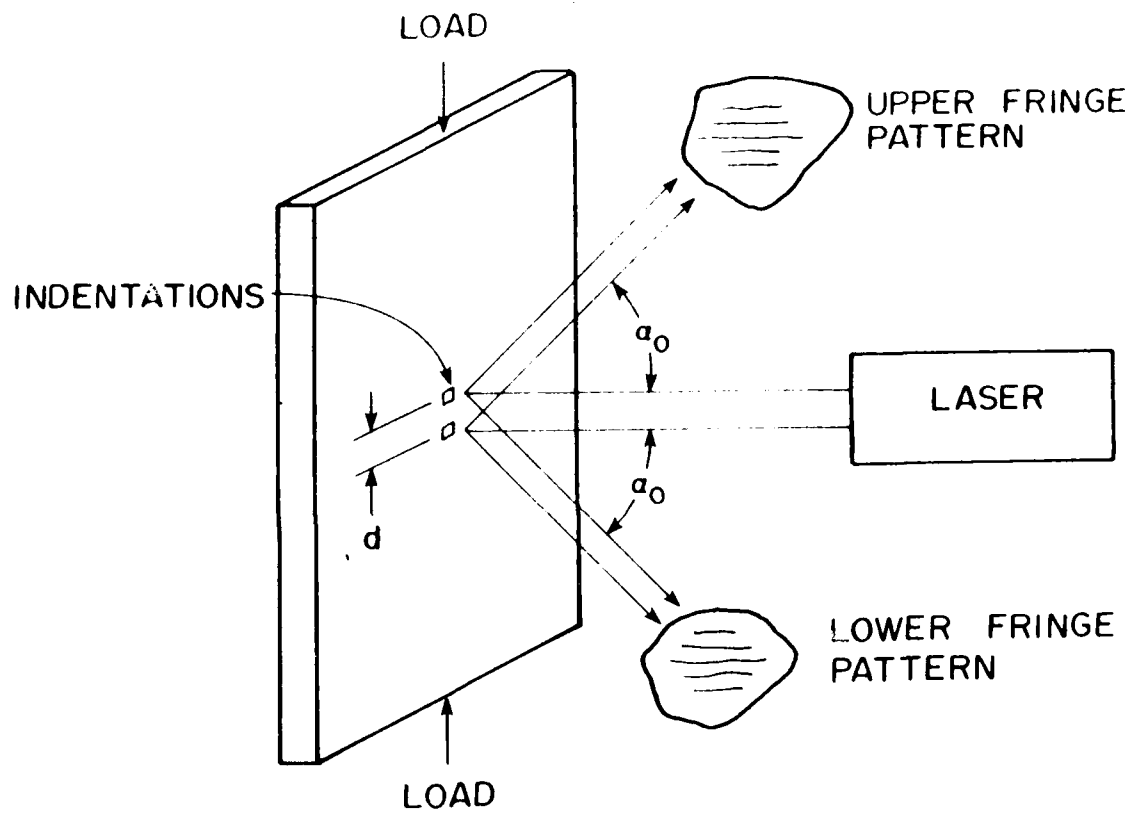


Figure 1. Schematic of the ISDG



Figure 2. Indentations across a fatigue crack.  
The spacing is 100 micrometers.

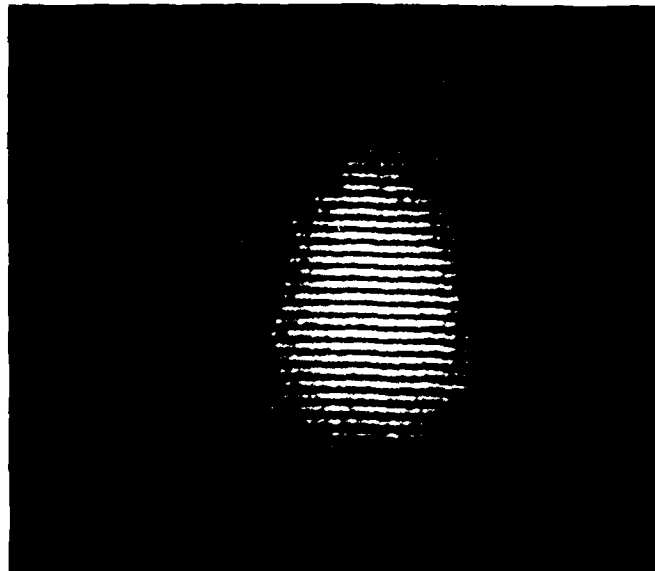


Figure 3. A photograph of a fringe pattern.

beam as positive, the rigid-body part is eliminated. The governing equation for relative displacement,  $\Delta d$ , is then:

$$\Delta d = \frac{\Delta m_u + \Delta m_l}{2} \frac{\lambda}{\sin \alpha_0} \quad (5)$$

where  $\Delta m_u$  and  $\Delta m_l$  are relative fringe motions of the upper and lower patterns, and  $\alpha_0$  is a fixed observation position. The  $\Delta m$  are measured as a fraction of the spacing between fringes, i.e.  $\Delta m = 1$  means a fringe has moved to occupy the spacing of an adjacent neighbor. In the averaging of Equation 5, fringe motion is defined as positive if it is toward the incident laser beam. Note that rigid-body motion which is not parallel to the load axis causes errors not eliminated by Equation 5; fortunately, that motion is small in most laboratory setups.

The quantity  $\lambda / \sin \alpha_0$  is a calibration factor for the measurement.  $\lambda$  is  $0.633 \mu\text{m}$  for He-Ne laser light, and  $\alpha_0$  is approximately  $42^\circ$  because of the shape of the Vicker's diamond. Therefore, the calibration constant is approximately 1 micrometer. If one is to measure smaller displacements, then one must measure  $\Delta m$  with greater resolution. The next section describes a minicomputer-based system for real-time measurements with a resolution on the order of  $0.02 \mu\text{m}$ .

#### Minicomputer-Based System

The approach to measuring smaller fringe movements is to use a servocontrolled scanning mirror and a slit-covered photomultiplier tube (PMT) to sample the fringe position. Figure 4 is a schematic of the system and shows two scanners - each controlled by the minicomputer. In addition, the load applied to the specimen in the electrohydraulic test machine is controlled by the minicomputer.

Figure 5 is an overview of the test system. The electrohydraulic test machine is by MTS and has a 90 kilonewton load capacity, but uses a Lebow model 3170 load cell with a capacity of 9 kilonewtons. A locally constructed resistance furnace surrounds the specimen; it has quartz windows for the entering laser beam, the exiting fringe patterns, and for observation of the specimen during a test. It is heated by a Research, Inc. model 646 power controller in conjunction with an Omega Model 4002 temperature controller using a chromel-alumel thermocouple. Fans are used to cool the load cell and the scanners. The 5 milliwatt laser is from, Ealing, model 25-0860, and is



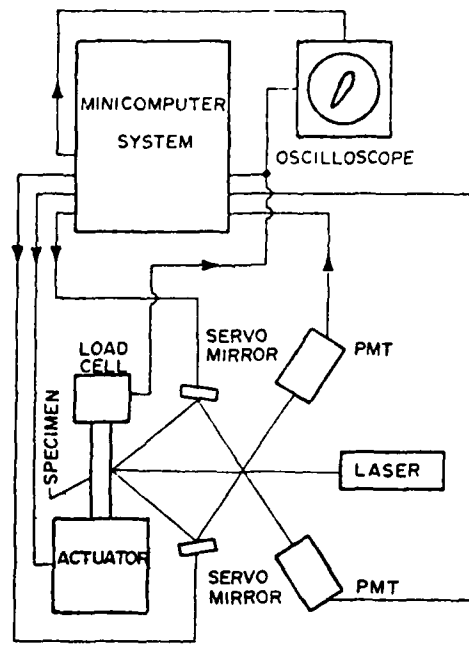


Figure 4. Schematic of ISDG System

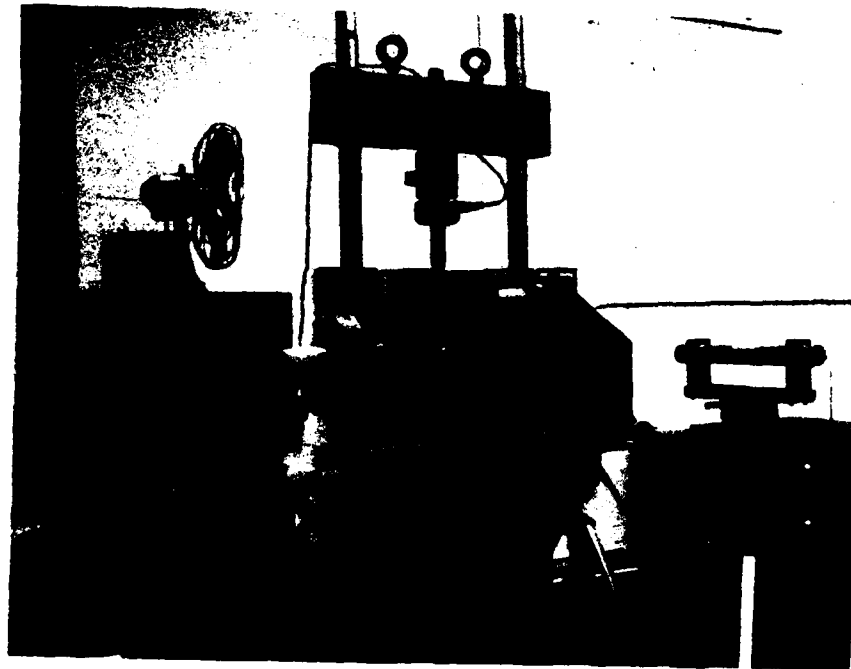


Figure 5. Overview of ISDG System

mounted on a fine-thread X-Z stage for easy positioning of the laser beam on the indents.

The scanner and PMT mounting board is shown in Figure 5; it is mounted on a tripod and an X-Y stage. Figure 6 is a closeup of one of the scanning mirrors and the PMT enclosure. The scanners are from General Scanning, Inc. - model G-100 PDT. They are heated above room temperature with an electric heating tape; the temperature is measured with a thermistor. Movement of the mirror as well as temperature control is effected by a Model CCX01 control unit, also from General Scanning. The mirror units are mounted on a finned aluminum conductor which dissipates heat associated with the galvanometer type drive unit. The front surface mirror is 7 x 16 mm in size with the long dimension perpendicular to the fringes. Each mirror unit is mounted on a microscope stage positioning device (not shown) which permits movement parallel to and perpendicular to the fringes. The mirror control unit has an amplitude and position control; one aligns the fringe pattern by positioning the mirror in the fringe pattern and then rotating it to reflect the fringes onto the PMT.

RCA model 4840 PMTs and model PF1042 power supplies are used. The PMT is side-opening and enclosed in a minibox. The power supply is the cylindrical box with wires in Figure 6. The aperture to the PMT is covered with an interference filter and then a mask with a slit approximately 1 mm wide; these are mounted in an aluminum holder. The white paint on the mask is useful in viewing the fringes for aligning. The 13.5 volts DC required by the power supplies is provided by a Tektronix 501-2 rack-mounted power supply. Output from the PMTs (nominally - 10 millivolts) is inverted and amplified by Tektronix model 502 amplifiers. A Gould model 0S1400 digital storage oscilloscope is used to monitor the PMT outputs.

Figure 7 is an overview of the minicomputer system. The basic unit is a DEC MINC minicomputer with 16 channels A/D, 4 channels D/A, and a VT105 graphics terminal. It is augmented with a DEC RL01 10-Mbyte disk, LA120 line printer, and a Houston Instruments Model DP 101 digital plotter. Programming is done in FORTRAN IV. The minicomputer and disk drive are protected by a Topaz model 70306 line surge protector.

#### Measurement Strategy

There are basically four parts to a minicomputer program for a particular experiment:



Figure 6. Closeup of scanning mirror and PMT



Figure 7. Overview of minicomputer system

1. A setup part in which the data files are named; load ranges, time intervals, and other parameters specified.
2. An initialization part where the fringes are aligned and spacing and location determined.
3. The actual test program where load signals are sent to the test machine and displacement measurements are made.
4. A displacement measurement subroutine which measures the fringe motion and converts it into a displacement value; this subroutine is repeatedly called in part 3.

In this section, part 2 will be discussed briefly and part 4 in some detail.

The initialization part starts with a loop that simply sweeps the fringes across the slit of the PMT. The loop generates in 256 increments a sawtooth analog output of + 5 volts at a frequency of 13 Hz. The sawtooth signal is attenuated at the servomirror controller to adjust the angle of rotation of the mirror. The position adjustment of the controller is used to center the pattern on the PMT. Figure 8a is a plot of intensity versus angle when the angle of rotation is large enough to sweep all the fringes that impinge on the mirror past the slit (the plot was taken from the storage oscilloscope). While this loop is running, the mirrors, PMT amplifiers, and mirror controllers are adjusted to get the desired signal. Figure 8b is an example of a typical final adjustment - 3 minimums centered in the sweep.

On keyboard command the rest of the initialization takes place. A single 256 increment sweep generates and stores a signal like the one in Figure 8b. That data is processed to determine the location of the central minima, CH1 and CH2, and the spacings MSP1 and MSP2 for the two fringe patterns.

The basic measurement strategy is to follow the center minimum of Figure 8b as it moves left or right. The mirrors are rotated only 60 increments (instead of 256), and as the minimum moves left or right, the mean output voltage is adjusted so that the next sweep will include the moving minimum. All this is accomplished with the subroutine SND described below. Figure 9a is a plot of the PMT output for

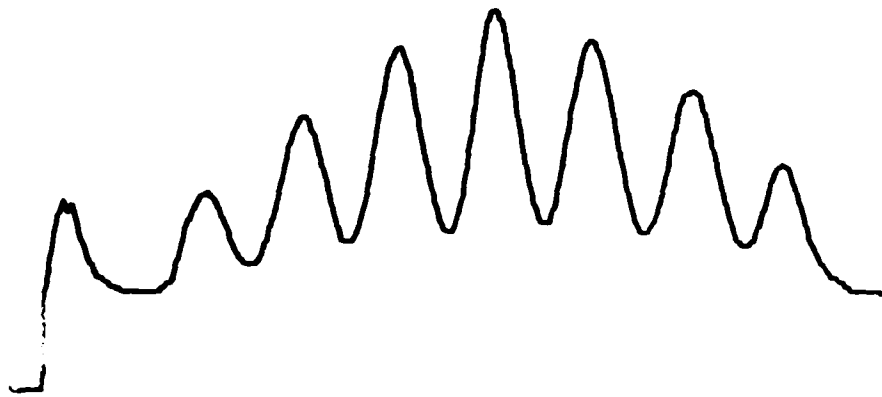


Figure 8a - Sweep of entire fringe pattern

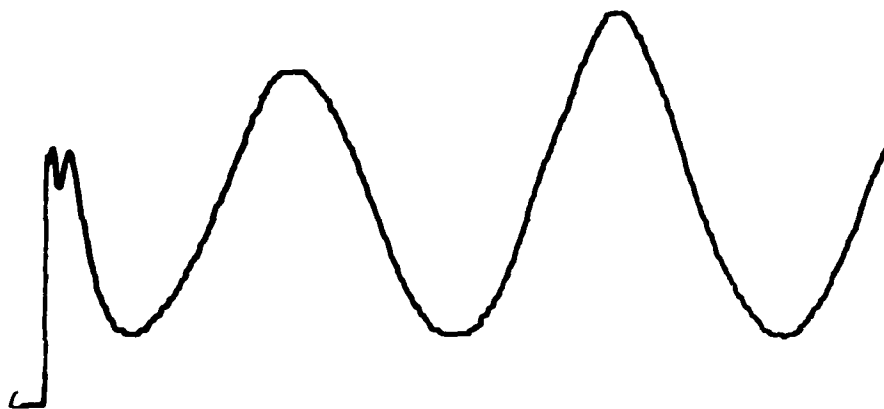


Figure 8b - Attenuated mirror sweep adjusted for test

one channel when the fringe is moving very little. Computation of the amount of fringe motion and updating of the mean position takes place during the flat portions at minimum voltage. Figure 9b is a plot when the fringe is moving to the left, and Figure 9c is when its moving to the right. From Figure 9, one sees that each displacement measurement takes 100 ms with half the time devoted to scanning and the other half to computing.

Figure 10 is a listing of the subroutine SND. NPTS and NAV were parameters in the original version, but they have been set at 60 and 10 respectively. NPTS is the number of increments the mirror sweeps. NAV is the number of data points averaged in a sliding average to smooth out the fringe intensity prior to locating the minimum. CC is a constant related to the calibration factor in Equation 5; it includes the fringe spacings MSP1 and MSP2 which are also constants for a particular setup.

CH1 and CH2 are the locations of the minima before the sweep was run, and CH1N and CH2N are locations afterward. The difference is related to the displacement; see line 53. The signs are different on channels 1 and 2 because the mirrors sweep in the same angular direction.

When the fringe has moved more than one spacing (see Figure 8b), the subroutine directs the mean position of the mirror back to the center of the adjacent fringe. Displacements on the order of 100 micrometers can be measured by this strategy. NDSP is the integer value of the total measured displacement; whereas NDSP0 is a temporary value stored every time either mirror is shifted a complete fringe. ISH is a counter (-1, 0, +1) indicating whether channel 1 (ISH = -1) or channel 2 (ISH = +1) has shifted an entire fringe. The logic of the subroutine is such that NDSP is computed, the mean position is shifted one fringe spacing if necessary, and NDSP0 is computed for use on the next scan.

#### Correction for Large Displacement

The minicomputer system measures fringe motion as a physical movement of the minimum position and divides by the original spacing to compute  $\Delta m$ . If the spacing is 100 increments of mirror motion, and the minimum moves 5 increments between scans, then  $\Delta m = 0.05$ . However, the spacing between fringes changes as the distance between indentations changes, and it is necessary to correct for that fact.

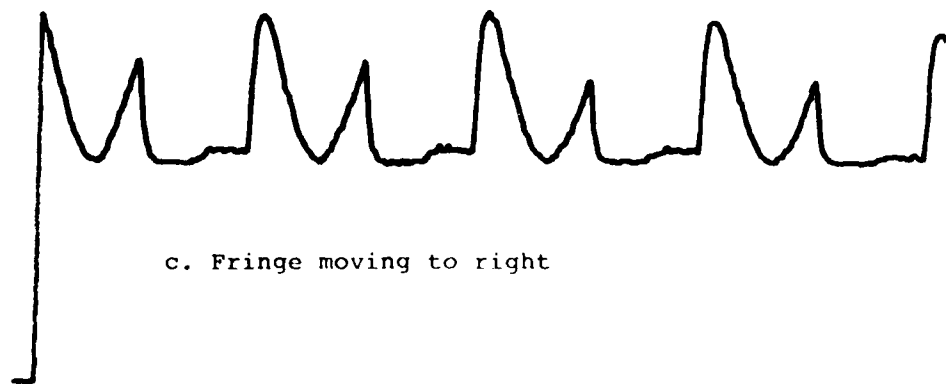
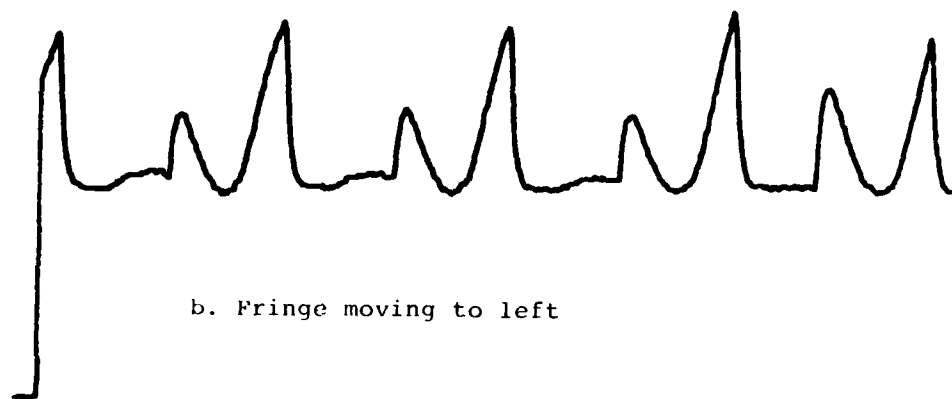
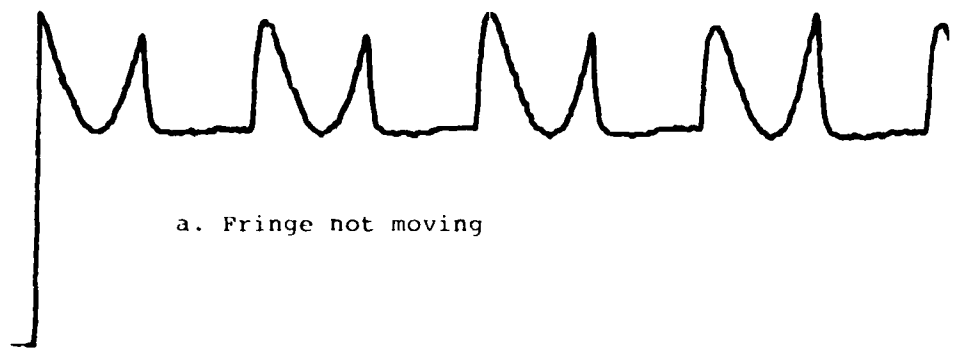


Figure 9 - Successive scans about selected fringe minimum

```

C ***** subroutine SMD *****
0001 SUBROUTINE SMD(NPTS,MSP1,MSP2,CH1N,CH2N,CH1,CH2,NAV,CC,NDSP,NDS
0002 INTEGER T1,T2,CH1,CH2,CH1N,CH2N
0003 INTEGER*4 NDSP,NDSPO,NDS
0004 DIMENSION T1(60),T2(60),IV1(60),IV2(60)
0005 ISH=0
0006 258 DO 260 J=1,NPTS
0007     JI=J
0008     T1(J)=CH1-8*((NPTS/2)-JI)
0009     T2(J)=CH2-8*((NPTS/2)-JI)
0010 260 CONTINUE
0011     DO 270 J=1,NPTS
0012     CALL AOUT(T1(J),0,1)
0013     CALL AOUT(T2(J),1,1)
0014     CALL AIN(IV1(J),0,1)
0015     CALL AIN(IV2(J),1,1)
0016 270 CONTINUE
0017     JS=NPTS/2
0018     CALL AOUT(T1(JS),0,1)
0019     CALL AOUT(T2(JS),1,1)
0020     IMPT1=0
0021     IMPT2=0
0022     DO 280 KJ=1,NAV
0023     IMPT1=IV1(KJ)+IMPT1
0024     IMPT2=IV2(KJ)+IMPT2
0025 280 CONTINUE
0026     IV3=IMPT1
0027     IV4=IMPT2
0028     CH1=T1(1)
0029     CH2=T2(1)
0030     N9=NPTS-NAV-1
0031     DO 300 KK=2,N9
0032     KT=KK+NAV-1
0033     IV3=IV3+IV1(KT)-IV1(KT-NAV)
0034     IV4=IV4+IV2(KT)-IV2(KT-NAV)
0035     IF(IV3.GE.IMPT1)GO TO 290
0037     IMPT1=IV3
0038     CH1=T1(KK)
0039 290 IF(IV4.GE.IMPT2)GO TO 300
0041     IMPT2=IV4
0042     CH2=T2(KK)
0043 300 CONTINUE
0044 304 IF(ISH)305,308,306
0045 305 CH1N=CH1
0046     NDSPO=NDSP-CC*100.*(CH2-CH2N)
0047     ISH=0
0048     GO TO 336
0049 306 CH2N=CH2
0050     NDSPO=NDSP-CC*100.*(CH1N-CH1)
0051     ISH=0
0052     GO TO 336
0053 308     DSP=((CH1N-CH1)+(CH2-CH2N))*CC*100.
0054     NDS=DSP+.5
0055 310 NDSF=NDSPO+NDS
0056 250 IF((CH1N-CH1).LE.(8*MSP1))GO TO 252
0058     CH1=CH1+8*MSP1
0059     ISH=-1
0060     GO TO 258
0061 252 IF((CH1-CH1N).LE.(8*MSP1))GO TO 254
0063     CH1=CH1-8*MSP1
0064     ISH=-1
0065     GO TO 258
0066 254 IF((CH2-CH2N).LE.(8*MSP2))GO TO 256
0068     CH2=CH2-8*MSP2
0069     ISH=-1
0070     GO TO 258
0071 256 IF((CH2N-CH2).LE.(8*MSP2))GO TO 336
0073     CH2=CH2+8*MSP2
0074     ISH=1
0075     GO TO 258
0076 336 RETURN
0077     END

```

Figure 10. Listing of the displacement measuring subroutine.



Repeating Equation (4):

$$d \sin \alpha = m\lambda \quad (6)$$

Differentiating both sides and setting  $\Delta m = 1$  gives:

$$\Delta \alpha = \frac{\lambda}{d \cos \alpha} \quad (7)$$

for the spacing between fringes located at an arbitrary angle  $\alpha$ . But,  $\alpha$  is fixed at  $\alpha_0$ , so

$$\Delta \alpha = \frac{\lambda}{d \cos \alpha_0} \quad (8)$$

Displacement is given by:

$$\Delta d = \Delta m \frac{\lambda}{\sin \alpha_0} \quad (9)$$

Let

$$\Delta m = \frac{\Delta \theta}{\Delta \alpha} \quad (10)$$

where  $\Delta \theta$  is the number of increments of mirror motion between the minimum of successive scans. Then:

$$\Delta d = \frac{\Delta \theta}{\Delta \alpha} \frac{\lambda}{\sin \alpha_0} \quad (11)$$

Now, let:

$$\text{NDSP} = \frac{\Delta \theta}{\Delta \alpha_0} \frac{\lambda}{\sin \alpha_0} \quad (12)$$

$$\text{where } \Delta \alpha_0 = \frac{\lambda}{d_0 \cos \alpha_0} \quad (13)$$

NDSP is the relative displacement measured by the subroutine SND.

Dividing (11) by (12) and using (8) and (13) yields:

$$\frac{\Delta d}{\text{NDSP}} = \frac{d}{d_0} = \frac{d_0 + \Delta d}{d_0} \quad (14)$$

from which

Equation (15) is the correction for large displacement and is incorporated in the main program by statements like:

```
DSP2=NDSP  
DSP3=DSP2/(1-DSP2/D0)  
IDSP(NQ)=DSP3+.5
```

Figure 11 is a plot of the load-displacement measured on compact tension specimen 6-035 at room temperature. That specimen load had been used for 4 creep experiments with small displacements, but still had good indentations. The average final crack length which was determined after the specimen had been broken apart is 23.08 mm. Indentations were located at a position 16.73 mm from the load-line. After some initial nonlinear behavior because of crack closure, the elastic result is quite straight until almost 100 microns total displacement. One of the fringe patterns became too fine to resolve with the slit-covered PMT which caused erroneous results after approximately 90 microns. The elastic compliance was calculated at the indentations' location following the procedure of Saxena and Hudak (12). The parameters were  $a/W = 0.58$ ,  $x/W = 0.42$ ,  $E = 203 \times 10^3$  MPa, width  $B = 10$  mm, and  $W = 40$  mm. The calculated compliance is  $1.05 \times 10^{-2}$  microns/nt; whereas, the measured compliance for the region between 500 and 2000 pounds (see Figure 11) is also  $1.05 \times 10^{-2}$  microns/Nt. This is certainly a fortuitous agreement, but does indicate that the measurement system is working correctly.

#### Specifications for the ISDG

The extensive testing in the NASA-sponsored Benchmark Notch Test program (6) provided sufficient data for evaluation of the ISDG. The following specifications arise from that work plus the current program.

Gage Length - 100 micrometers is used in this work, but it could be reduced to 50 micrometers. Smaller indentations (approximately 10 micrometers square) have been used with a gage length of 30 micrometers.

Range - approximately 100 micrometers has been demonstrated. With finer slits on the PMTs and a more powerful laser, the range could be extended to 400 micrometers without difficulty.

Sampling Rate - 11 samples per second. This can be speeded up with faster mirrors and computer hardware.

Relative Uncertainty -  $\pm 3\%$  with an additional uncertainty of  $\pm 0.015$  micrometer. For example a measured displacement of 1.0 micrometers would have an uncertainty of  $\pm .045$  micrometers. The  $\pm 3\%$  is associated with determination of the angle  $\alpha$ , and the  $\pm 0.015$  micrometer arises from the effects of electrical and optical noise on the determination of minimum positions. The results in Figure 11 show that this is a very conservative assessment of the relative uncertainty.

Temperature Range - to 730 C on this superalloy material. Vapor deposited protective coatings could be used to extend this range.

C07102

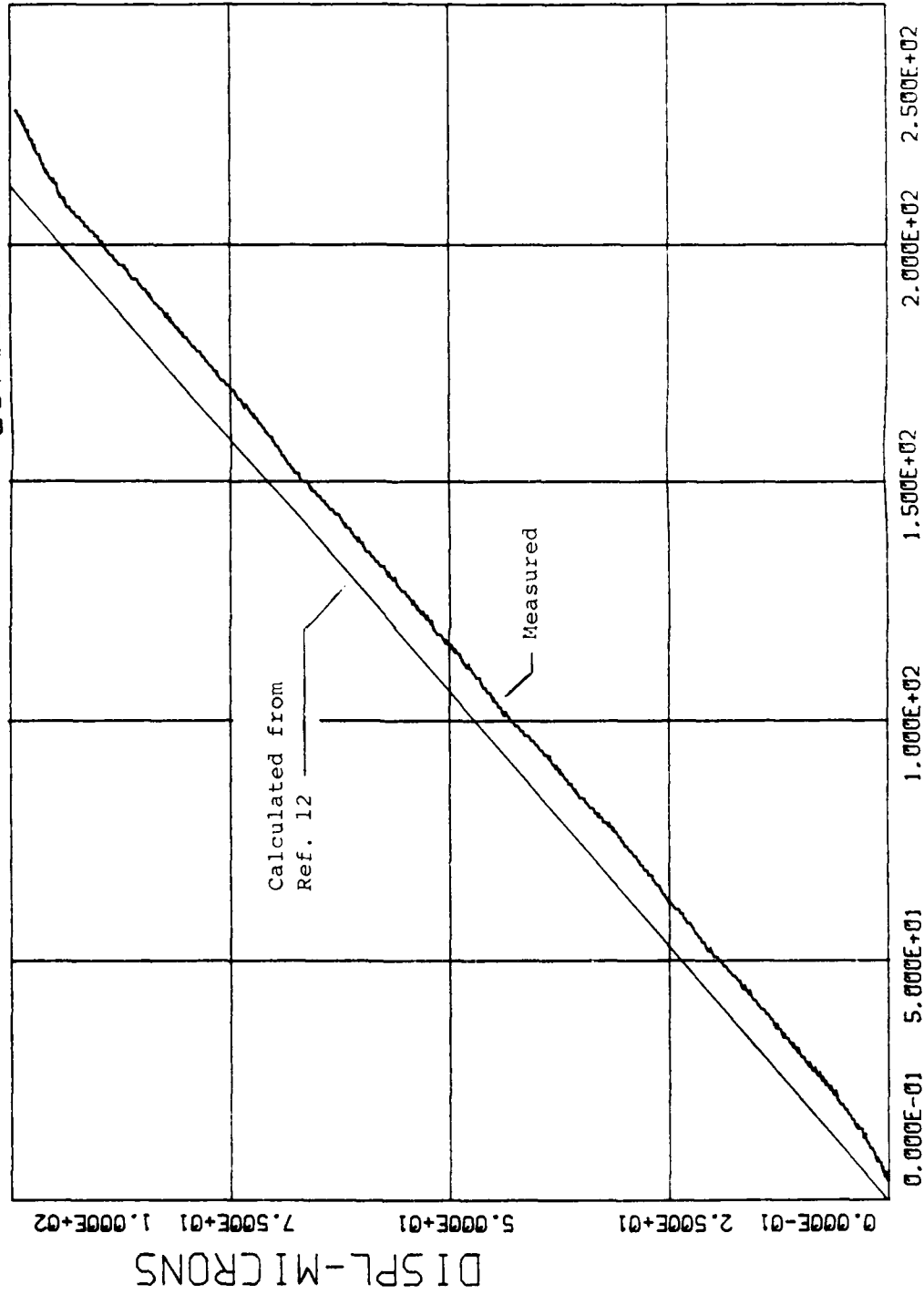


Figure 11. A check of large displacement measurement.

## EXPERIMENTAL PROCEDURES

Material and Specimens

The material used was Inconel 718, a nickel-based superalloy widely used in the turbine disks of aircraft jet engines. It was given a standard heat treatment of 968C for 1 hour, quench, 718C for 8 hours, and air cool. In another study (6), the elastic modulus at 650C was determined to be  $161 \times 10^3$  MPa for a similarly treated version of 718. The material used in this work was tested in a separate study (13) at various strain rates, and the modulus at 650C found to be  $164 \times 10^3$  MPa at the slowest strain rate of 10- per second.

The specimens were the standard compact tension geometry with overall dimensions of 48 mm by 50 mm with a dimension of  $w = 40$  mm from the load line to the furthest edge. They were machined to a thickness of 10.0 mm from 12.5 mm thick plate with the notch oriented in the T-L configuration. All machining was done by Metcut Research Associates, Inc. of Cincinnati, Ohio. Specimens were precracked at room temperature to an initial crack length,  $a$ , of 14 mm as measured from the load line.

Before precracking, specimens were mechanically polished on various grades of silicon carbide paper with the final polish using 1.0 micron diamond paste on a felt wheel. After precracking, the specimens were pre-oxidized at 650C for one hour. It had been learned from earlier work on similar materials that indents applied after this preoxidization remain reflective at temperature for long times. Several (usually 4) experiments were run on each specimen with precracking at room temperature and a new set of indents near the crack tip between tests.

Loading Apparatus

All loading was done in the electrohydraulic test machine under computer control. Special grips of alloy 713C were purchased for the high temperature tests. A wedge-shaped section was cut from these grips to permit exit of the two fringe patterns for indents at the tips of the shorter cracks. Figure 12 is a photograph of a specimen in the grips.

Specimens were heated in a locally constructed resistance furnace which has 3 quartz ports for the incident laser beam and the two fringe patterns. Two viewing ports are also included. Figure 5 showed the furnace mounted on

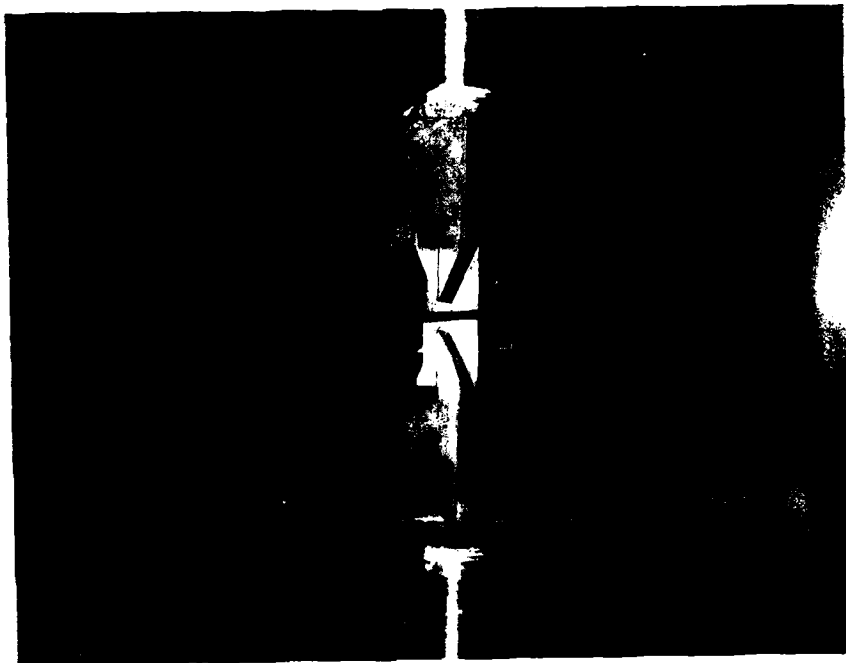


Figure 12. A compact tension specimen in the special grips.

the test machine. The load links are quite long, and a fan blowing on the load cell keeps it at ambient temperature. A thermocouple was pushed in contact with the specimen and provided the signal for the temperature controller which held the specimen at the test temperature + 2C. It took approximately one hour to heat the specimen up and stabilize at a temperature of 650C.

## SECTION IV

### CREEP THRESHOLD MEASUREMENTS

The underlying theme behind this part of the research program was to study the use of the ISDG to measure crack opening displacement under creep conditions. With its high sensitivity and good long-term stability, the ISDG should enable determination of threshold creep values in minimal time. An earlier study of IN-100, with less sophisticated measurements, is reported in reference 14.

#### Loading Schedule

A separate program, CRTH, was written to apply the load and make the ISDG measurements. The loading schedule is shown schematically in Figure 13. A very small load was applied to the specimen as it was heated. After the test temperature was reached, a larger initial load was applied, but it was still less than half the to-be-applied creep load. The laser beam was then adjusted to its final position. At this point, the ISDG was initialized as described earlier; this took only a couple of minutes. The final increment of load was applied to reach the creep load. This rate of loading was the same as used for subsequent compliance measurements.

Two seconds after the creep load was reached, the first compliance was automatically taken. The load was dropped at a linear rate to 445 newtons below the creep load and then immediately reapplied. Displacement measurements were made (every 20 seconds except for one 5-hour test) automatically, and compliance data taken on command from the keyboard. Each compliance measurement took 50 seconds, and most tests lasted 30 minutes. Load displacement and time were displayed on the terminal to permit monitoring of the test.

After a creep test at temperature, the specimen was precracked at room temperature in preparation for another test. Four tests could be run on one specimen while staying in the middle region.



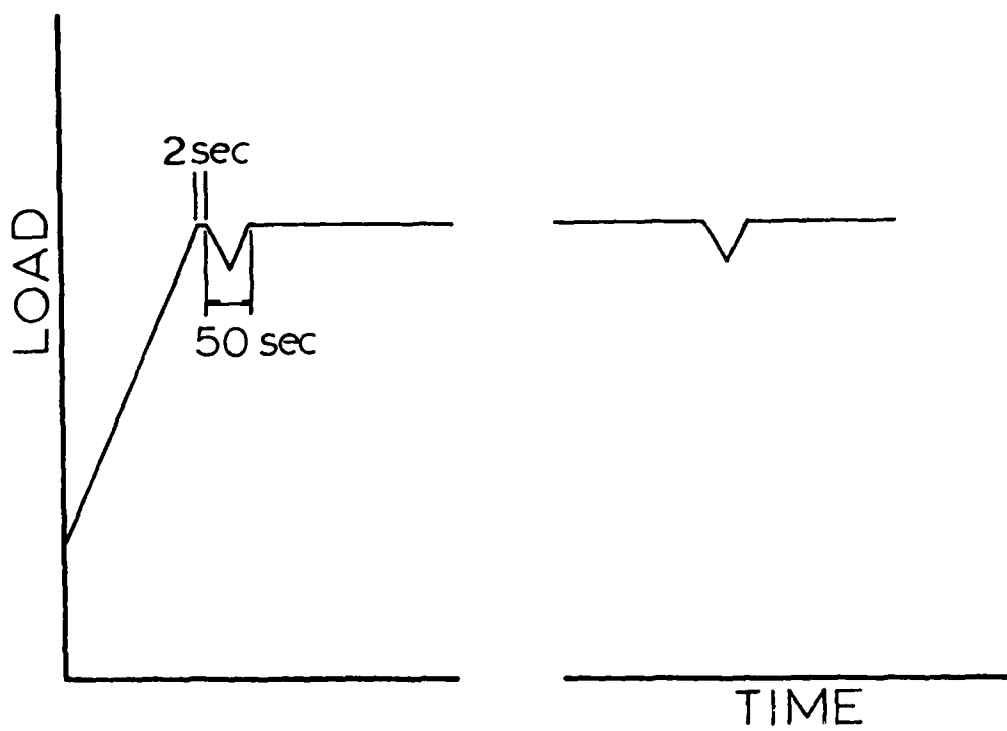


Figure 13. Loading schedule for creep tests.

## Data Presentation

The creep displacement data and compliance data were stored in separate files on the 10-Mbyte disk and plotted after completion of the test. Figure 14 shows the results from test 21092 which was at a high stress intensity factor. Approximately 2.6 micrometers of creep occurred during this 30 minute test. The vertical "tick" marks indicate when the command compliance measurements were made.

Compliances were also determined after the tests by fitting a least-squares straight line to each set of unloading/loading data. Figure 15 is a plot of the 4 compliances of test 21092; there are 20 points for unloading and 20 for reloading. The fitted straight lines extend past the 445 newton (100 lb) compliance load increment so that the left intercepts may be shown. The rightmost data points on each compliance correspond to the displacement at the tick marks in Figure 14. The data analysis program printed out the slopes, intercepts, and the correlation coefficients.

## Results

The results of 9 tests are summarized in the following tables. Plots of creep displacement and compliances are given in Appendix 1 for all 9 tests.

Table 1 presents the surface crack length measurements - all from the load line - along with the creep stress intensity factor (SIF) and total creep displacement.  $a_{is}$  is the initial crack length on the side with the indents, and  $a_{is}$  is the location of the indents. The difference gives the distance of the indents behind the crack tip ( $r$ ) which is usually 0.4 mm or less. This gives a ratio of  $r/a$  of 0.03 or less. Kobayashi (15) states that the "local region" wherein linear elastic displacement calculations are valid is  $r/a \leq 0.05$ .

Table 2 gives information on the calculated and measured compliances. The measured ones are simply the slopes of the straight lines of Figure 15. Calculated values are obtained using linear elasticity equations; the linear behavior of Figure 15 verifies this process. The compliance at a point  $r$ , behind the crack tip is given by

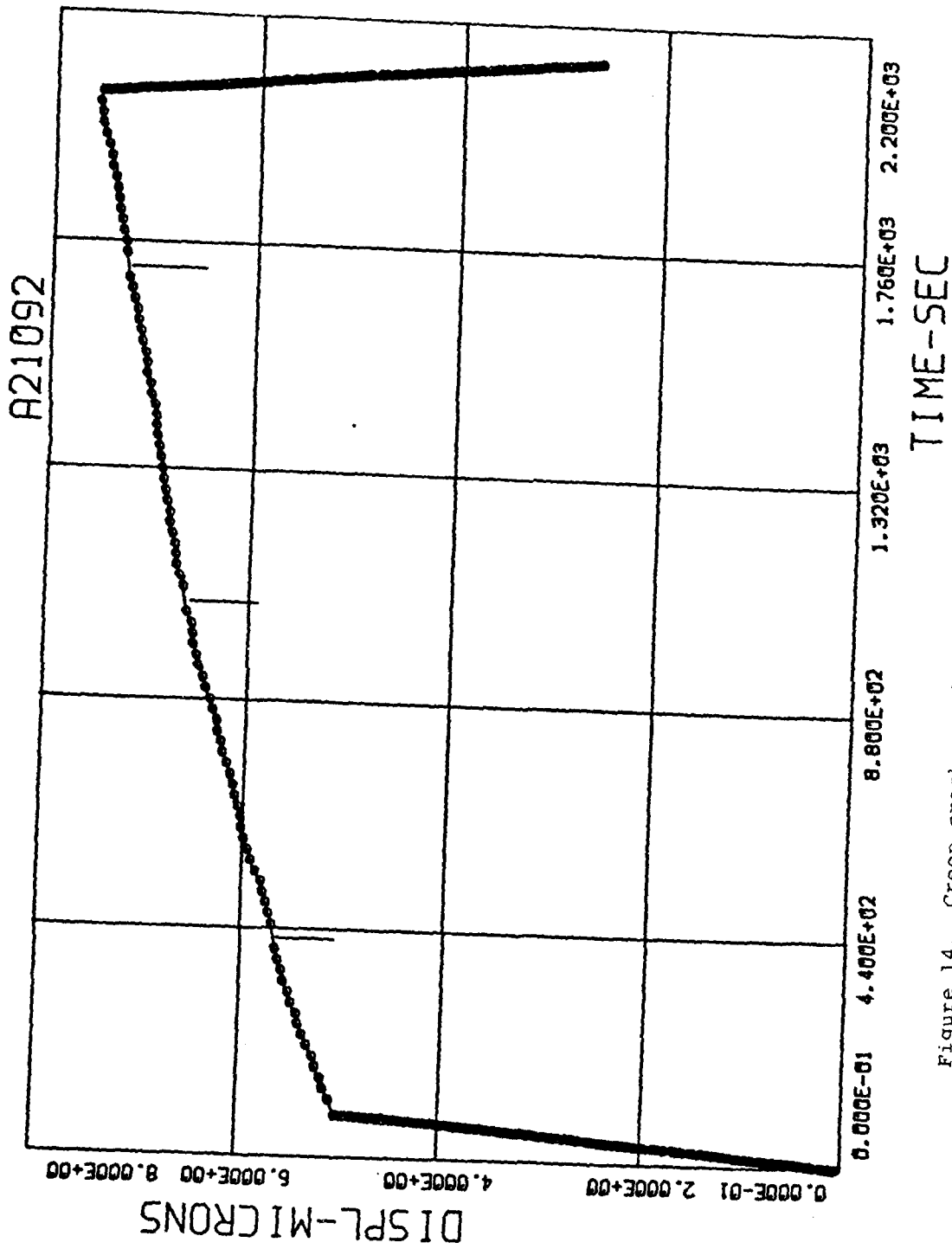


Figure 14. Creep crack opening displacement for Test 21092.

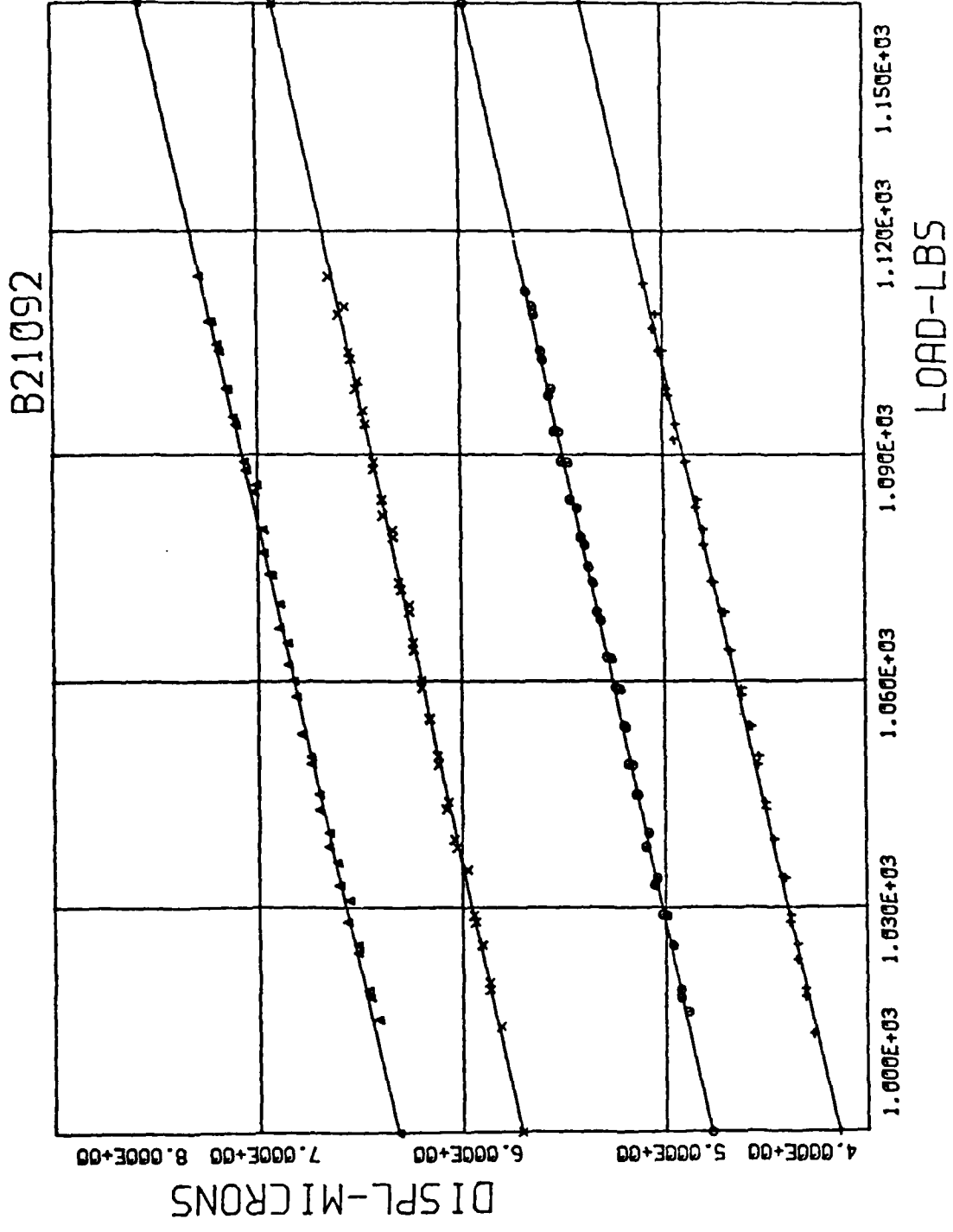


Figure 15. Measured compliances for test 21092.

TABLE 1

CRACK LENGTHS, LOADS, AND CREEP DISPLACEMENTS  
FOR THE CREEP TESTS

Test Number	Specimen Number	Initial SIF	Indents Locations	Initial Surface Crack Length	Final Surface Crack Length	Creep Displacement
		$K_{I_1}$ MPa-m <sup>1/2</sup>	$a_{I_s}$ mm	$a_{i_s}$ mm	$a_{f_s}$ mm	$\delta_c$ mm
10092	6-038	22.0	13.66	14.58	14.74	1.85
13092	6-038	13.7	16.50	16.84	16.90	0.65
16092	6-038	23.5	21.68	22.04	22.10	3.25
17092 (5 hrs)	6-035	11.0	13.92	14.32	14.38	0.18
20092	6-035	16.5	16.70	16.90	17.00	1.05
21092	6-035	22.0	18.72	18.92	19.02	2.55
22092	6-035	16.5	22.08	22.14	22.28	1.00
23092	7-039	19.2	13.58	13.90	13.94	1.15
24092	7-039	13.7	16.38	16.64	16.66	0.72

TABLE 2

CALCULATED AND MEASURED COMPLIANCES FOR THE  
CREEP TESTSCOMPLIANCES  $10^{-3} \text{ in}^2/\text{Nt}$ 

Test Number	calculated		measured			calculated
	$C_{is}$	$C_1$	$C_2$	$C_3$	$C_4$	$C_{fs}$
10092	2.08	1.84	2.16	1.96	2.20	2.27
13092	1.49	1.88	1.19	--	--	1.60
16092	2.18	2.42	2.35	2.45	2.54	2.48
17092	1.32	1.64	1.61	1.40	1.37	1.41
20092	1.06	1.50	1.63	1.40	1.49	1.34
21092	1.30	1.88	1.80	1.80	1.89	1.60
22092	0.72	2.12	2.21	2.22	2.15	1.58
23092	1.25	1.50	1.43	1.51	1.45	1.44
24092	1.24	1.52	1.44	1.37	1.43	1.31

$$C = \frac{4F^2(1-\nu^2)}{WE} \sqrt{\frac{a}{W}} \left[ \frac{1}{2} + \frac{3}{8} \left( \frac{a}{W} \right)^2 + \frac{5}{16} \left( \frac{a}{W} \right)^4 \right] \quad (16)$$

where E is the elastic modulus and  $\nu$  is Poisson's ratio. W is the specimen width from the load line, and F is the stress intensity factor variation with a. The compliances  $C_1$  and  $C_2$  are calculated from the initial and final crack lengths  $a_{i1}$  and  $a_{i2}$ .  $C_1$ ,  $C_2$ ,  $C_3$ , and  $C_4$  are the measured compliances with  $C_3$  being the one taken 2 seconds after reading the creep load.

The measured compliances of Table 2 show a lot of scatter. They do not increase uniformly with time even when there is considerable crack growth. Calculated compliances tend to be smaller than those measured. For example, the measured compliances of test 16902 change very little, but there was considerable creep displacement.

In his extensive study of creep in compact tension specimens of IN-100(1), Donath noted that compliances taken soon after the creep load was reached usually were smaller than the initial loading compliance. Table 3 supports this observation;  $C_1$  is the compliance computed from the last 110 Newtons of initial loading. This is not surprising because the final portion of the loading leads to nonlinear deformation around the crack tip, but the compliances taken after the creep load is reached show linear behavior.

The cracks are of course not perfectly straight through the specimen, and Figure 16 is a photograph of specimen 6-035 after it was broken open at room temperature. The last three tests are clearly visible and show a gentle curvature with reasonably uniform creep crack growth. The creep growth, as evidenced by the dark bands, show the familiar striations perpendicular to the crack front. These bands are dark because the fresh material surfaces were exposed to high temperatures; whereas, the intermediate fatigue crack growth for the first test on this specimen is hard to see because the initial precrack is stained. The specimens were precracked; then cleaned with soapy water, acetone, and methanol successively; these solutions seeped into the precrack and stained it at high temperature.

Crack length measurements - both initial and final - were made after the specimens were broken open. An X-Y

TABLE 3

## FIRST COMPLIANCES FOR THE CREEP TESTS

Test Number	Final Loading Compliance $10^{-3} \mu\text{m/Nt}$	First Incremental Compliance - $C_1$ $10^{-3} \mu\text{m/Nt}$
10092	2.60	1.84
13092	2.01	1.88
16092	3.00	2.42
17092	1.75	1.64
22092	1.73	1.50
21092	2.30	1.88
22092	2.43	2.12
23092	1.70	1.50
24092	1.75	1.52





Specimen 6-035

Figure 16. Crack surface after four tests.

microscope with a resolution of 0.025 mm was used, and measurements were made at the 2 sides plus 5 intermediate points. The average values of these initial and final crack lengths are presented in Table 4 as  $\bar{a}_i$  and  $\bar{a}_f$ . They are of course larger values than the surface measurements of Table 2. The standard deviation of the 7 measurements was 0.5 mm or less. Compliances based on these crack lengths are also given as  $\bar{C}_i$  and  $\bar{C}_f$ . These compliances are larger than those of Table 2 primarily because  $r$  is larger.

Figure 17 is a plot of the crack growth rate versus  $K$  where the growth rate is taken from the data of Table 4, i.e. based on final average data after the specimen is broken open. This illustrates the scatter inherent in creep crack growth experiments. For examples, the two tests at 13.7 MPa-m<sup>3/2</sup> were conducted on separate specimens with very nearly identical initial crack lengths, yet the amount of creep crack growth was very different.

### Discussion

Since the distance of the indents behind the crack tip is much less than the crack length, it is clear that " $r$ " is most affected by an extension of the crack. The relative changes in  $F_1$ ,  $a$ , and  $\sigma$  in Equation 16 are much smaller. So, the relative uncertainty in  $C$  is approximately.

$$\frac{\Delta C}{C} \approx \frac{1}{2} \frac{\Delta r}{r} \quad (17)$$

This means that if one wishes to use compliance changes to infer crack growth, it is best to make measurements near the crack tip. But from a practical viewpoint, it also means that any nonuniform crack growth, "tunneling" ahead of the crack, or other irregularities in creep crack growth greatly affect the measurement value of  $C$ .

It is believed that local irregularities contribute to the scatter in the measured compliances of Table 2 because the indents are so close to the tip. Earlier work (14) on center-cracked panel specimens of IN-100 at 730C with indentations located near the specimen centerline showed that the compliances increased uniformly with crack growth. Those compliance measurements, made far away from the crack tip, produced much smoother and more sensible results. Measurements by Macha et al (16) agree very well with elastic calculations, but they were made on aluminum specimens with nice, straight crack fronts and no plastic deformations or creep involved. The excellent agreement of Figure 11 which was taken at room temperature on specimen

TABLE 4  
 AVERAGE CRACK LENGTHS AND COMPLIANCES FOR  
 THE CREEP TESTS

Test Number	Average Crack Lengths		Compliances	
	$\bar{a}_i$	$\bar{a}_f$	$\bar{C}_i$	$\bar{C}_f$
	mm	mm	$10^{-3} \mu\text{m}/\text{Nt}$	$10^{-3} \mu\text{m}/\text{Nt}$
10092	14.94	15.42	2.28	2.76
13092	17.32	17.44	2.15	2.33
16092	22.38	22.70	2.84	3.57
17092	15.08	15.30	2.17	2.40
20092	17.44	17.62	2.03	2.29
21092	19.58	19.98	2.56	3.19
22092	22.96	23.08	3.36	3.64
23092	14.94	15.18	2.39	2.64
24092	17.68	17.86	2.74	2.96

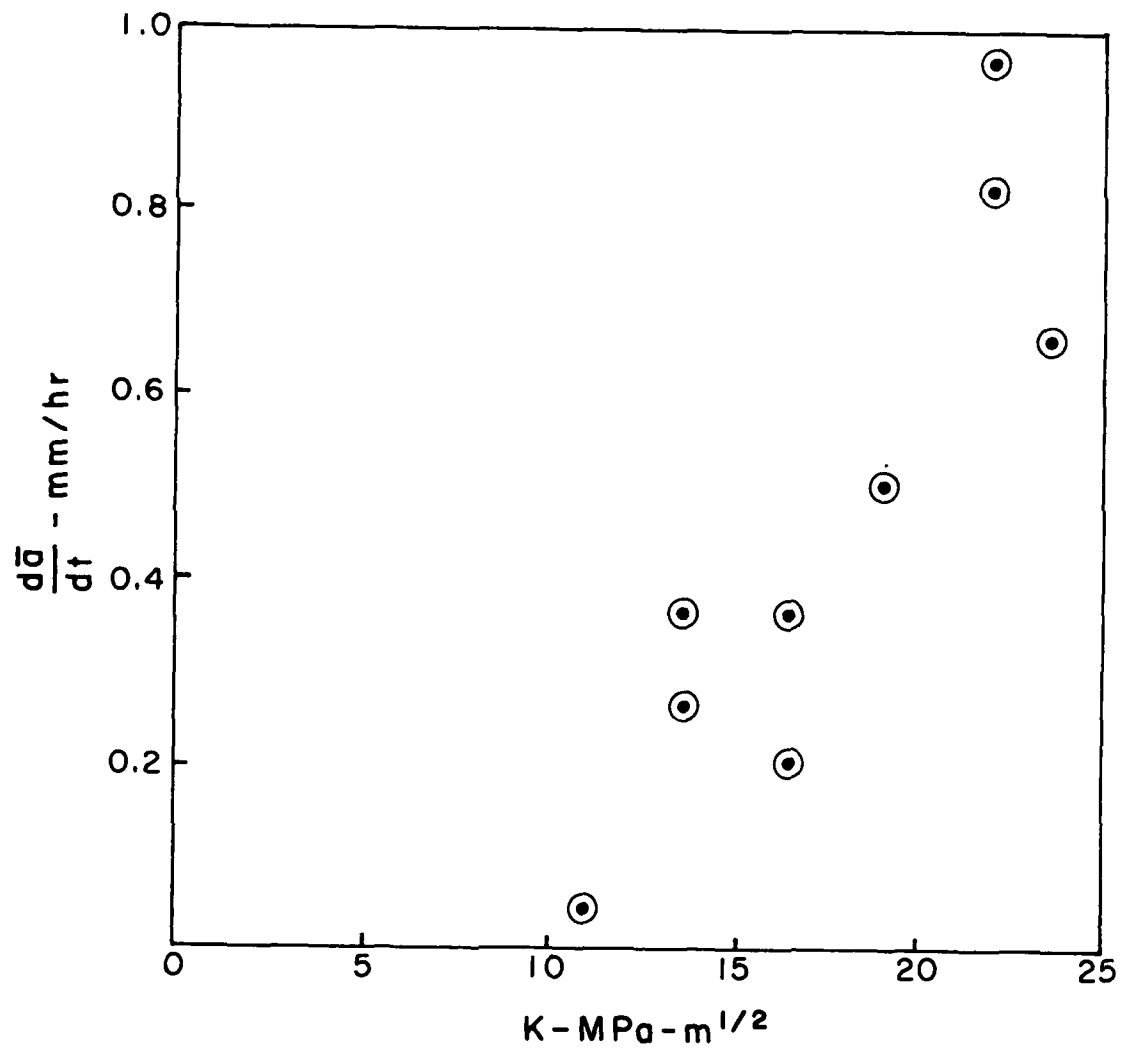


Figure 17. Average crack growth rate versus K.

6-035 was obtained for indentations 6.4 mm behind the crack tip.

It is reasonable to compute the elastic component of the crack opening displacement by multiplying the changes in compliance computed from crack length measurements by the creep load. That component should be simply due to the crack growth; the rest would arise from creep of the material. Calculations based on surface crack length measurements do in general yield an opening displacement smaller than the measured . . . . However, calculations based on average crack lengths produce larger than . . . . This is another example of the experimental conditions not matching the linear elastic model - at least near the crack tip.

However, if the primary purpose of a series of tests is to quickly establish a creep threshold value, that can easily be done. Figure 18 is a plot of the crack opening displacement rate divided by the first measured compliance - It shows that the creep rate normalized by the specimen compliance is reasonably linearly related to the magnitude of the stress intensity factor. Extrapolation to zero crack growth gives a threshold value of 10.4 MPa-m<sup>1/2</sup> which is consistent with the results from test 17092 at the lowest K for 5 hours. This is quite a bit lower than the 16 MPa-m<sup>1/2</sup> reported by Sadananda and Shahinian (17) for Alloy 718 at 649C in tests lasting 200 hours. So, by measuring creep crack opening displacement with the ISDG and removing the geometry effects by dividing by the measured compliance, one can establish a threshold value.

One can also fit a straight line to the data of Figure 17 and establish a threshold value without any sophisticated measurements at all. But the normalized ISDG data shows less scatter and also permit one to evaluate the creep growth before the specimen is broken open. This is useful in getting optimal usage from multiple tests on the same specimen.

### Conclusions

The ISDG works well for crack opening displacement measurements on superalloys at high temperature. Figures 14 and 15 show that the data is smooth and that displacements on the order of 0.02 micrometers are resolved. Furthermore, the minicomputer - controlled system makes data acquisition and subsequent analysis very easy. The realtime display of crack opening displacement during a creep experiment is especially useful.

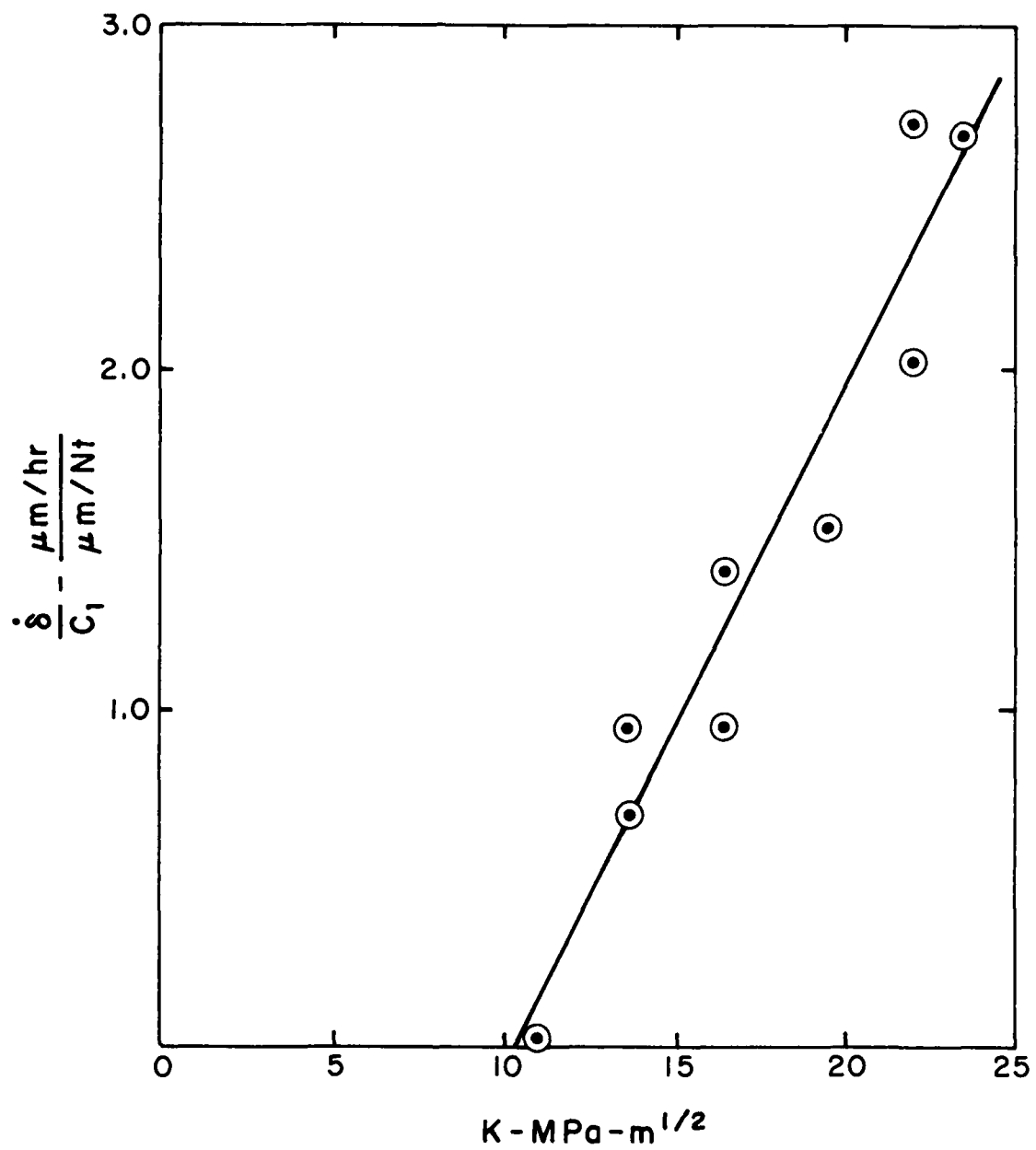


Figure 18. Normalized crack opening displacement rate versus K.

Incremental compliance measurements near the crack tip are not modelled well by linear elastic fracture mechanics. The three-dimensional nature of the problem as well as deviations such as curved crack fronts preclude this. Furthermore, irregularities in local crack tip behavior during creep growth contribute to scatter in the measured compliances. Incremental compliances measured near the tip did not prove useful in either establishing a threshold value or inferring the amount of creep crack growth.

Measurements of creep crack opening displacement normalized by the first measured incremental compliance did prove useful in establishing a threshold stress intensity factor for creep - it is  $\sim 10\text{MPa}\cdot\text{m}^{1/2}$  for Inconel 718 at 650C. The advantage of the ISDG is that one knows within a very few minutes (certainly within a few hours for very low creep loads) whether creep is occurring. It is much more sensitive and easy-to-use than other techniques. This realtime information is useful for efficient planning of experiments to establish threshold values.

## SECTION V

### FATIGUE THRESHOLD MEASUREMENTS

Just as increasing crack opening displacement identified creep in the previous section, one would expect an increasing relative displacement between minimum and maximum loads to identify fatigue crack growth. The ISDG is not nearly fast enough to permit fatigue loading for tens of thousands of cycles in a reasonable time, so the fatigue loading was interrupted periodically for an incremental displacement measurement.

#### Loading Schedule

A program, FATH, was written to fatigue load the specimen at a rate of approximately 20 Hz and periodically interrupt it for a complete measurement of displacement versus load through one cycle. Figure 19 is a schematic of the FATH loading schedule. An initial single cycle was applied without ISDG measurement in order to "seat" the specimen in the grips. Then the laser beam was adjusted and the initialization subprogram run. Next a single ramp cycle was run during which ISDG measurements were made. This single cycle was immediately and automatically followed by a sine function signal to fatigue load the specimen at approximately 20 Hz. This loading signal was periodically interrupted for a single ramp cycle. Each single ramp cycle took 24 seconds.

Early in this phase of the investigation, only the maximum and minimum displacements during the single cycle were recorded. Incremental displacement measurements in those early experiments showed similar behavior to the more complete results reported herein, but they are included in this report only in Table 5. There were six preliminary tests and six complete tests.

Again the specimens were precracked at room temperature between tests and finally broken open for crack shape measurements. All precracking and fatigue testing were done with an R ratio of 0.1.

#### Data Presentation

All of the various single cycle displacement-load data were stored in a single file; each single cycle record could be accessed independently. Figure 20 is a plot of the incremental displacement data for Test 12083 which was run for 50,000 cycles at  $\Delta K = 11.0 \text{ MPa}\cdot\text{m}^{1/2}$ . The lower plot with circle symbols is the crack opening displacement at the



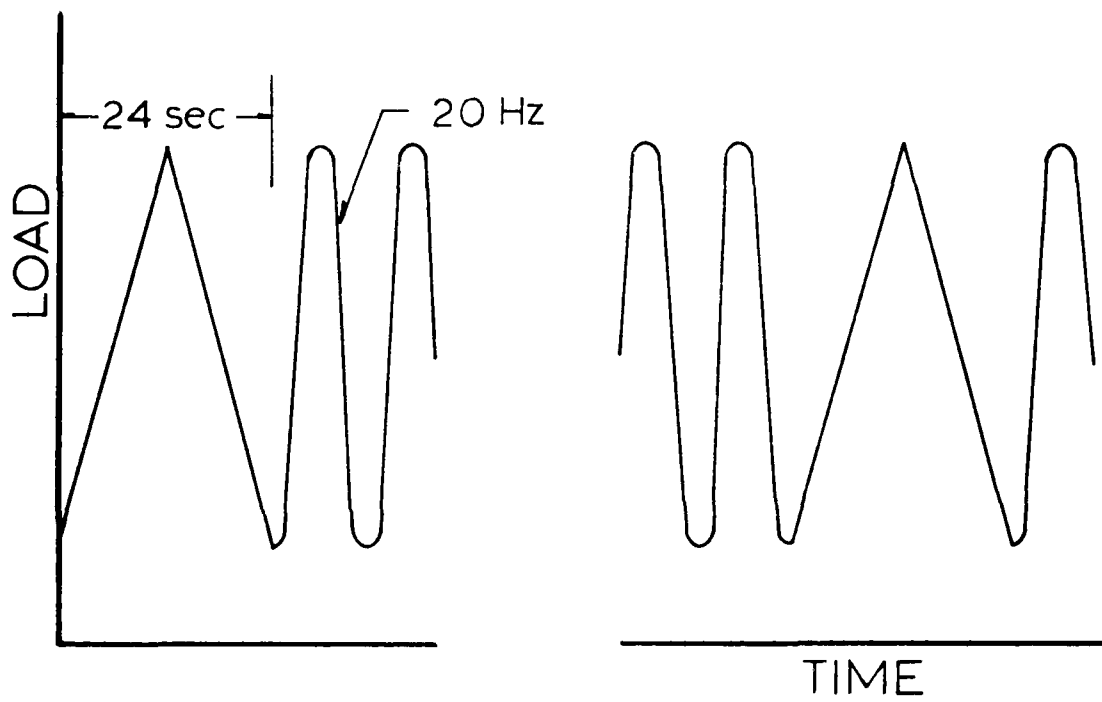


Figure 19. Loading schedule for fatigue tests.

A111083

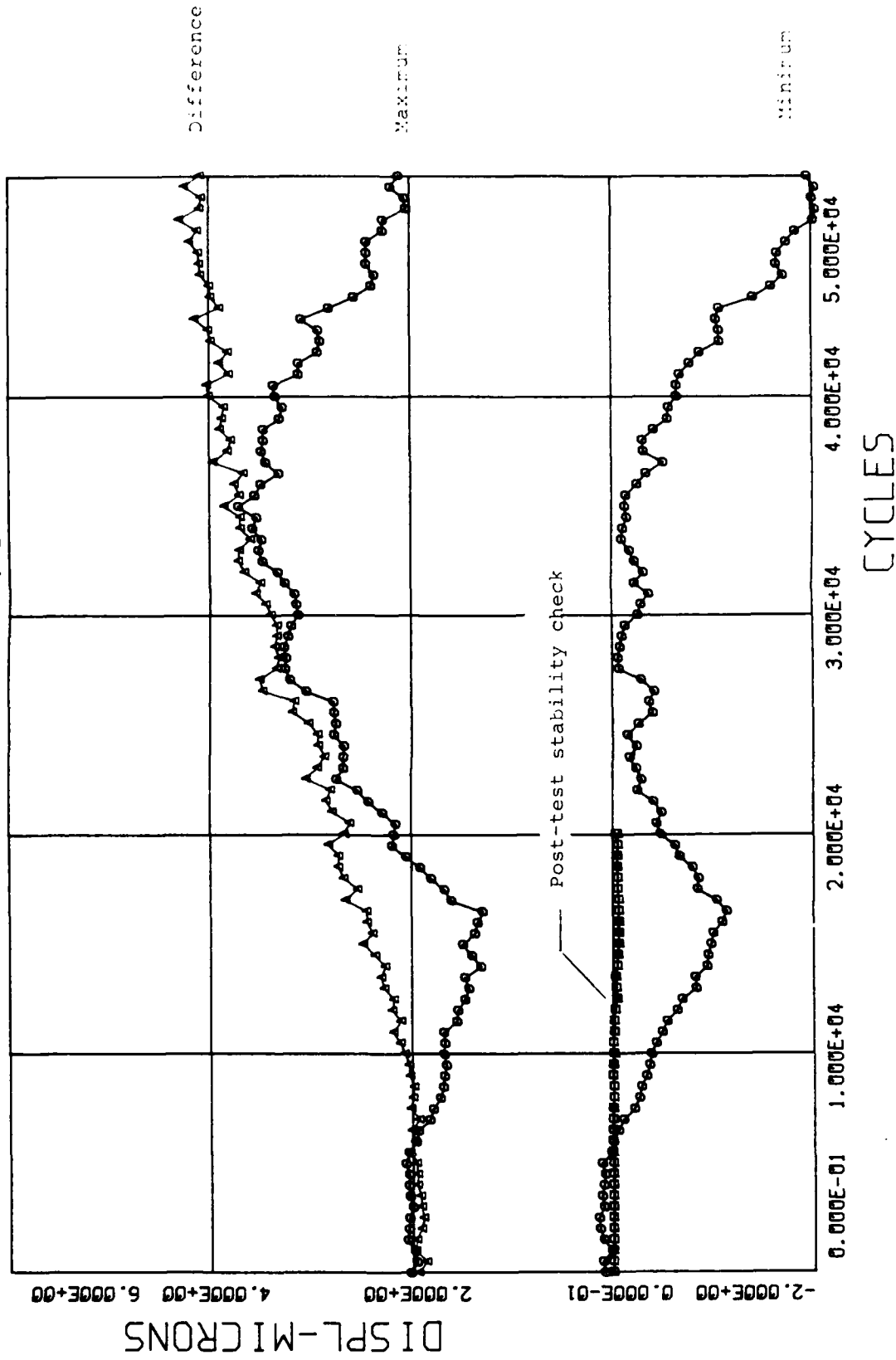


Figure 20. Crack opening displacement at minimum and maximum loads for Test 11083.

minimum load; the upper set of circles is shown at maximum load.

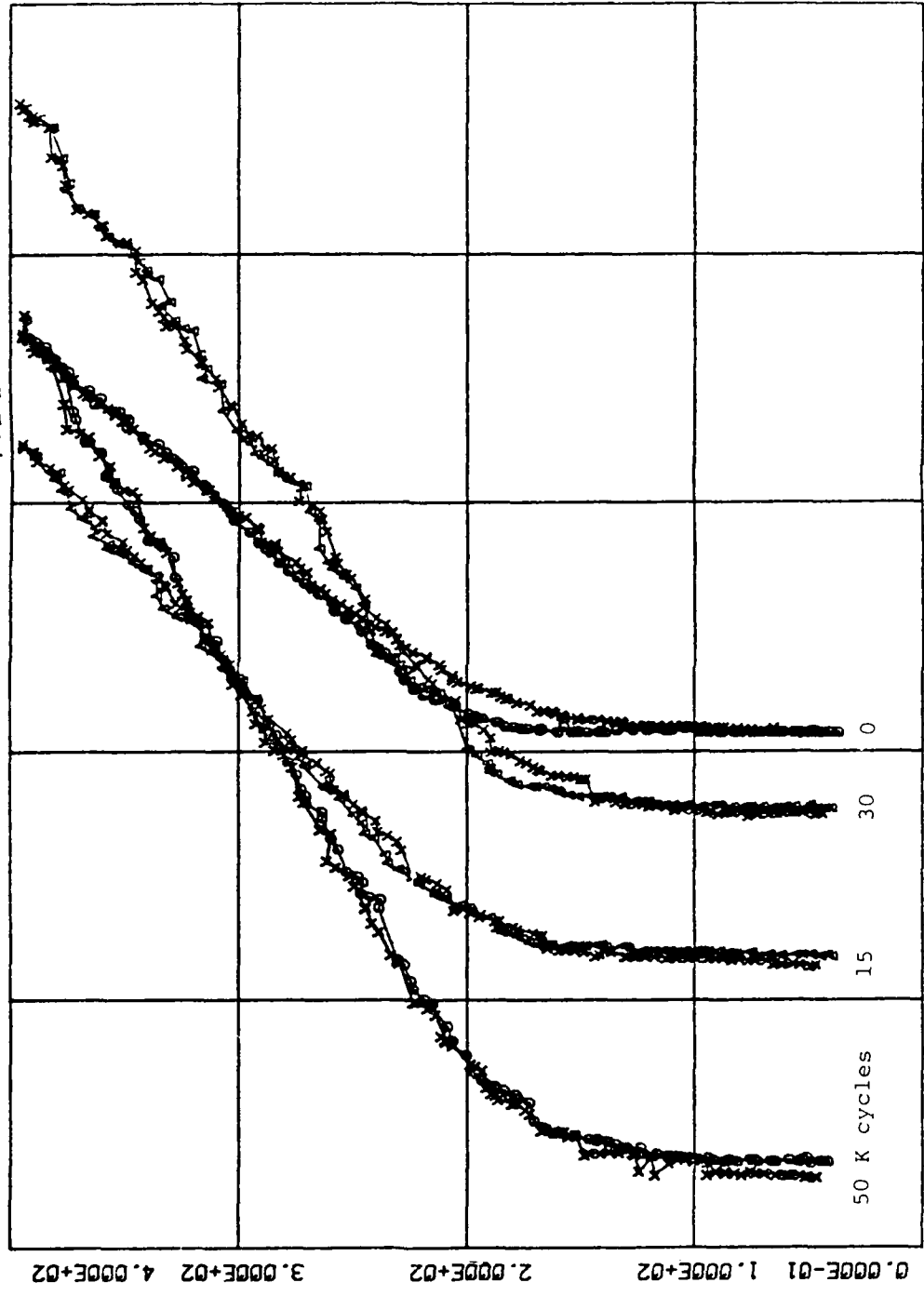
This decrease in crack opening displacement at minimum load was unexpected; however, it was observed in other tests which showed crack growth (including a preliminary test). Nevertheless, to assure that this was not a recent drift, immediately after the test was completed, a stability check was conducted by running the program on a zero load input disconnected from the test circuit. The triangle symbols on the zero displacement line are the results of this stability check - there is essentially no drift. The triangle symbols in Figure 20 are a plot of the incremental displacement which is seen to increase monotonically. This particular test did indeed show fatigue crack growth.

Figure 21 is a plot of four single cycles for test 11083. Note that the beginning and ending displacement in each case corresponds to the values on the lower plot in Figure 20. It is evident that the upper portion of each curve is linear - meaning that the specimen behaved in a linear elastic fashion after a particular opening load had been surpassed. This opening load is observed to decrease with cycling in Figure 21, and the compliance as measured from the upper or linear portion increases. Also, a bit of hysteresis is observed on the first recorded cycle.

The opening load can be more precisely defined if a straight line is fitted to the upper linear portion and the original data subtracted from this fitted line. Figure 22 illustrates this for the first recorded cycle of Test 11083. The original data is plotted as triangles (loading) and squares (unloading). A least-squares straight line is fitted to the upper portion; these two lines are drawn and marked with circles. Finally, the reduced data is plotted as crosses - the values being approximately zero in the upper region. Programs were written to do all this manipulation and to identify the opening load as that value where the reduced data deviated from zero by 10 percent of the maximum deviation (which occurs of course at zero load).

Some judgment was required in using this opening load program. The largest portion of the upper portion of the curve was used which would give a straight line correlation of 0.99 or better. Several trials were often required, but some of the data had correlations of better than 0.9995.

A11083

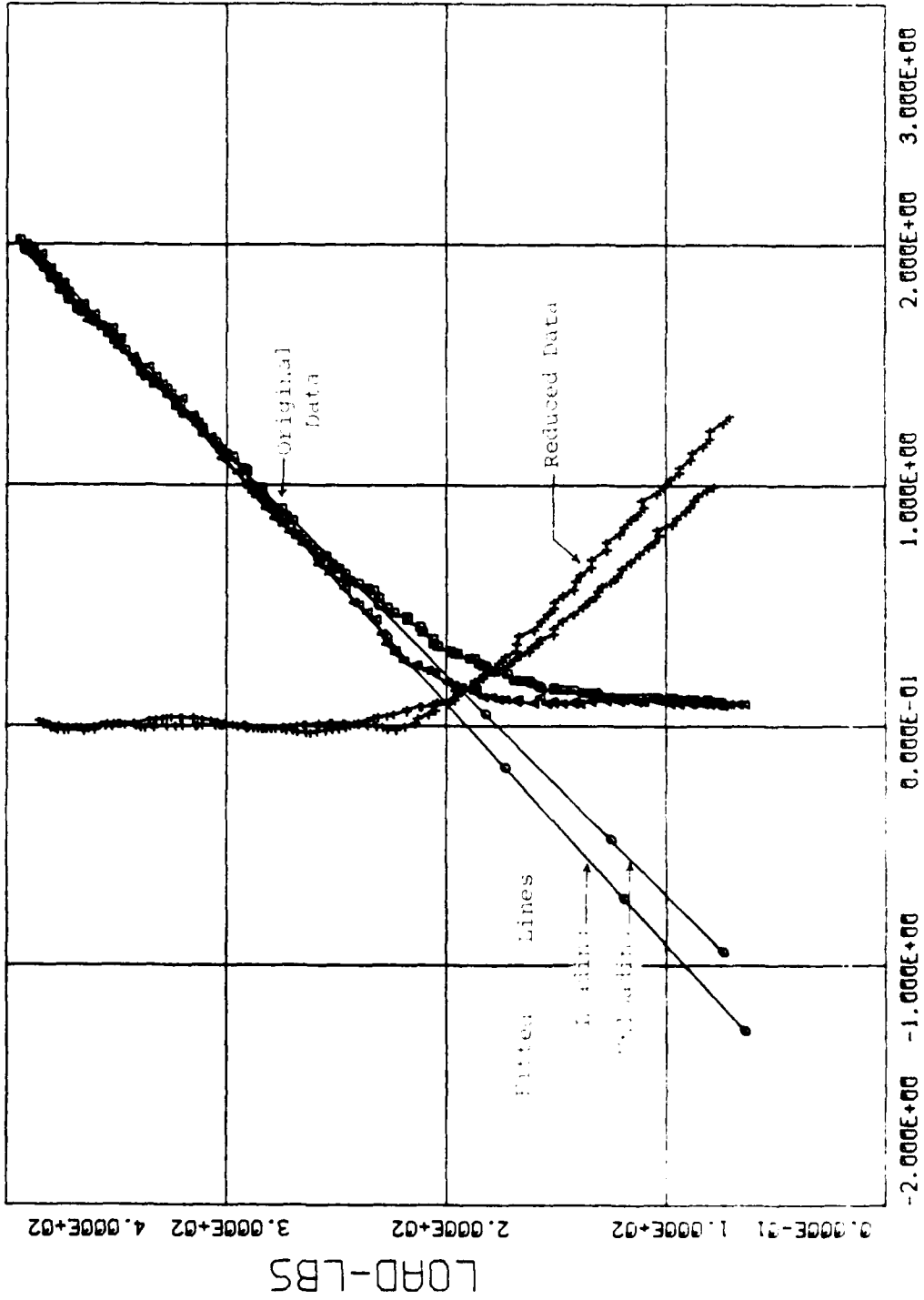


-2.400E+00 -1.200E+00 2.384E-07 1.200E+00 2.400E+00 3.600E+00

DISPL-MICRONS

Figure 21. Selected load-displacement plots for Test 11083.

A11083



DISPL-MICRONS

Plot of Load vs. Displacement for A11083 by P. J. Test 11/71.

## Results

The results of the six complete tests are summarized and max/min displacement versus cycles are presented in this section. Selected single cycle plots of load versus displacement and of the corresponding reduced data are included in Appendix 2. The average crack lengths were measured after the specimens were broken open.

Table 5 list the specimens, loading, initial average crack lengths, and average crack growth for all twelve tests. The results at  $\Delta K = 16.5 \text{ MPa}\cdot\text{m}^{1/2}$  and at  $\Delta K = 8.8$  are consistent, but there is variation in the results at  $\Delta K = 11.0 \text{ MPa}\cdot\text{m}^{1/2}$ .

Figure 23 is a plot of crack growth rate versus stress intensity factor range. Rates are computed simply from the data of Table 5, and the results are presented on the usual log-log plot. The inconsistencies in the growth rates at  $\Delta K = 11.0, \text{ MPa}\cdot\text{m}^{1/2}$  are quite evident there.

The surface crack lengths and compliances based on them are presented in Table 6. The measured compliances for the first and last cycles are compared with the calculated values, and again the measured values are higher. Behavior here is similar to that observed in the creep threshold experiments.

Detailed information on each of the six complete tests is given in Figures 24-35. The maximum and minimum crack opening displacements versus cycles are presented along with variations in compliances and opening loads. The opening load ratio is the load at which the crack opens divided by the maximum load. Information on the precracking load schedule is also given.

TABLE 5

CRACK LENGTHS, LOADS, AND AVERAGE CRACK GROWTH  
FOR THE FATIGUE TESTS

Test Number	Specimen Number	SIF Range	Average Initial Crack Length	Average Crack Growth	Total Cycles
		$\Delta k$	$\bar{a}_i$	$\bar{\Delta a}$	kilocycles
		$MP_a^{-1/2}$	mm	mm	
15073	7-034	16.5	15.28	1.18	17
03083	7-036	16.5	18.04	0.67	13
08083	7-037	16.5	19.79	0.42	11
21073	7-034	11.0	18.73	0.34	31.5
26073	7-037	11.0	15.61	0.65	48
11083	7-034	11.0	23.84	0.36	50
12083	7-037	11.0	23.40	0.0	80
16083	7-036	11.0	25.06	0.0	60
27073	7-036	8.8	21.29	0.0	100
29073	7-034	8.8	17.97	0.0	100
09083	7-036	8.8	21.79	0.0	100
17083	7-037	8.8	26.26	0.0	100

TABLE 6

## COMPLIANCES FOR THE FATIGUE TESTS

Test Number	Indents Location	Initial Surface Crack Length	Cycle	Calculated Compliance	Measured Compliance	Average Crack Growth
	$a_{is}$	$a_{is}$				$\bar{\Delta a}$
	mm	mm	kilocycles	$10^{-3} \mu m/Nt$	$10^{-3} \mu m/Nt$	mm
08083	18.43	18.60	0	1.16	1.68	0.42
			11	2.8	3.50	
11083	23.48	23.68	0	1.84	2.20	0.36
			50	3.19	4.00	
12083	22.86	23.00	0	1.45	2.46	0.00
			80	1.45	1.94	
16083	23.99	24.19	0	2.07	2.65	0.00
			60	2.07	2.29	
09083	21.67	21.82	0	1.29	1.55	0.00
			100	1.29	0.30	
17083	25.29	25.44	0	1.98	2.00	0.00
			100	1.98	1.37	

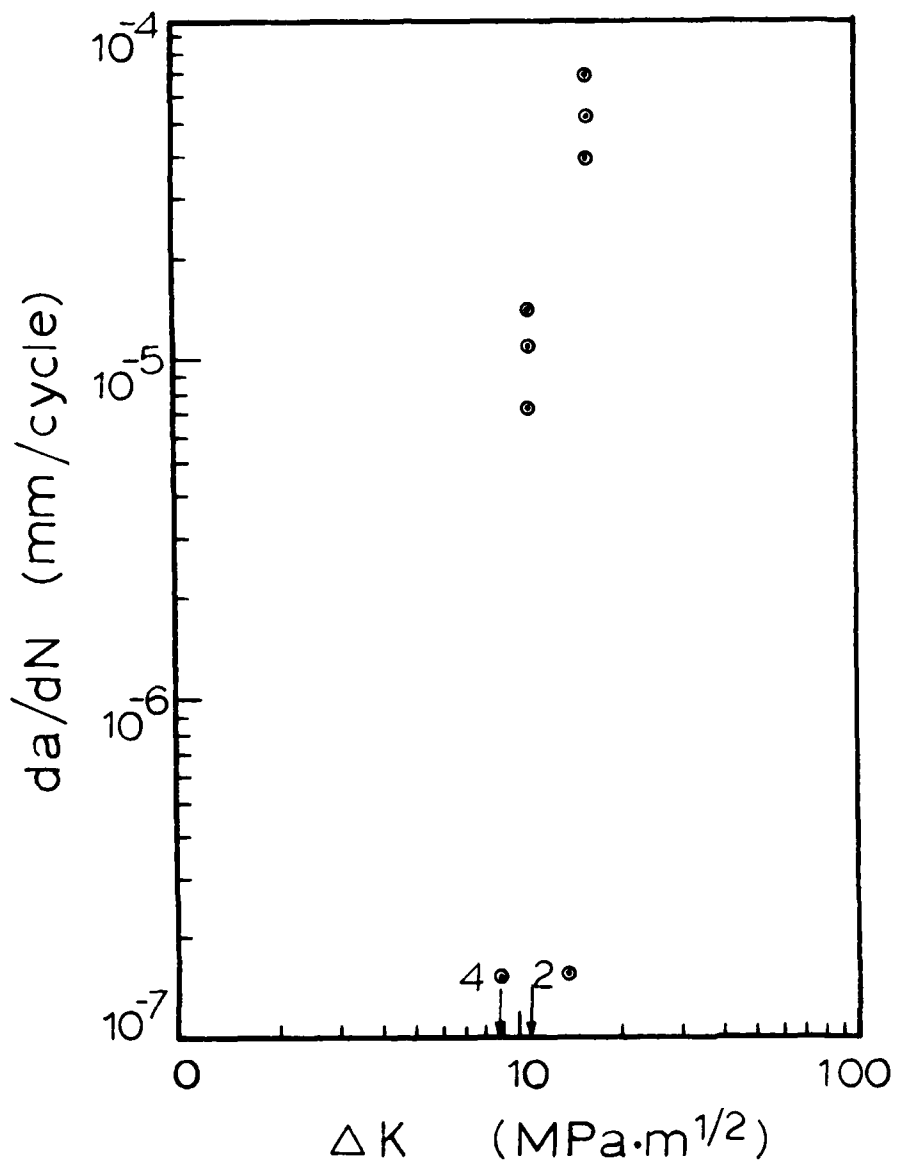


Figure 23. Crack growth rates for the fatigue threshold tests.



B08083

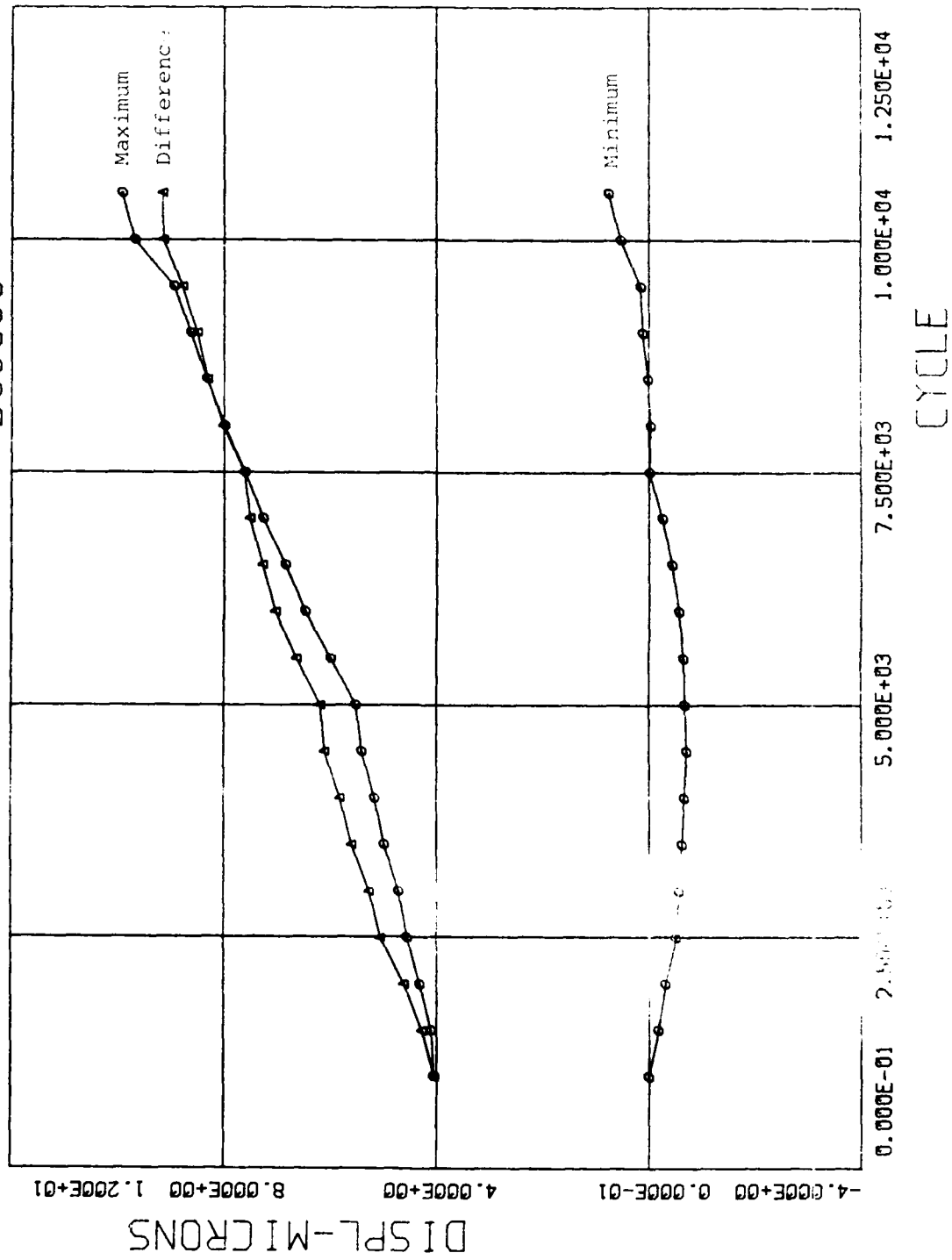


Figure 1. Opening displacements at minimum and maximum for Test 08083.

TEST NUMBER - 08083

$\Delta K$  (MPa-m<sup>1/2</sup>) - 16.5

TOTAL CYCLES (1000) - 10.5

AVERAGE CRACK GROWTH (mm) - 0.42

FINAL ROOM TEMPERATURE PRECRACKING

$\Delta K$  (MPa-m<sup>1/2</sup>) - 16.5

CYCLES - 5,000

CRACK GROWTH (mm) - 0.14

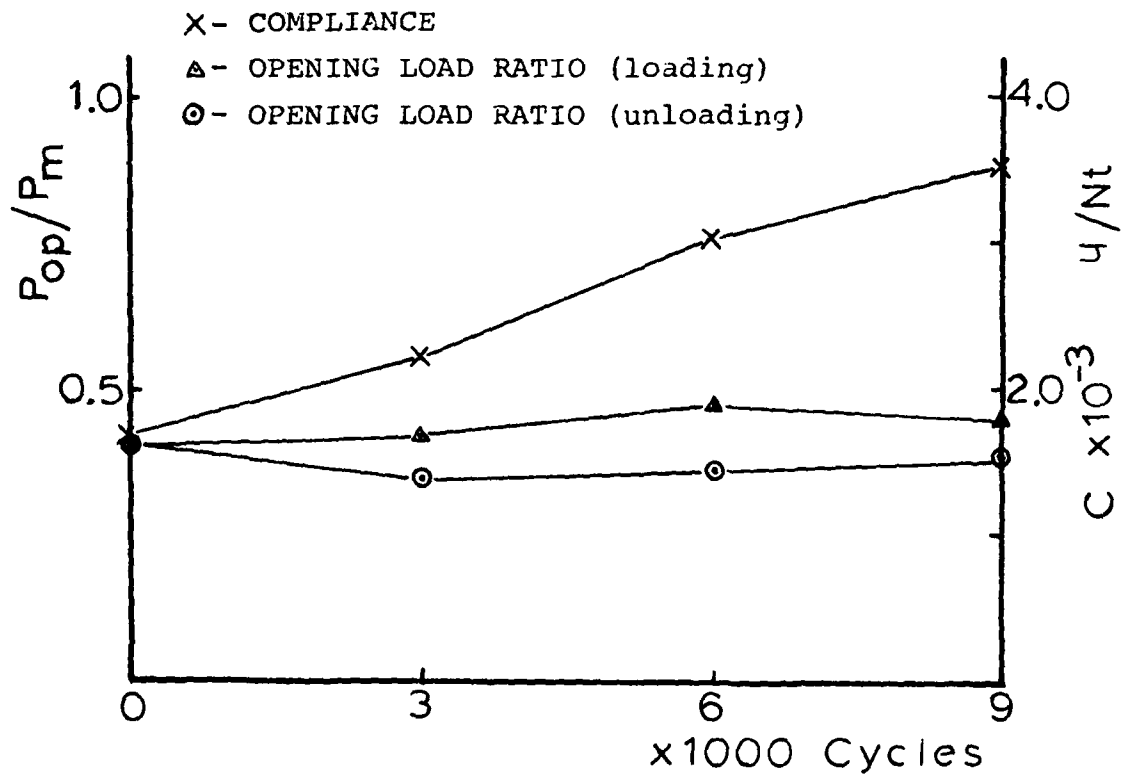


Figure 25. Information and data for Test 08083.

A11083

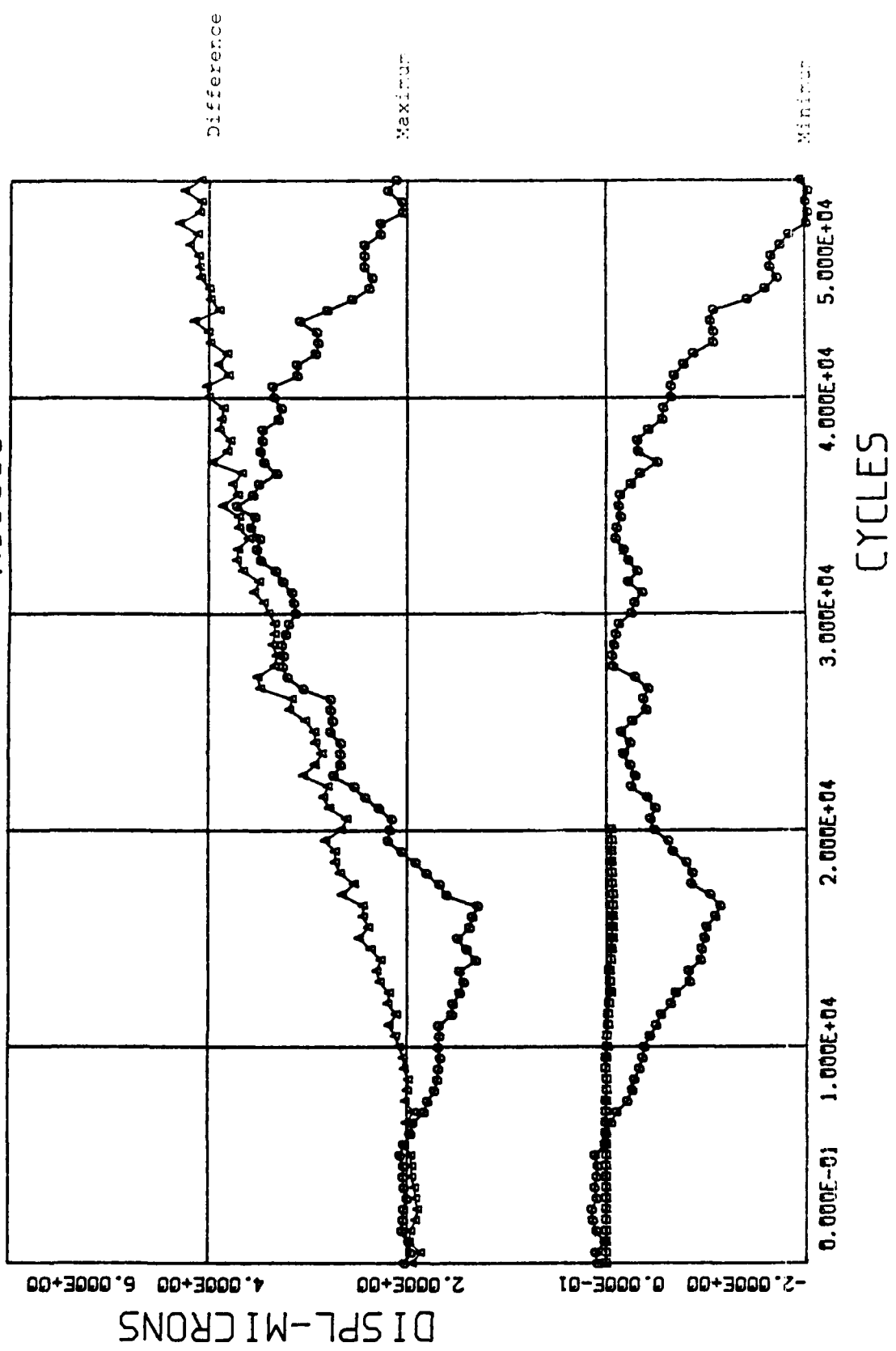


Figure 26. Crack opening displacements at minimum and maximum loads for Test 11083.

TEST NUMBER - 11083

$\Delta K$  (MPa-m<sup>1/2</sup>) - 11.0

TOTAL CYCLES (1000) - 50

AVERAGE CRACK GROWTH (mm) - 0.36

FINAL ROOM TEMPERATURE PRECRACKING

$\Delta K$  (MPa-m<sup>1/2</sup>) - 11.0

CYCLES - 65,000

CRACK GROWTH (mm) - 0.25

X - COMPLIANCE

Δ - OPENING LOAD RATIO (loading)

⊙ - OPENING LOAD RATIO (unloading)

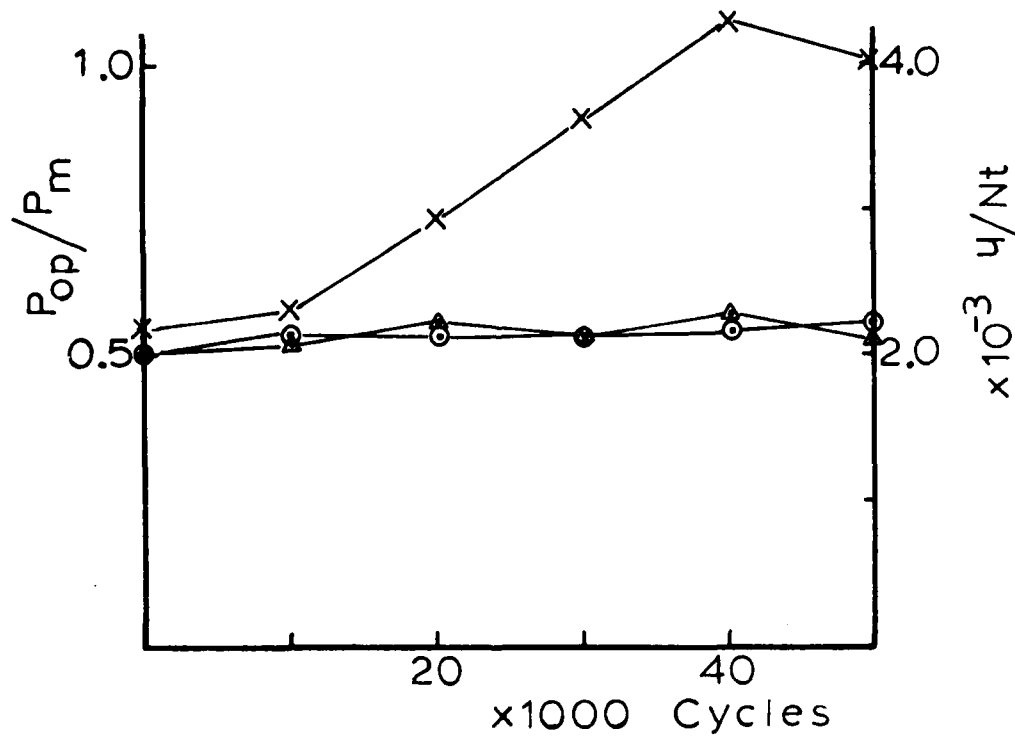


Figure 27. Information and data for Test 11083.

A12083

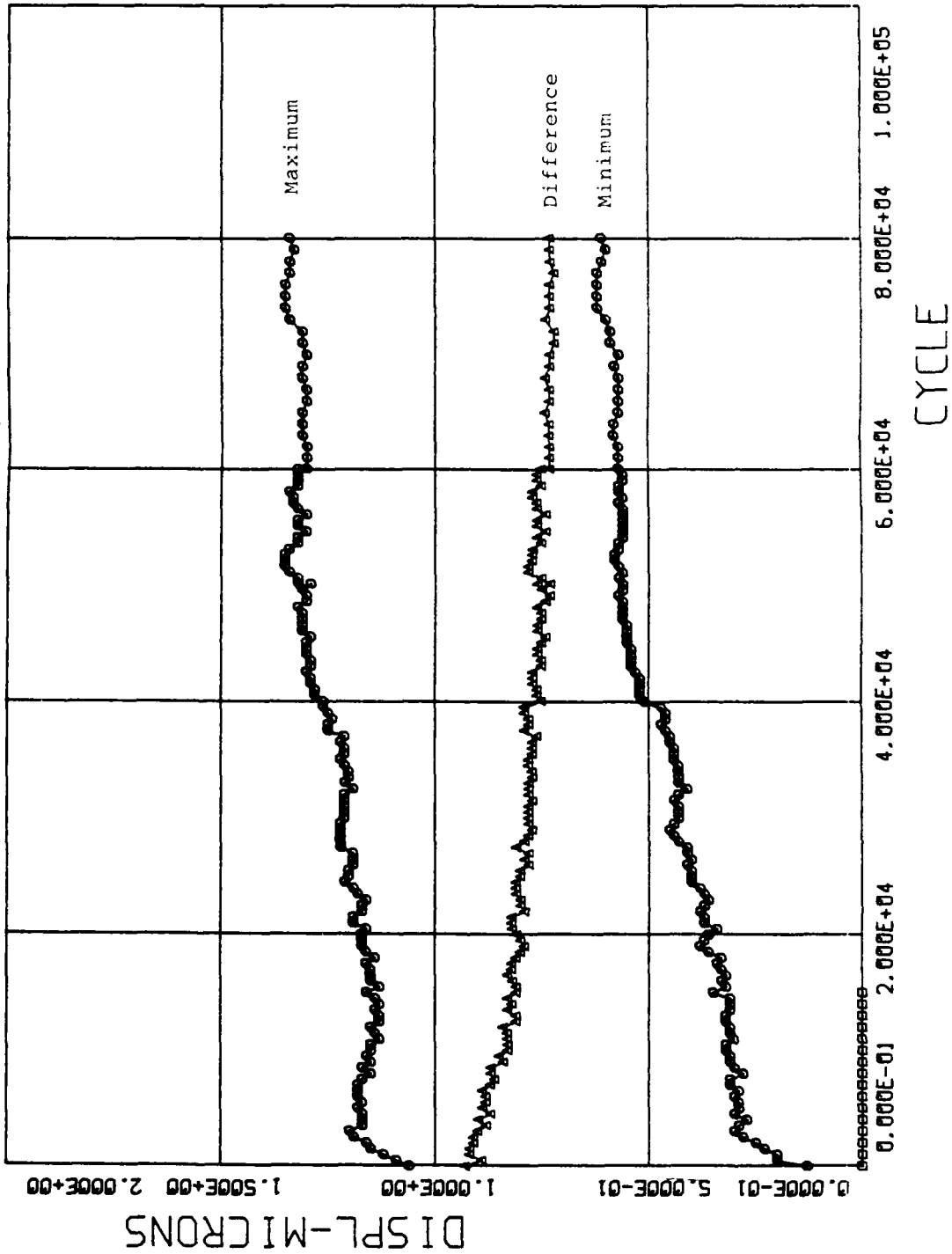


Figure 28. Creep crack opening displacement for Test 12083.

TEST NUMBER - 12083

$\Delta K$  (MPa-m<sup>1/2</sup>) - 11.0

TOTAL CYCLES (1000) - 80

AVERAGE CRACK GROWTH (mm) - 0.0

FINAL ROOM TEMPERATURE PRECRACKING

$\Delta K$  (MPa-m<sup>1/2</sup>) - 13.7

CYCLES - 20,000

CRACK GROWTH (mm) - 0.31

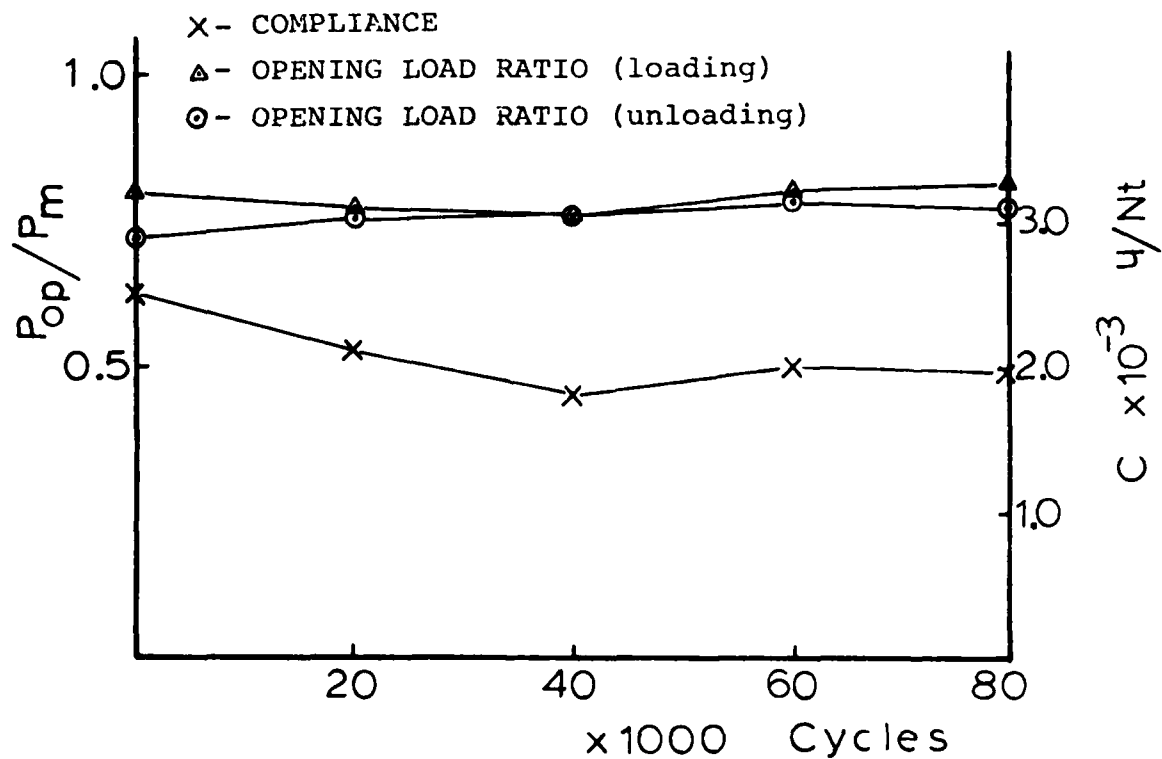


Figure 29. Information and data for Test 12083.

A16083

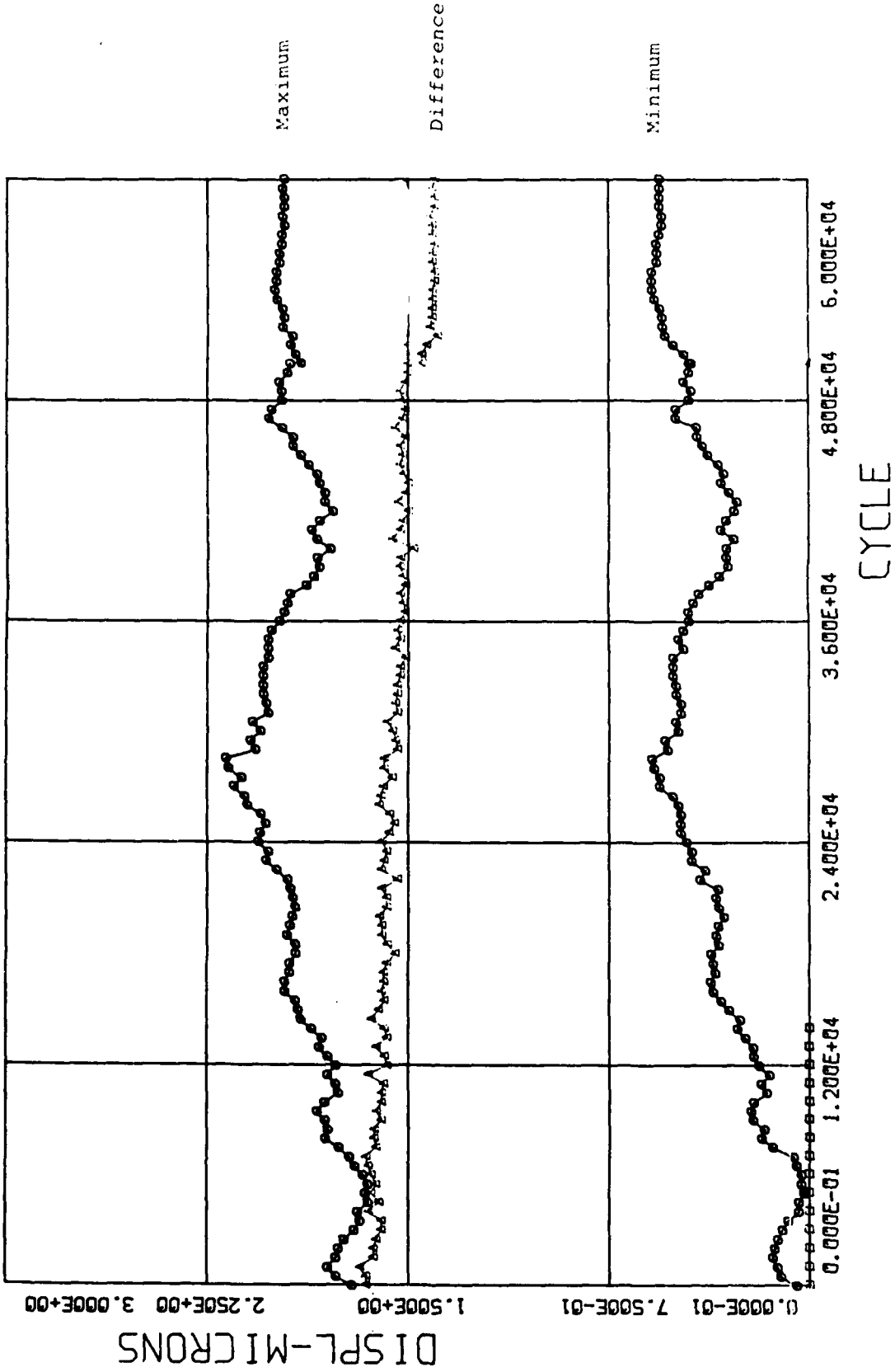


Figure 30. Crack opening displacement for Test 16003.

TEST NUMBER - 16083

$\Delta K$  (MPa-m<sup>1/2</sup>) - 11.0

TOTAL CYCLES (1000) - 60

AVERAGE CRACK GROWTH (mm) - 0.0

FINAL ROOM TEMPERATURE PRECRACKING

$\Delta K$  (MPa-m<sup>1/2</sup>) - 13.7

CYCLES - 110,000

CRACK GROWTH (mm) - 1.50

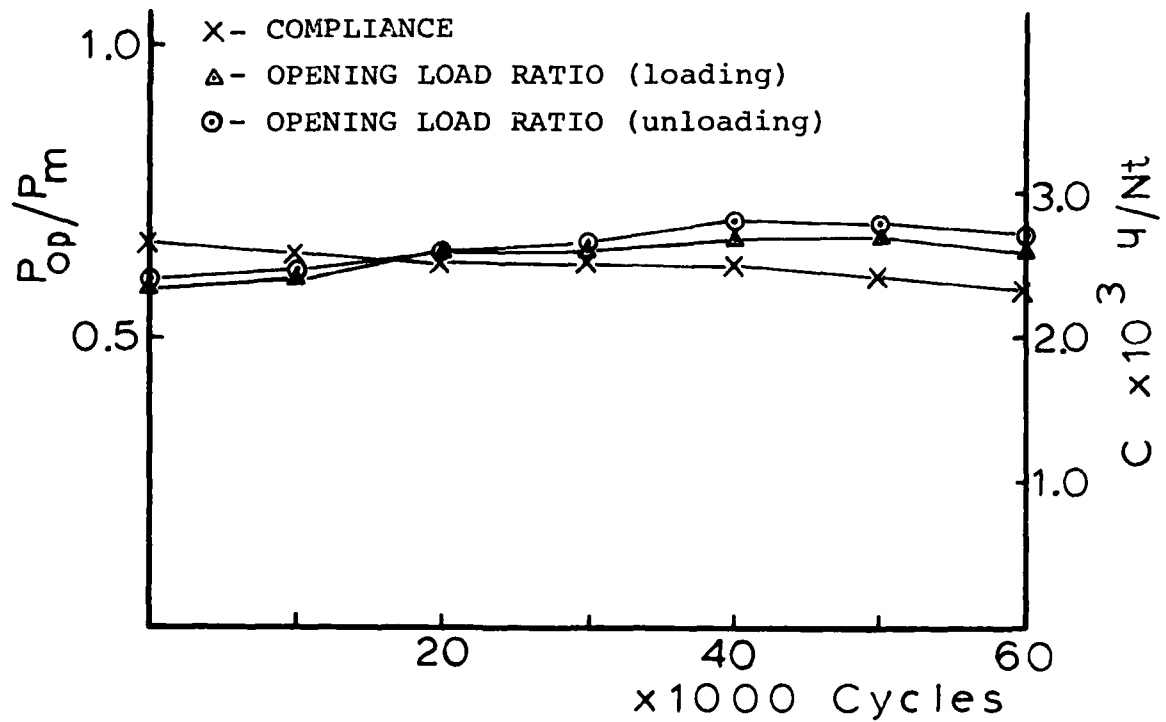


Figure 31. Information and data for Test 16003.



A09083

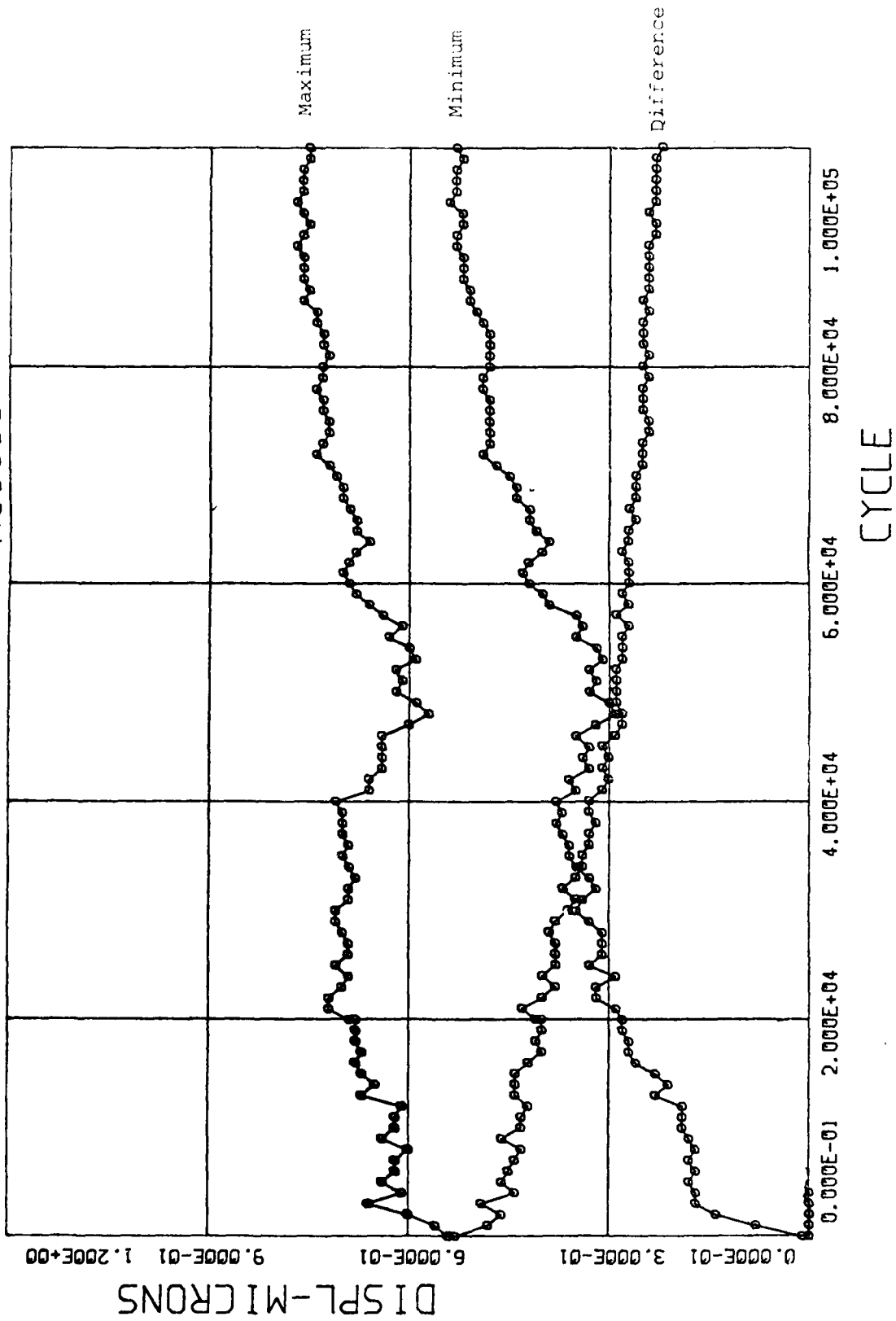


Figure 32. Crack opening displacement for Test 09083.

TEST NUMBER - 09083

$\Delta K$  (MPa-m<sup>1/2</sup>) - 8.8

TOTAL CYCLES (1000) - 80

AVERAGE CRACK GROWTH (mm) - 0.0

FINAL ROOM TEMPERATURE PRECRACKING

$\Delta K$  (MPa-m<sup>1/2</sup>) - 13.7

CYCLES - 65,000

CRACK GROWTH (mm) - 0.7

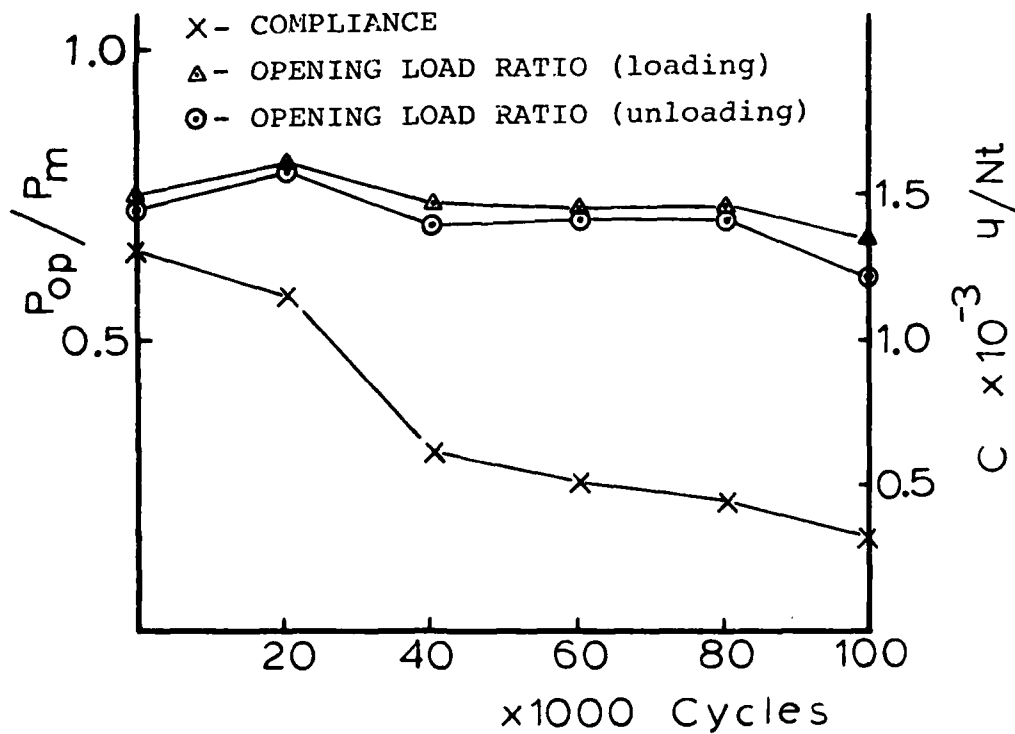


Figure 33. Information and data for Test 09083.

B17083

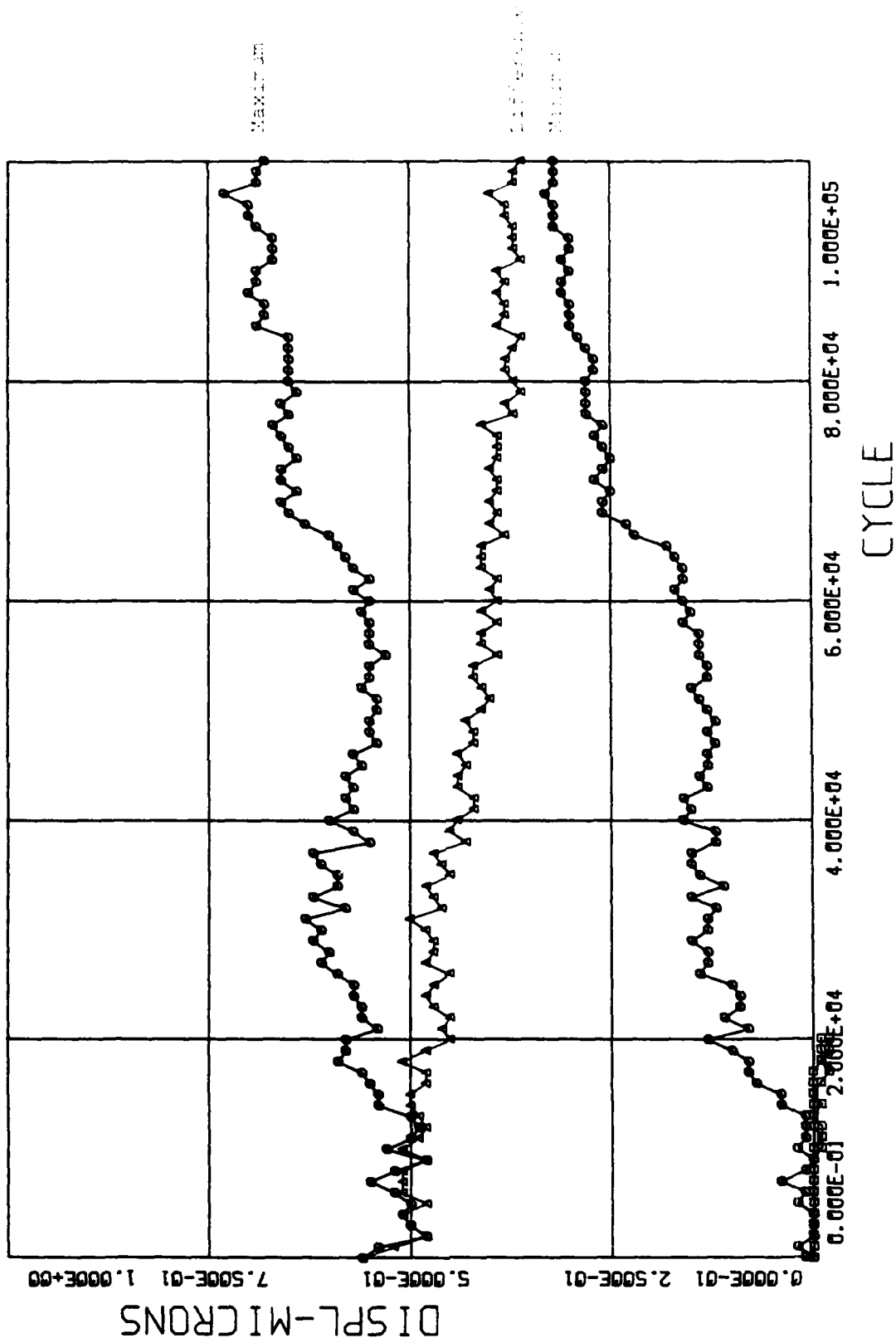


Figure 34. Crack opening displacement for Test 17083.

TEST NUMBER - 17083

$\Delta K$  (MPa-m<sup>1/2</sup>) - 8.8

TOTAL CYCLES (1000) - 100

AVERAGE CRACK GROWTH (mm) - 0.0

FINAL ROOM TEMPERATURE PRECRACKING

$\Delta K$  (MPa-m<sup>1/2</sup>) - 11.0

CYCLES - 80,000

CRACK GROWTH (mm) - 0.2

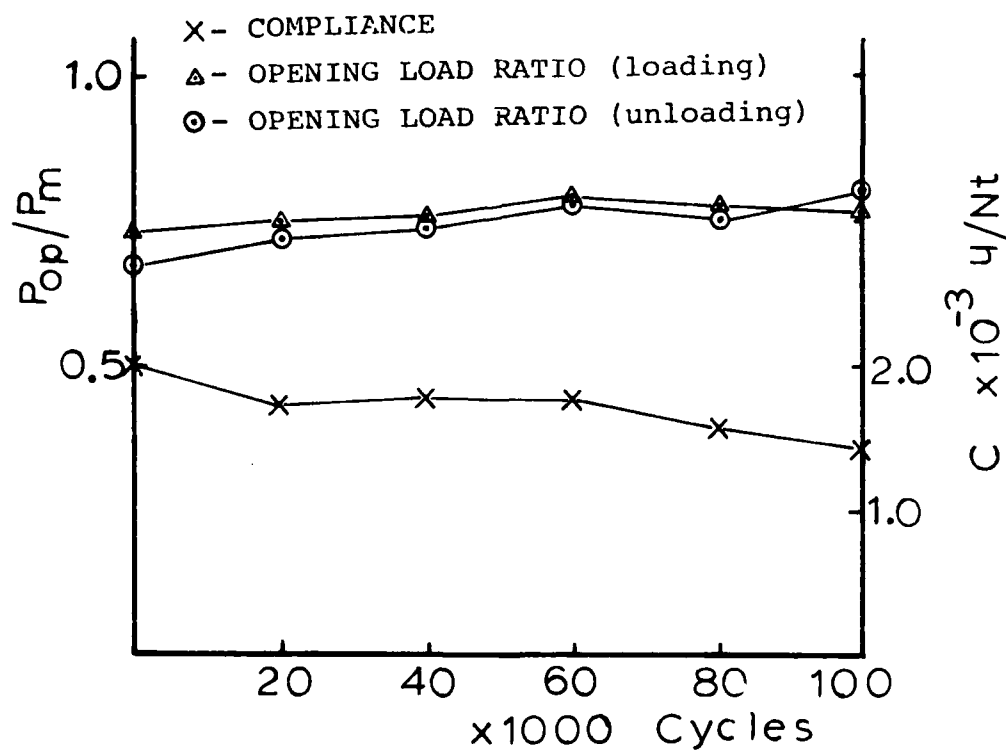


Figure 35. Information and data for Test 17083.

## Discussion

Table 5 shows inconsistencies in the crack growth data at  $\Delta K = 11.0 \text{ MPa}\cdot\text{m}^{1/2}$ . Three of the tests showed crack growth, and two did not. Results at higher and lower  $K_s$  were quite consistent. An examination of the precracking at room temperature offers an explanation. In those cases where the final precracking at room temperature was at  $\Delta K = 11.0 \text{ MPa}\cdot\text{m}^{1/2}$ , there was fatigue crack growth at 650C for  $\Delta K = 11.0 \text{ MPa}\cdot\text{m}^{1/2}$ . If the room temperature  $\Delta K$  was higher, there was no growth at 650C. It was impractical to precrack the specimens for the  $\Delta K = 8.8 \text{ MPa}\cdot\text{m}^{1/2}$  experiments at the same value at room temperature; the cracks simply would not grow. This strong dependence of high temperature behavior on room temperature precracking must be recognized in establishing threshold values.

If a crack grew under fatigue loading at 650C, the crack opening displacement (COD) at minimum load tended to decrease with cycling, and the difference tended to increase. Conversely, if the crack did not grow, the COD at minimum load tended to increase and the difference decrease. There is no ready explanation for this, but one must remember that very small displacements are being measured on the surface. If the crack doesn't grow, it is plausible to expect the crack surfaces to accumulate an oxide film which would possibly increase the COD at minimum load. If the crack grows, the situation is more complicated because the crack tip is moving away from the indents. This should lead to an increase in the minimum COD, but it doesn't.

The unexpected variations in absolute values of COD naturally lead one to question the stability of the measurement system, but Figure 26 shows the ISDG to be quite stable. The observed COD variations are apparently real physical behavior.

Examination of the odd-numbered figures 25-35 shows the compliance to stay more-or-less constant or decrease if there is no growth and to increase if there is growth. The compliances don't agree very well with those predicted (see Table 6) as was true for the creep experiments. The same reasons probably apply, namely three-dimensional effects and lack of perfectly straight crack.

The data recording and analysis procedures make establishment of the opening load easy. It stays more-or-less constant whether the crack grows or not. Unless the opening load ratio is greater than 0.5, there is no crack growth. Supposedly; then one could ascertain

whether or not the crack would grow by simply running one cycle of loading. Note that these results apply to measurements of COD very near the crack tip; a different ratio would likely be obtained at more remote locations.

### Conclusions

The ISDG works quite well for fatigue COD measurements. The automated system with regular interruptions for single cycle measurements makes testing quite easy. It is a very stable system, and one can decide whether or not a crack will grow with only a few kilocycles of testing. Furthermore, the extensive load-COD data can be used to study crack tip behavior.

The fatigue threshold for Inconel 718 at 650C is approximately  $11 \text{ MPa}\cdot\text{m}^{1/2}$ . Establishment of this value is highly dependent on the precracking procedure at room temperature.

## SECTION VI

### COD MEASUREMENTS AWAY FROM TIP

Both the creep and fatigue experiments show inconsistent agreement between calculated and measured compliances. These differences were attributed to three-dimensional effects which are very important when COD is measured very close to the crack tip. Presumably better agreement would be obtained if the COD was measured further away. Two additional experiments were run at a low and a high  $\Delta K$  to examine the effect of measurement location.

Note that as one moves back from the crack tip, the COD becomes larger, and this limits the response time of the ISDG. Finer load increments must be taken so that the fringes do not move too much between scans. Some of the single cycles load the specimen to less than the maximum load in fatigue.

#### Results and Discussion for $\Delta K = 8.8 \text{ MPa-m}^{1/2}$

A new specimen, Number 7-032, was precracked at room temperature with the final increment of crack growth, 0.45 mm, being at a  $\Delta K$  of  $11.0 \text{ MPa-m}^{1/2}$ . Figure 36 is a diagram of the crack obtained from measurements after the specimen was broken open. The curvature is typical of the cracks in the specimens used in the preceding section of fatigue threshold measurements. There was no growth at this low  $\Delta K$ , as expected. The locations of the COD measurement positions are also given as distances behind the surface crack tip on side B. Measurements were made at room temperature, Test 18123, and 650C, Test 19123.

Figure 37 shows the load-displacement at various locations behind the crack tip at room temperature. The opening load, i.e. the load above which the load-displacement becomes linear, is clearly dependent upon the measurement position. It becomes independent of position far enough away from the tip; this is consistent with the results of Macha, et al (18).

Load-displacement plots at two positions at room temperature and 650C are shown at Figure 38. The change in slope at high temperature is of course explained by the change in elastic modulus. The opening load ratio decreases at high temperature; the reduced stiffness of the surrounding specimen material may explain this. It is also possible that there is some thermal stress relief of the residual stresses behind the crack tip. Note that the maximum load at 650C was not up to the  $\Delta K$  of  $8.8 \text{ MPa-m}^{1/2}$  ;

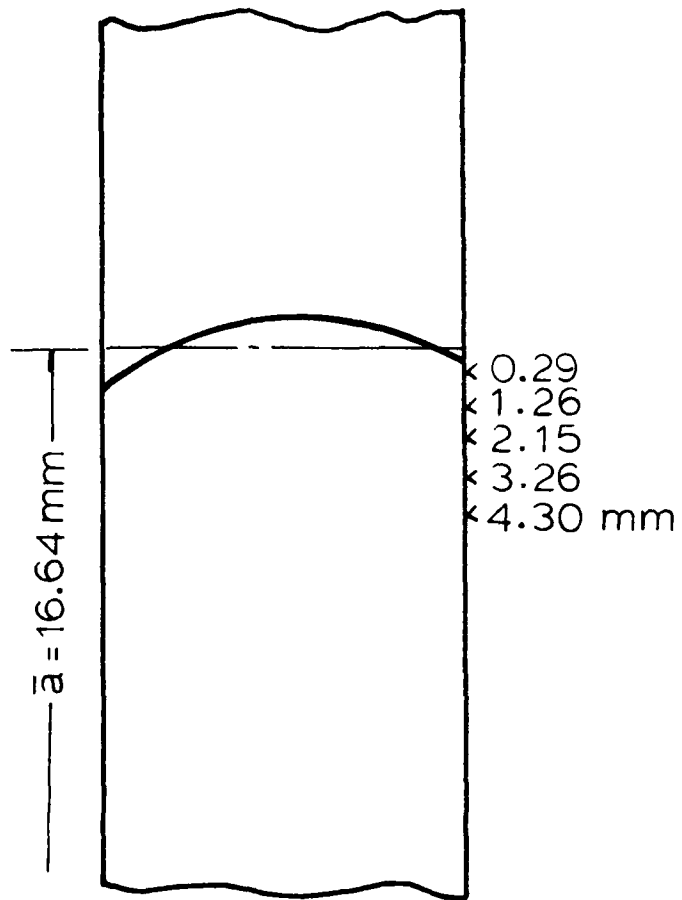


Figure 36. Schematic of crack for Tests 18123 and 19123.



A18123

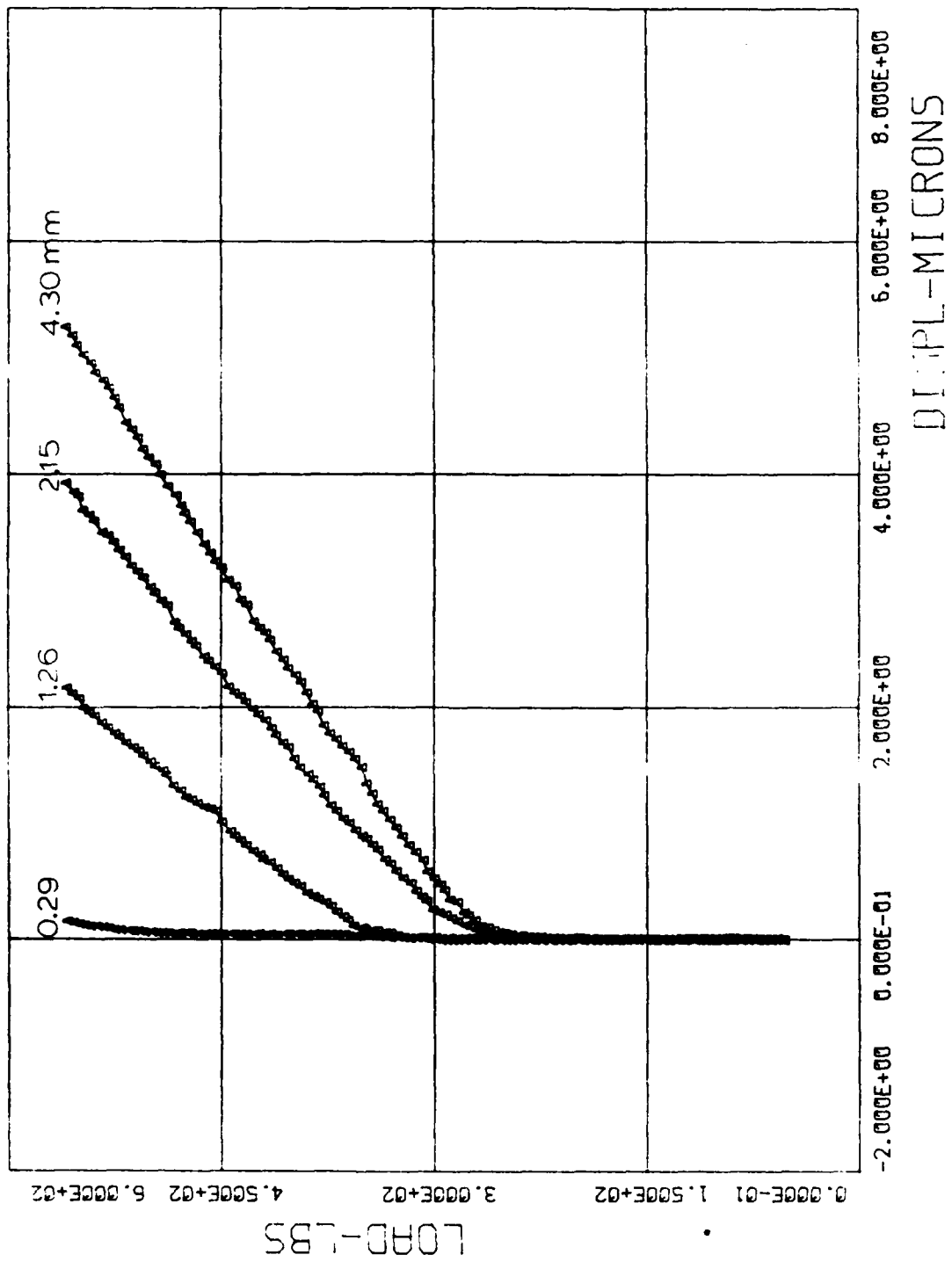


Figure 37. Load-displacement plots at various positions behind the crack tip.

C19123

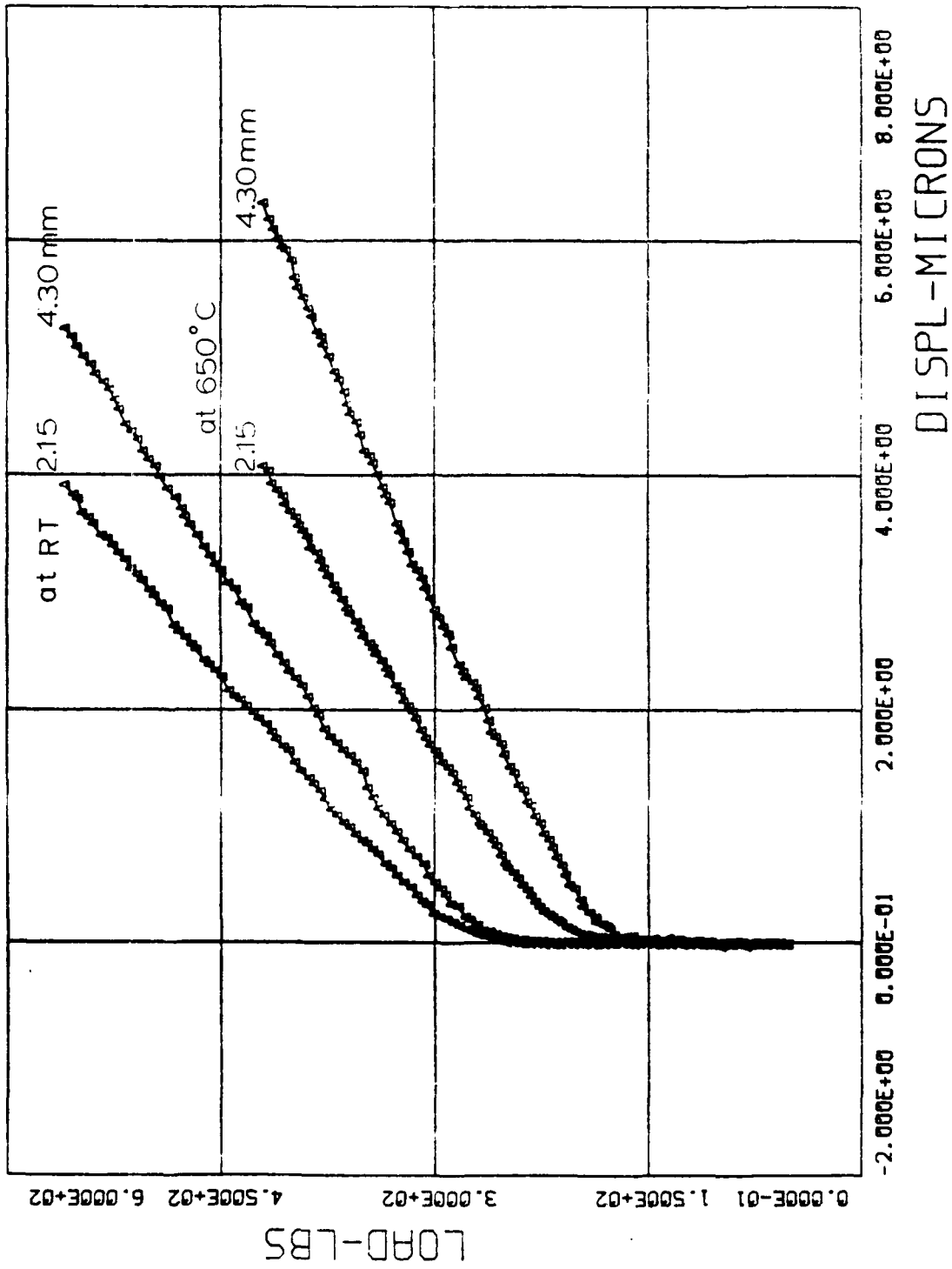


Figure 38. Load-displacement plots at two positions at 100 and 650C.

these load cycles were taken before the final fatigue testing at 650C.

It was desired to run a very long test at  $\Delta K = 8.8$  MPa- $m^{1/2}$  in order to verify that there was no crack growth at this SIF range. Figure 39 shows the minimum and maximum COD and their difference for 480,000 cycles. That test ran 6 hours and 45 minutes. These CODs were measured at the position 3.26 mm behind the crack tip and do not show a decrease in the difference as did the earlier experiments with measurements closer to the tip. However, the absolute values of COD did increase with cycling.

Figure 40 plots selected single cycles during test 19123. There is some sharpening of the "knee" of the curve, but the slopes and the opening load ratios remain essentially the same. Figures 39 and 40 show that there should be no crack growth, and the final examination after the specimen was broken open confirm that fact.

Table 7 summarizes comparisons between calculated (following reference 12) and measured compliances. Elastic modulus of  $213 \times 10^3$  MPa and  $160 \times 10^3$  MPa were used in the calculations. There is actually better agreement at high temperature than at room temperature. However, if one looks back at Figure 36 and speculates on the 3-D effects and consequences of slight misalignments in loading, it is surprising that the agreement is as good as it is. The perfect agreement of Figure 11 was obtained for COD measurements 2 mm further back from the tip.

#### Results and Discussion for $\Delta K = 16.5$ MPa- $m^{1/2}$

Specimen 7-032 was then precracked at room temperature with the final increment being 0.36 mm at  $\Delta K = 16.5$  MPa- $m^{1/2}$ .

Figure 41 shows the initial and final cracks and the COD measurement positions.

These fatigue loads were fairly high, and rapid growth was expected. The first few loading cycles were of particular interest, and complete load-displacement measurements were made for the first 20 cycles. Figure 42 shows the first and twentieth cycles. These were to a load equivalent to  $K = 16.5$  MPa- $m^{1/2}$ , and the first cycle was the first time the specimen had experienced that maximum load at 650C. There is some increase in the minimum load COD on the first cycle; this increase becomes smaller as the specimen is cycled. The CODs of Figure 42 were measured at the 0.30 mm position behind the surface tip. Earlier experiments had shown the minimum load COD change on the

J19123

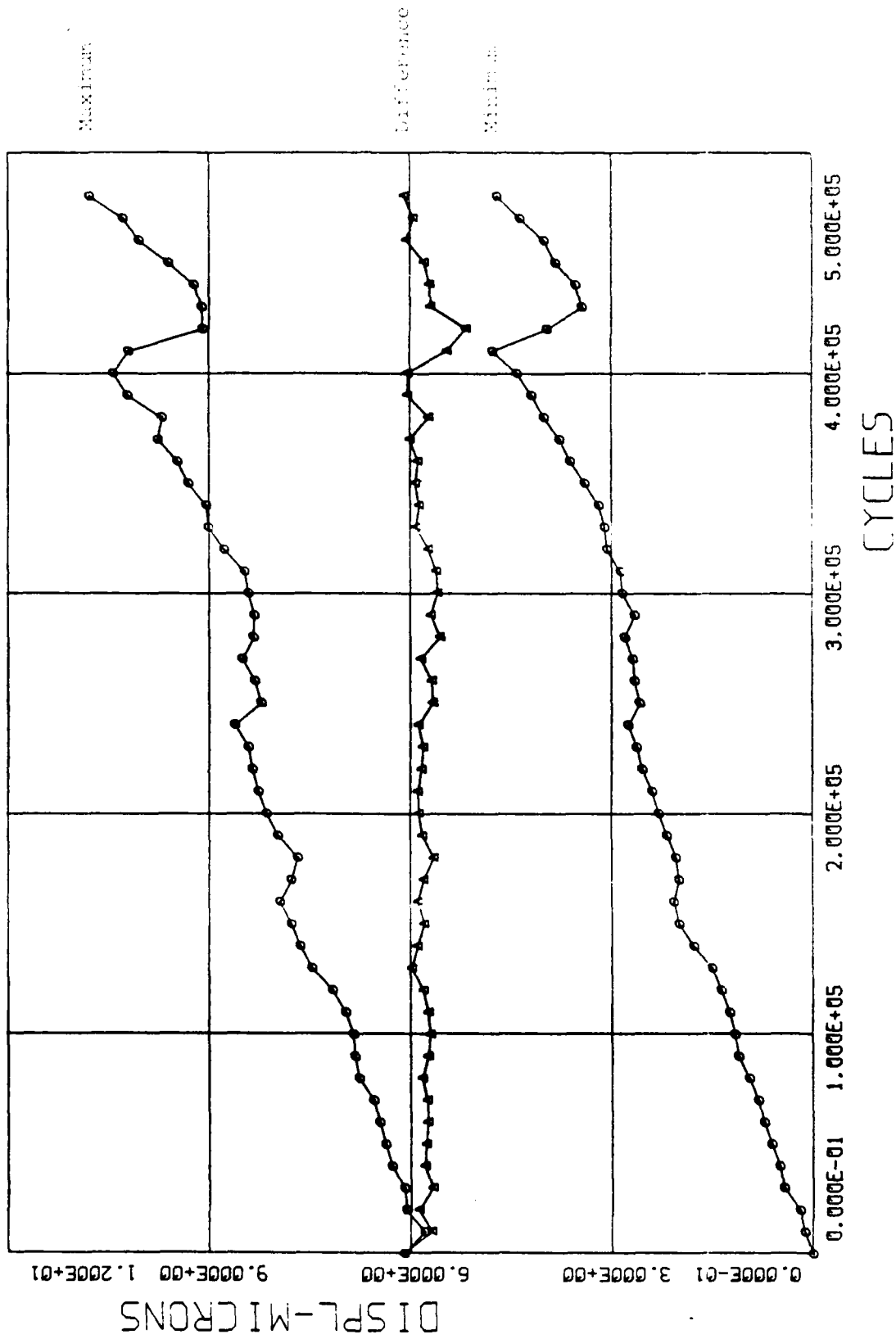


Figure 39. Crack opening displacements and their difference for Test J19123.

J19123

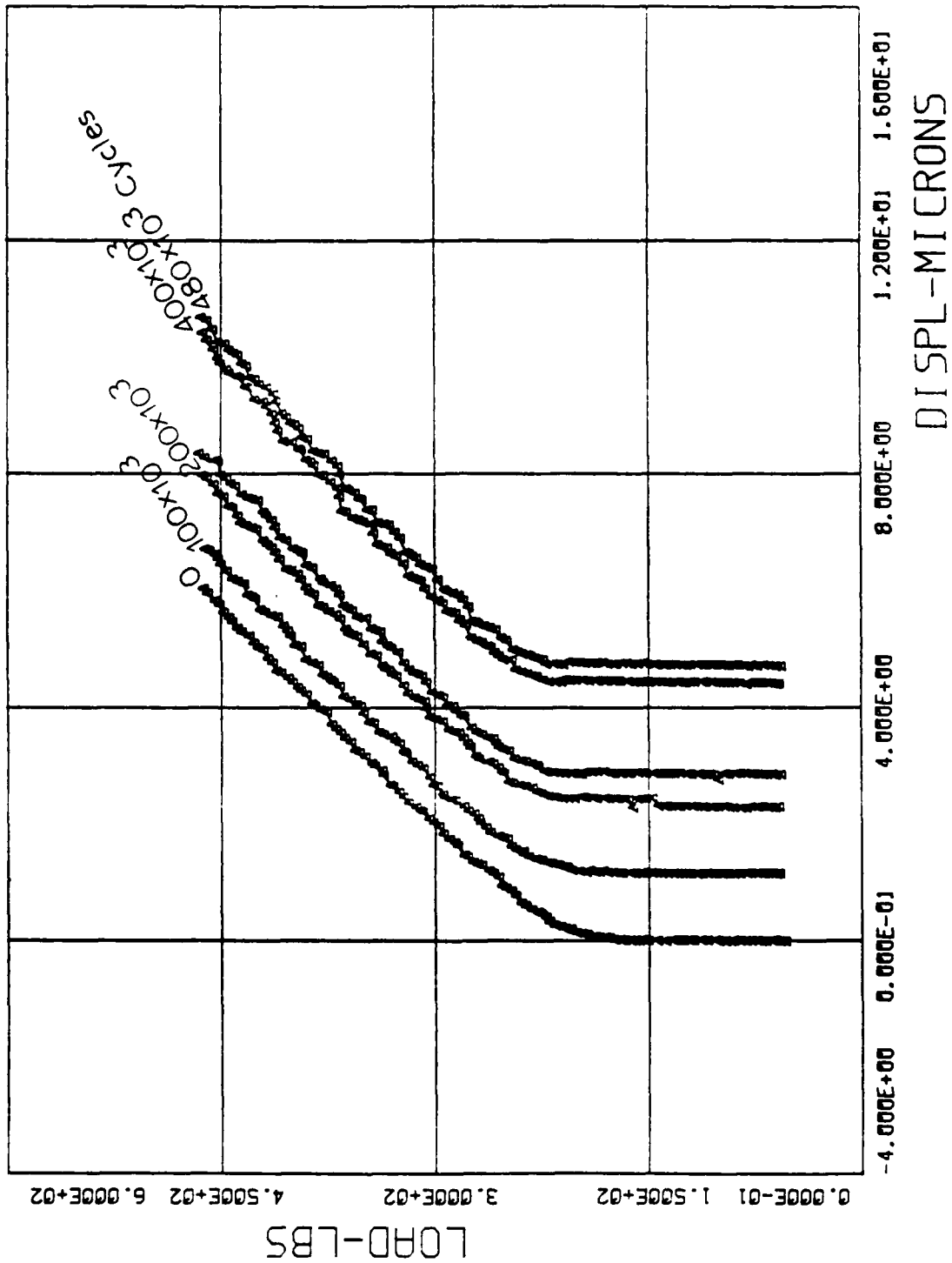


Figure 40. Single cycle load-displacement plots at various cycles for Test 19123.

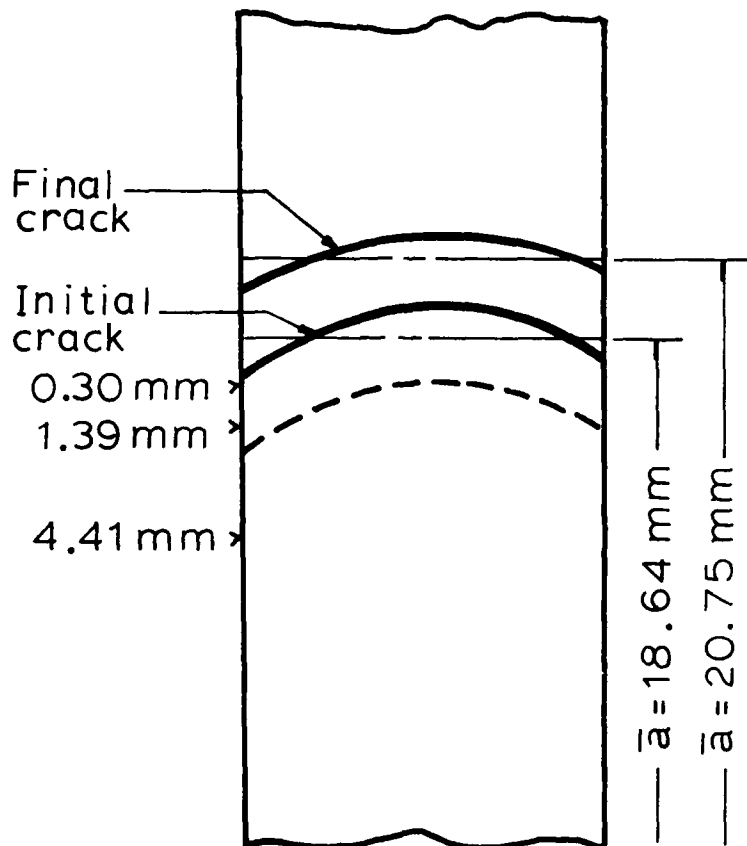


Figure 41. Schematic of the cracks before and after Test 21123.

D21123

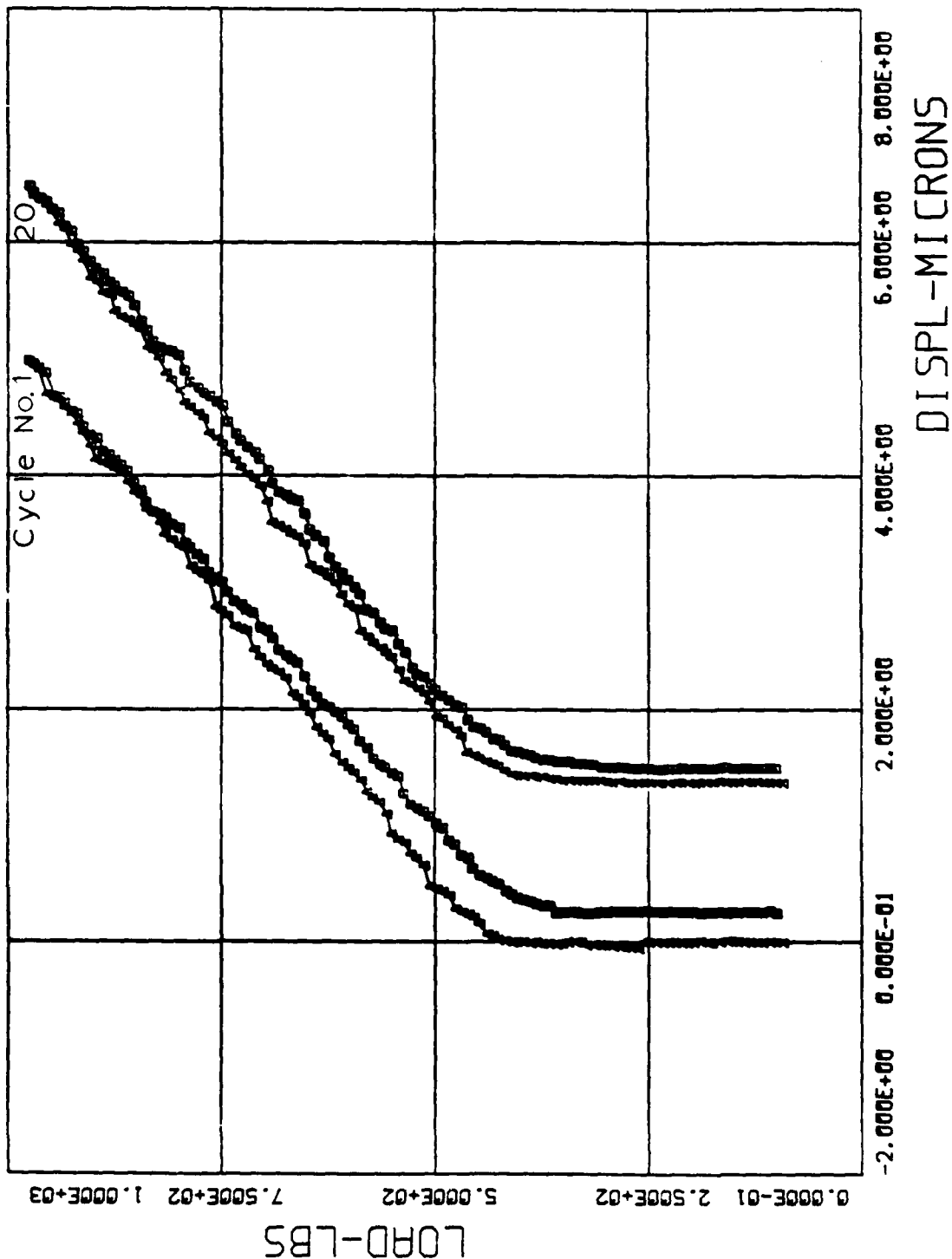


Figure 42. First and twentieth cycles of Test 21123.

TABLE 7

## COMPLIANCES MEASURED AWAY FROM THE CRACK TIP

Indents Location mm behind tip	Compliance at 200°		Compliance at 650°	
	$10^{-2}$ $\mu\text{m}/\text{Nt}$		$10^{-2}$ $\mu\text{m}/\text{Nt}$	
	Calculated	Measured	Calculated	Measured
1.26	1.24	1.02	1.66	1.53
2.15	1.48	1.42	1.98	1.98
3.26	1.78	1.58	2.38	2.37
4.30	2.04	1.84	2.72	2.80

first cycle, but no difference for later cycles. It appears that this change occurs fairly early and dies out. It may indicate that the crack grows (or blunts) more in the first few cycles than in subsequent ones.

Figure 43 shows the incremental COD measured at the 4.41 mm position. This loading was started after the initial 20 cycles, so it re-starts at the minimum load COD equal to zero. Also, these single cycle measurements did not load the specimen to the maximum  $\Delta K$ . These results are consistent with earlier ones.

Load-displacement for selected cycles during test 21123 are shown in Figure 44; all measured at the 4.41 mm position. The change in slope of the upper portion as well as the decrease in opening load ratio is evident. This measurement position is far enough behind the crack tip (originally at 4.41 mm and finally at 6.32 mm) that the opening load ratio should be independent of position. The decreasing ratio may be the effect of growing away from the residual plastic zone left by the room temperature precracking.

Table 8 compares the measured and calculated compliances - all at 650° - for the initial and final cracks. The agreement isn't as good as for Test 19123, but note that the load-displacement curves are not as straight in the upper region. The crack grew 1.91 mm (from an average initial value of 18.84 mm to a final average of 20.75 mm) in 25,000 cycles. This was a 10% change in crack length; whereas the measured compliances changed 65% at 4.41 mm and 154% at 1.39 mm. If one were able to divide the compliance<sub>2</sub> changes into 50 parts (i.e. resolve compliance to  $0.05 \times 10^{-2}$   $\mu\text{m}/\text{Nt}$ ), then one could resolve increments of crack growth of 0.04 mm. This resolution is reasonable with the ISDG.



E21123

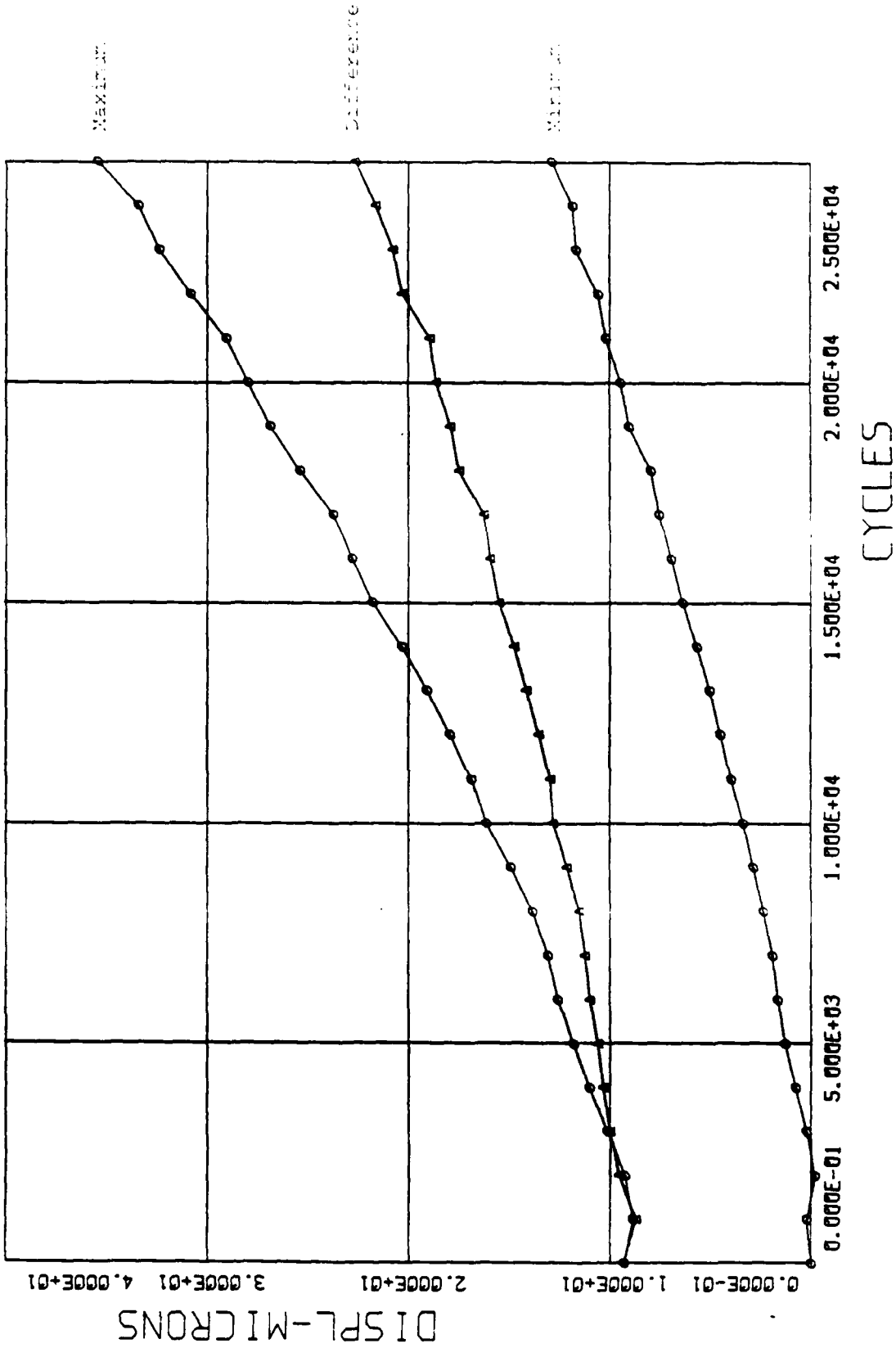
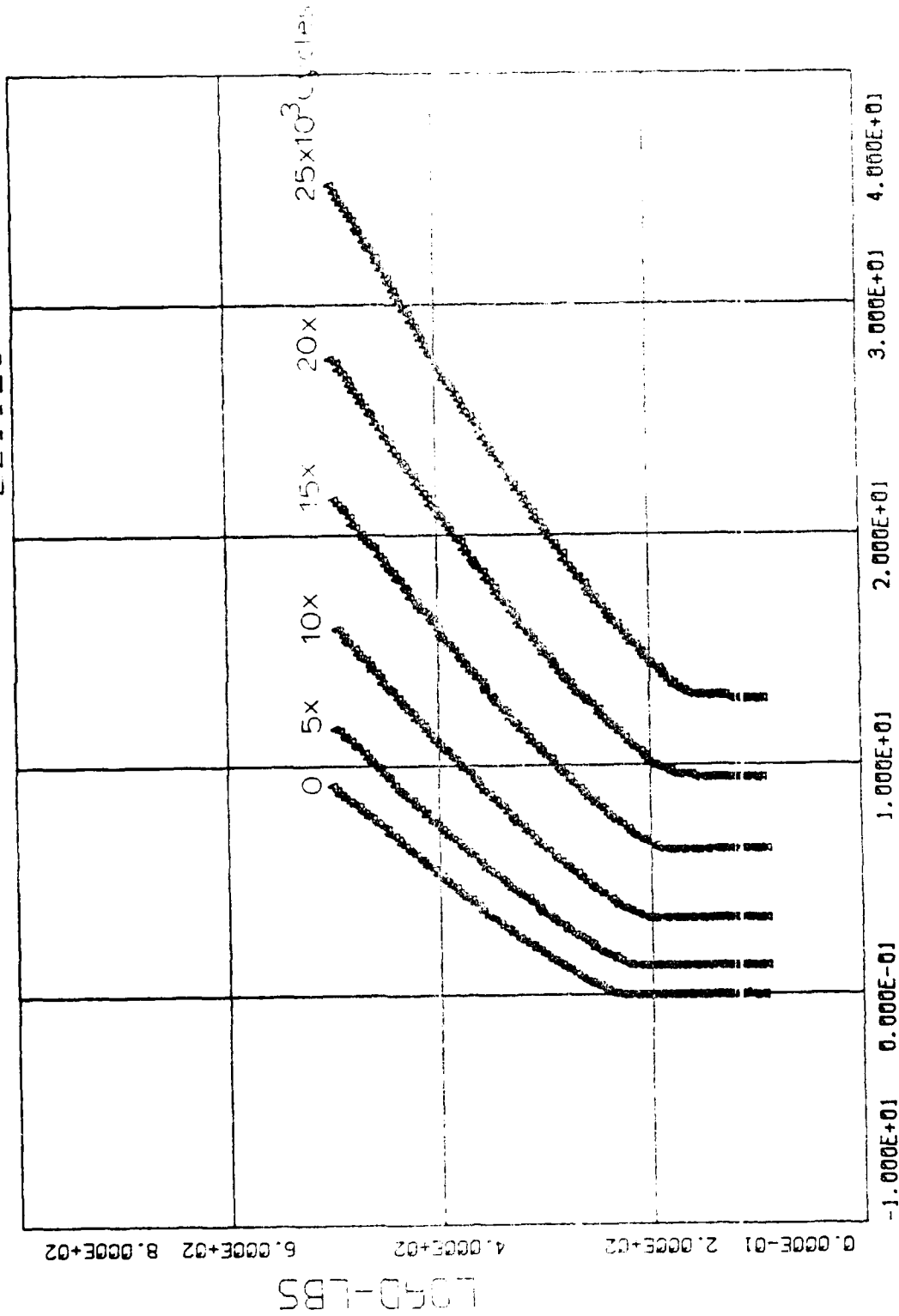


Figure 43. Crack opening displacements measured 4.41 mm behind tip and their difference for Test 21123.

E21123



DISPL-MICRONS

Figure 44. Load-displacements for selected single cycles of test 21123.

TABLE 8

INITIAL AND FINAL COMPLIANCES MEASURED AWAY  
FROM THE CRACK TIP

Indents: Location mm behind tip initially	Initial Compliance		Final Compliance	
	$10^{-2}$ $\mu\text{m}/\text{Nt}$		$10^{-2}$ $\mu\text{m}/\text{Nt}$	
	Calculated	Measured	Calculated	Measured
1.39	2.20	1.59	3.39	4.04
4.41	3.47	3.76	4.91	6.20

## SECTION VII

## CONCLUSIONS

The ISDG is quite stable for even long term measurements. There was no drift in a test of 500,000 cycles lasting 6 hours and 45 minutes. That test, conducted at  $\Delta K = 8.8 \text{ MPa}\cdot\text{m}^{1/2}$ , showed no crack growth, little change in the single cycle load-displacements, and no change in the incremental COD.

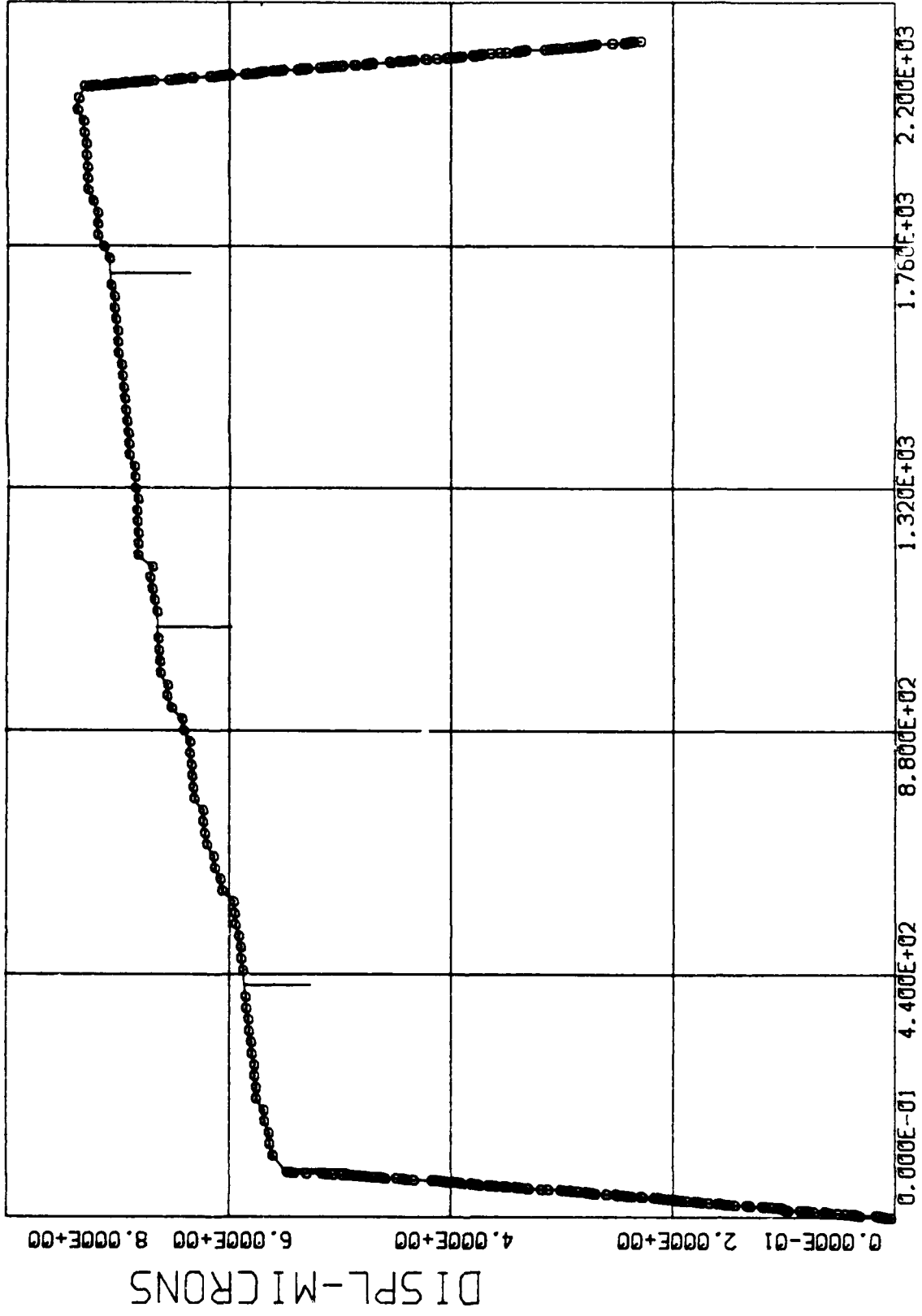
Compliances measured further away from the crack tip give better agreement with calculated values. In other words, they are a more reliable measure of crack position. This is true in spite of the fact that COD measurements are made at distances from the crack tip that are less than one-half of the specimen width and the crack front is curved. Since the crack is curved, there is some question as to what the crack length really is.

Even if the compliance measurements don't accurately locate the absolute position of the crack, changes in compliance can resolve crack growth increments of 0.04 mm. The ISDG system can do this on an automatic, non-contacting basis at 650C.

APPENDIX A  
CREEP TEST RESULTS

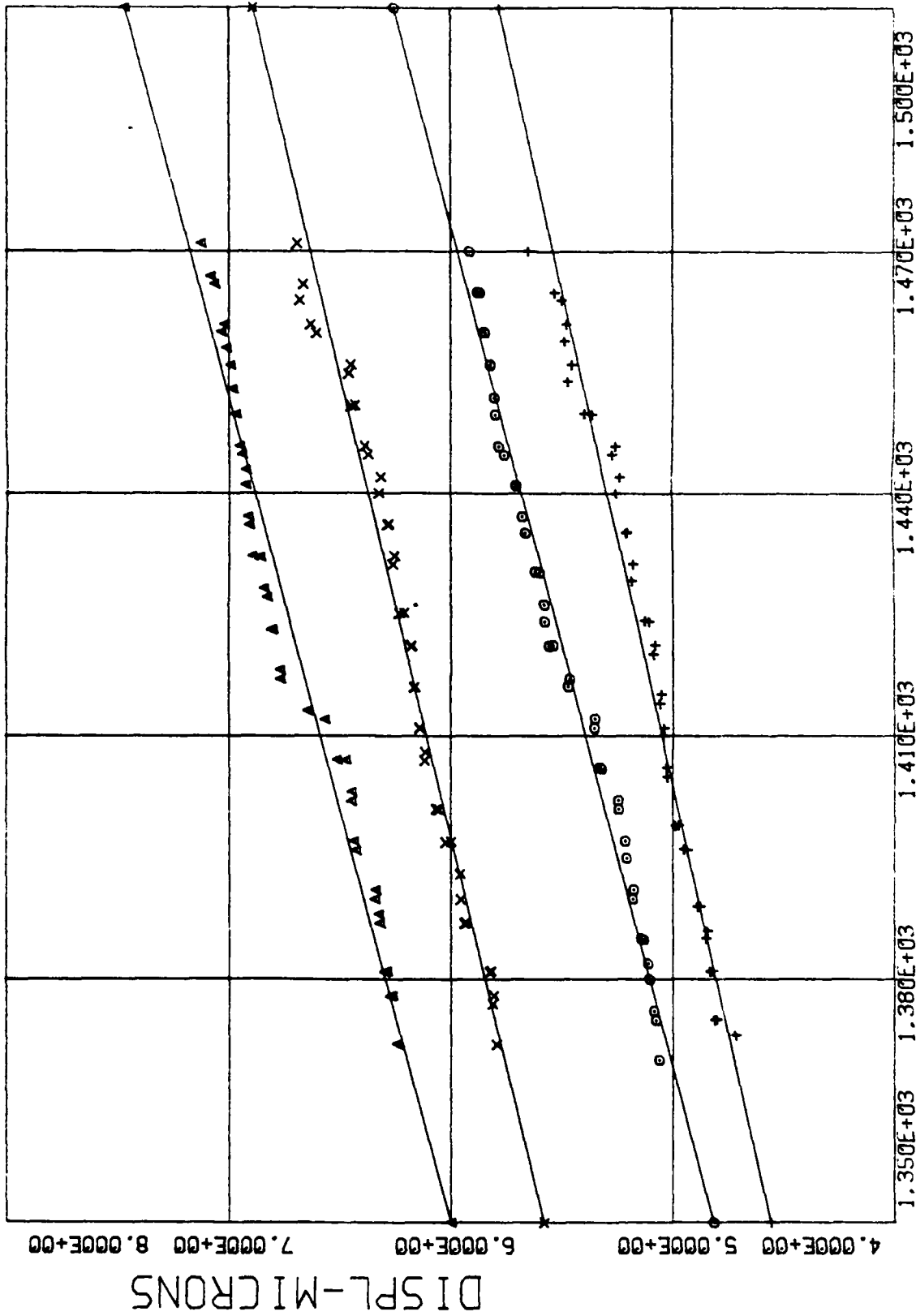
Creep displacement and compliance results for the 9 creep tests.  
See Table 1, page 28, for details on loading, crack lengths, and indentation  
locations.

A10092



TIME--SEC.

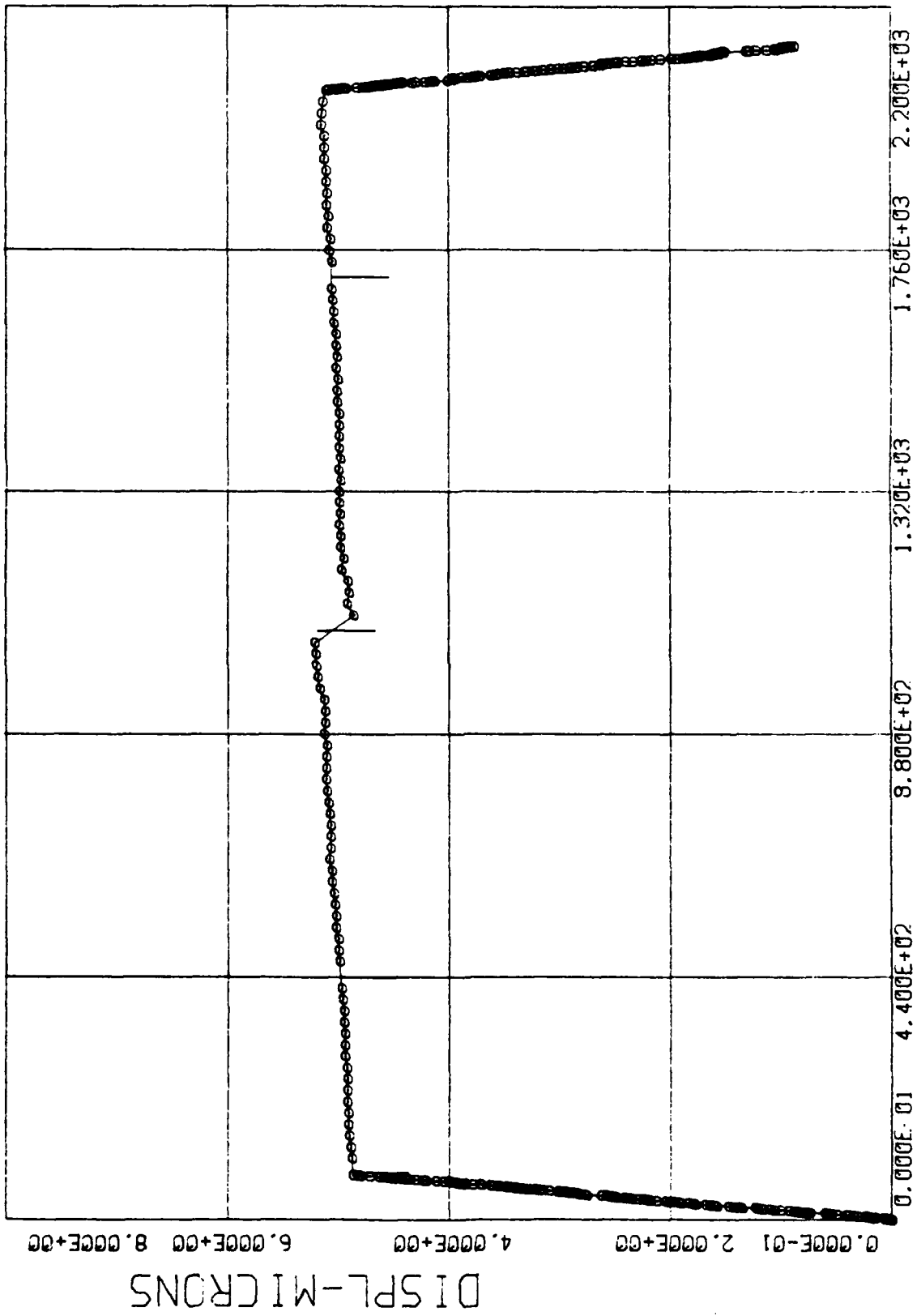
B10092



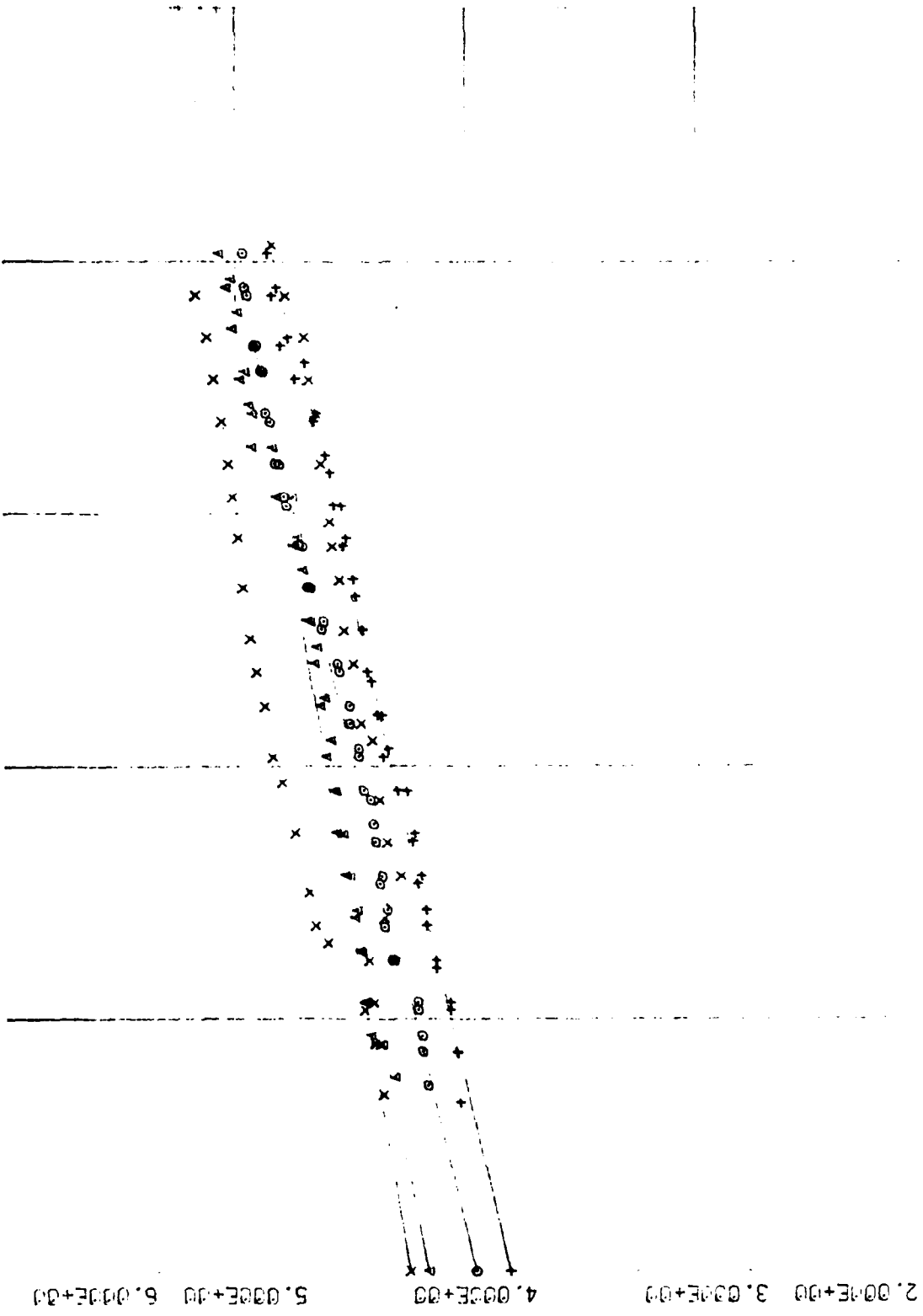
LOAD-LBS

DISPL-MICRONS

A13092



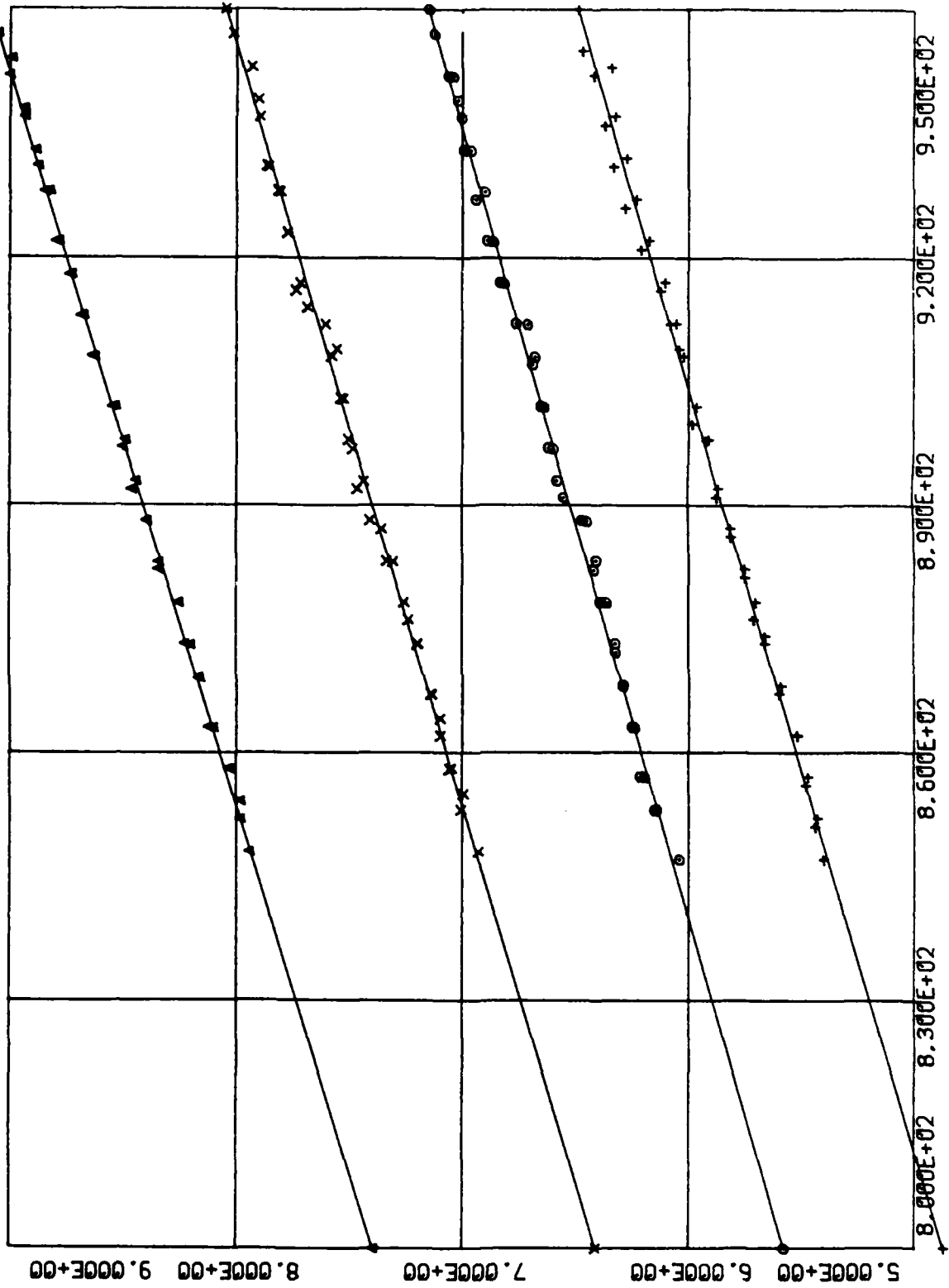
013792



DI PRL-RI ENVA



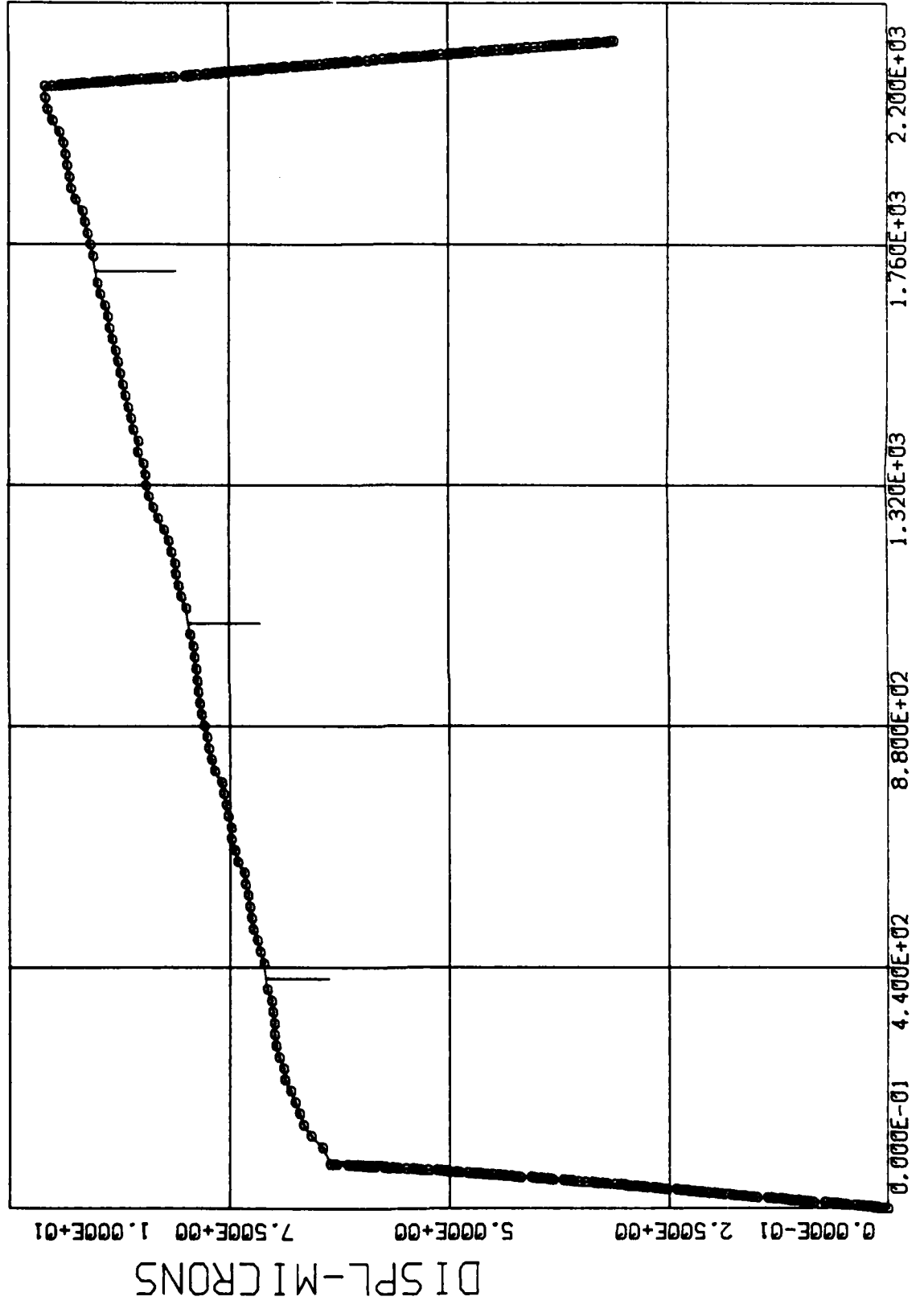
B16092



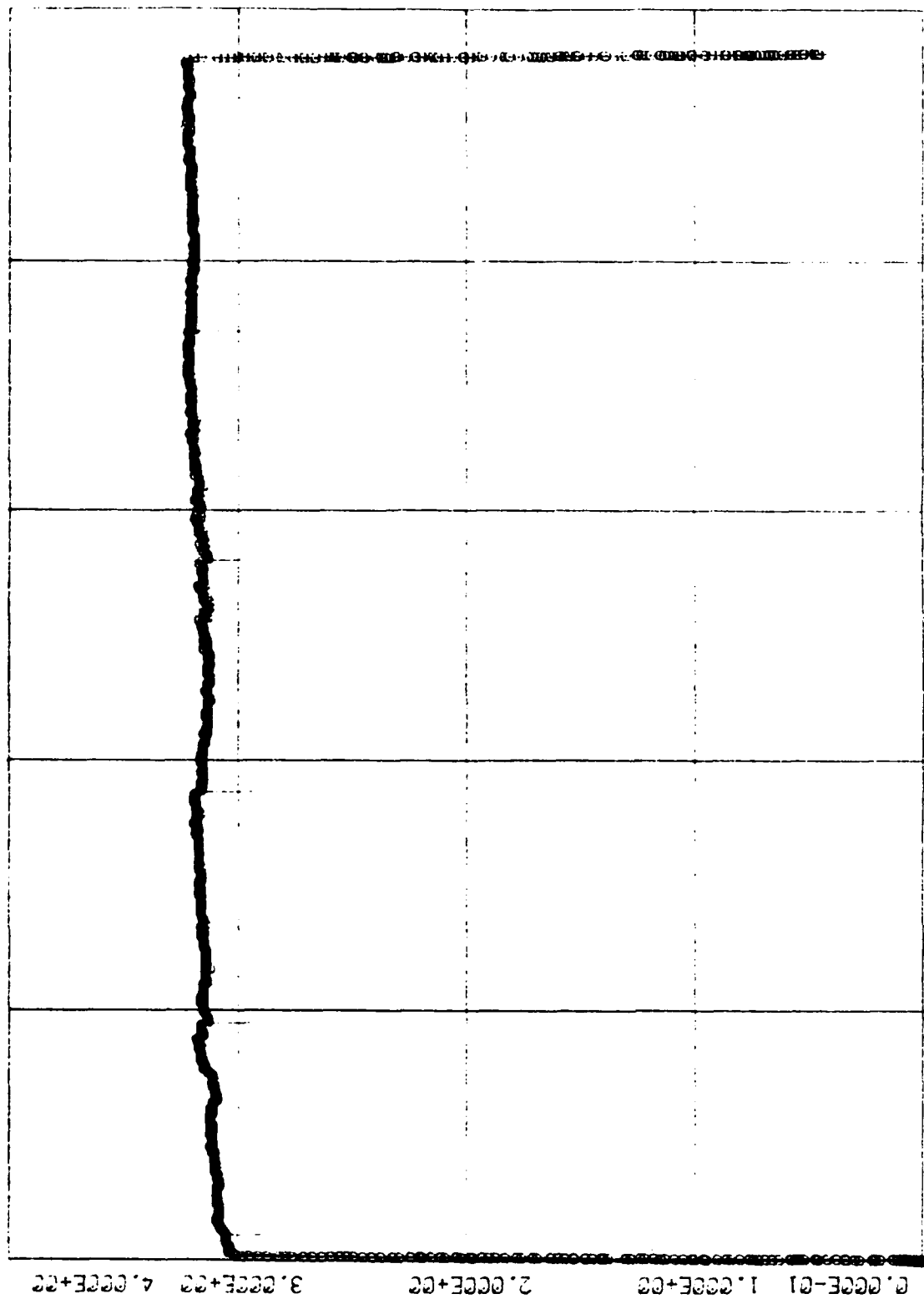
LOAD-LBS

DI SPL-MICRONS

A16092



C17092

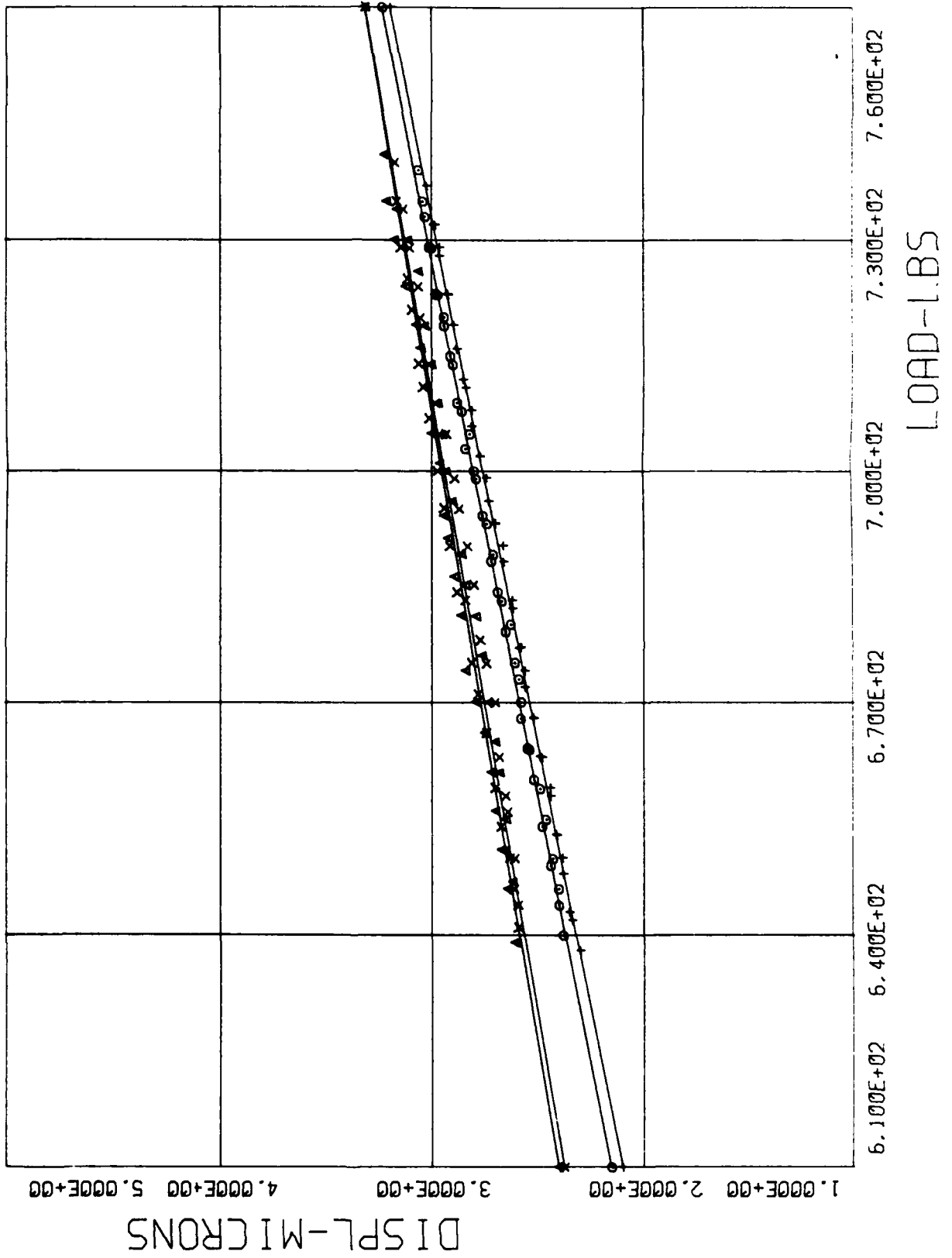


DISPL-MI (RMS)

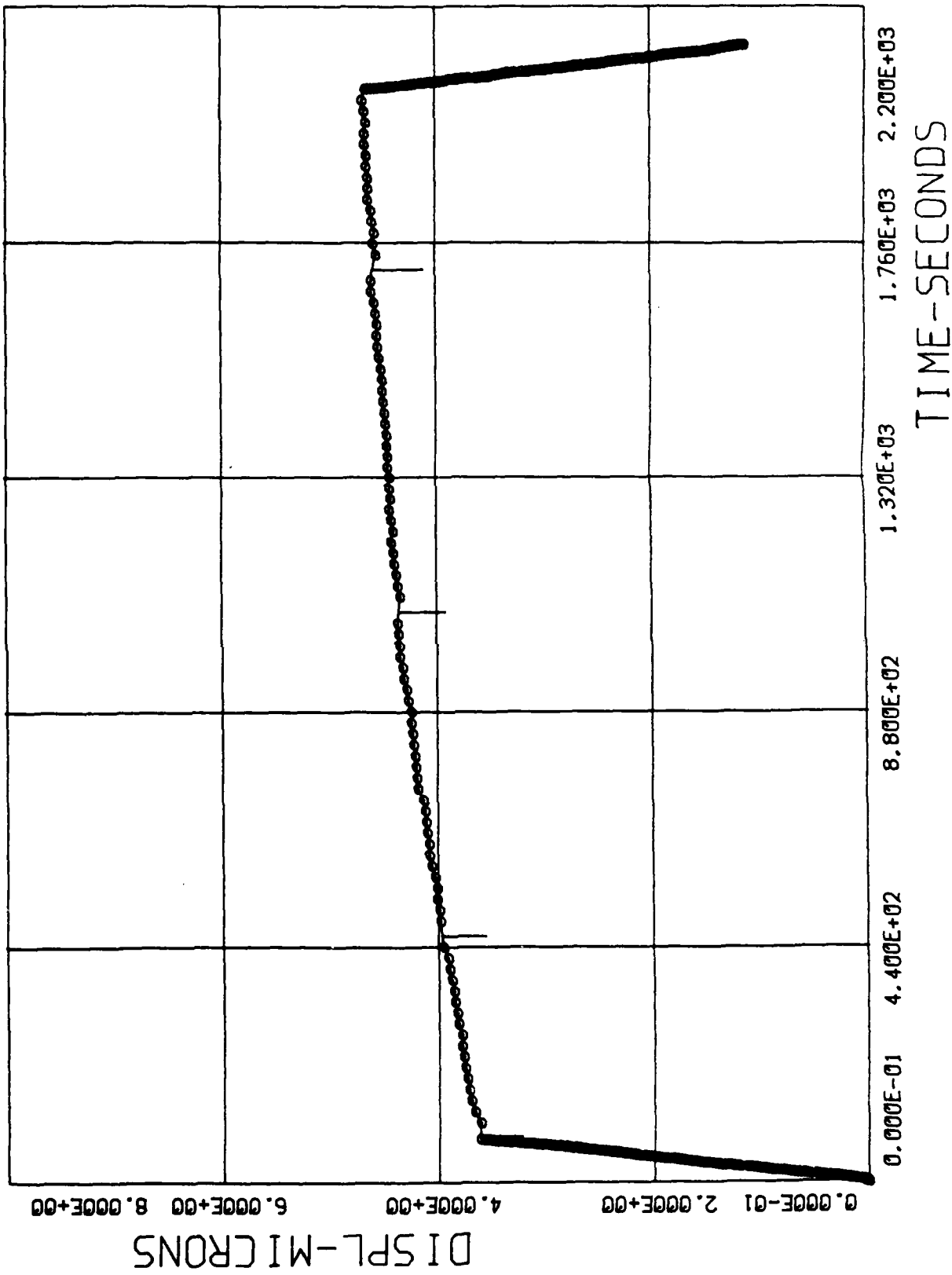
0.000E+00 4.000E+03 8.000E+03 1.200E+04 1.600E+04 2.000E+04

TIME-SEC

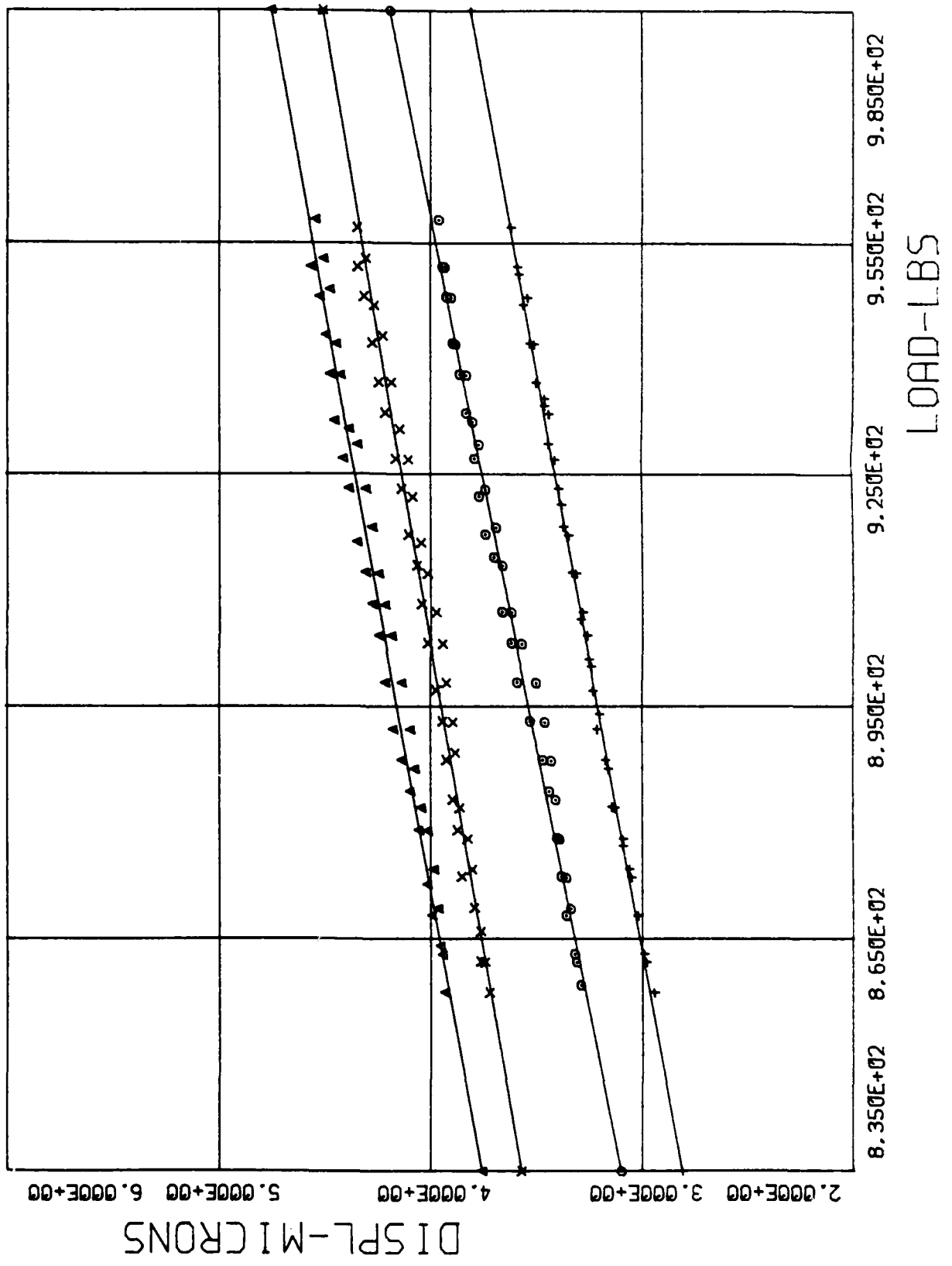
D17092



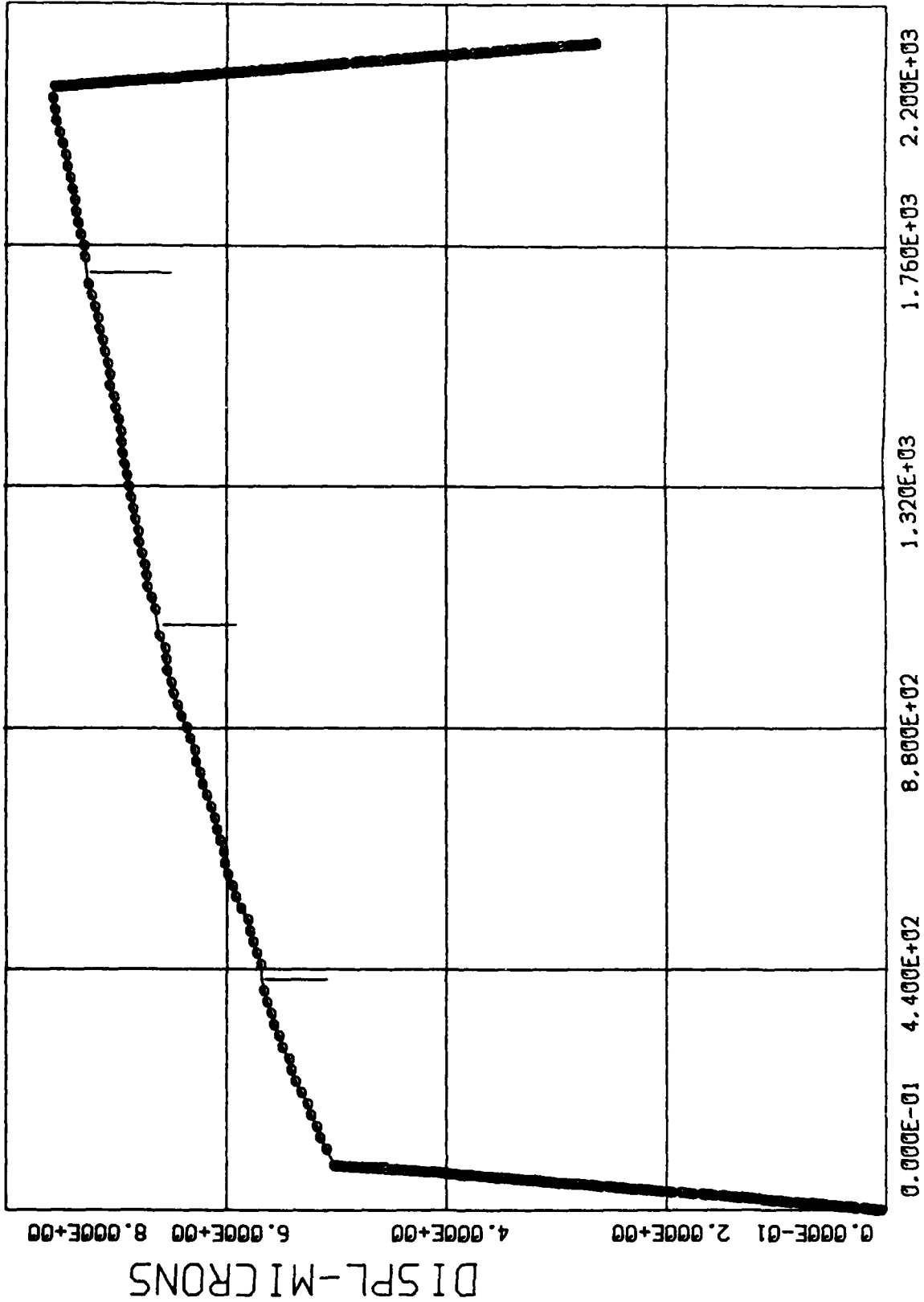
A20092



B20092



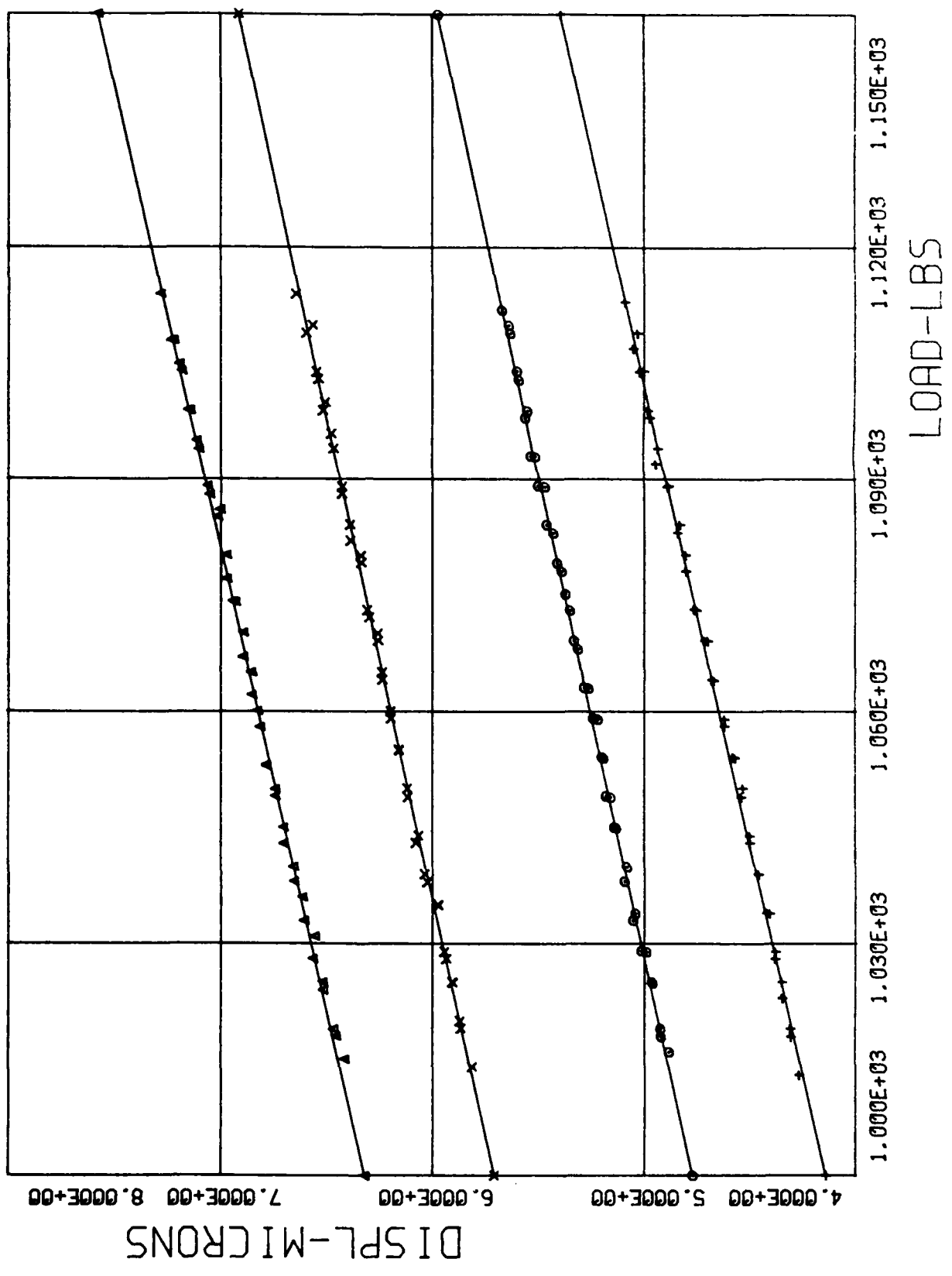
A21092



DISPL-MICRONS

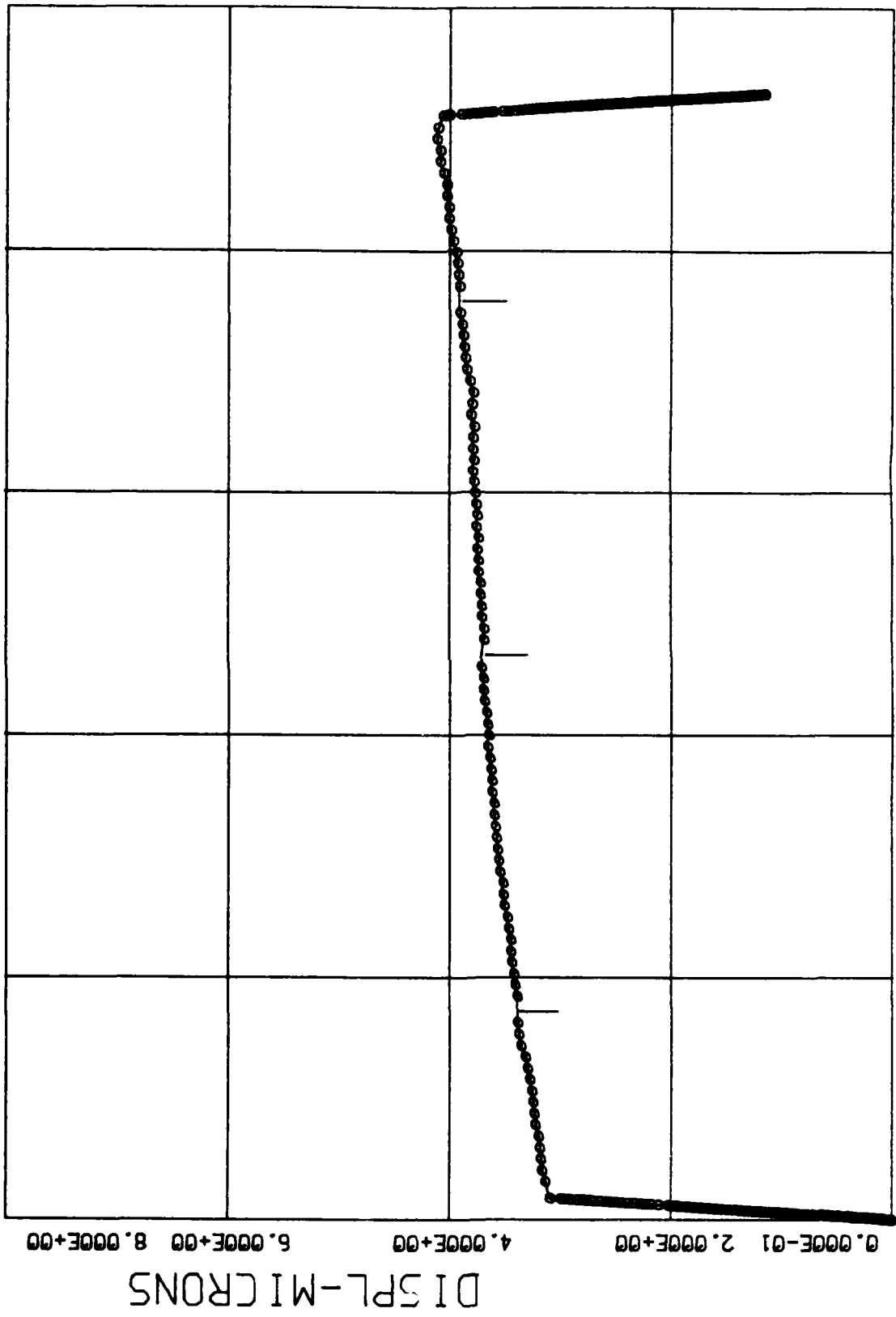
TIME-SEC

B21092





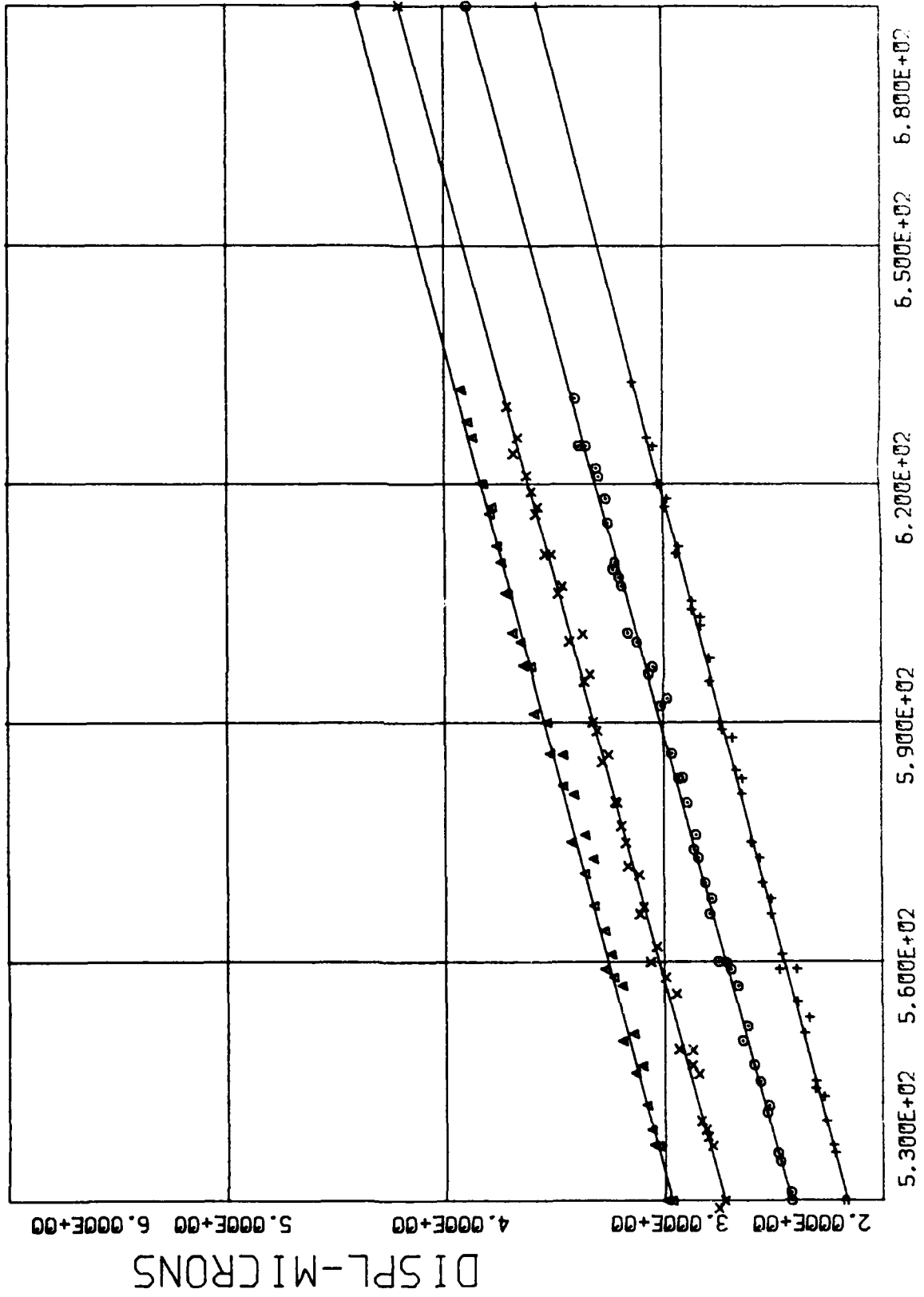
A22092



0.000E-01 4.400E+02 8.800E+02 1.320E+03 1.760E+03 2.200E+03

DISPL-MICRONS

B22092



LOAD-LBS

DISPL-MICRONS

AD-A142 675

A NEW OPTICAL TECHNIQUE FOR RAPID DETERMINATION OF  
CREEP AND FATIGUE THRE. (U) JOHNS HOPKINS UNIV  
BALTIMORE MD W N SHARPE APR 84 AFWAL-TR-84-4028

2/2

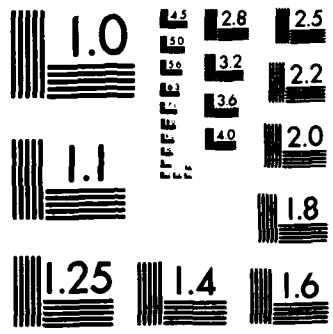
UNCLASSIFIED

F33655-81-K-5014

F/G 20/11

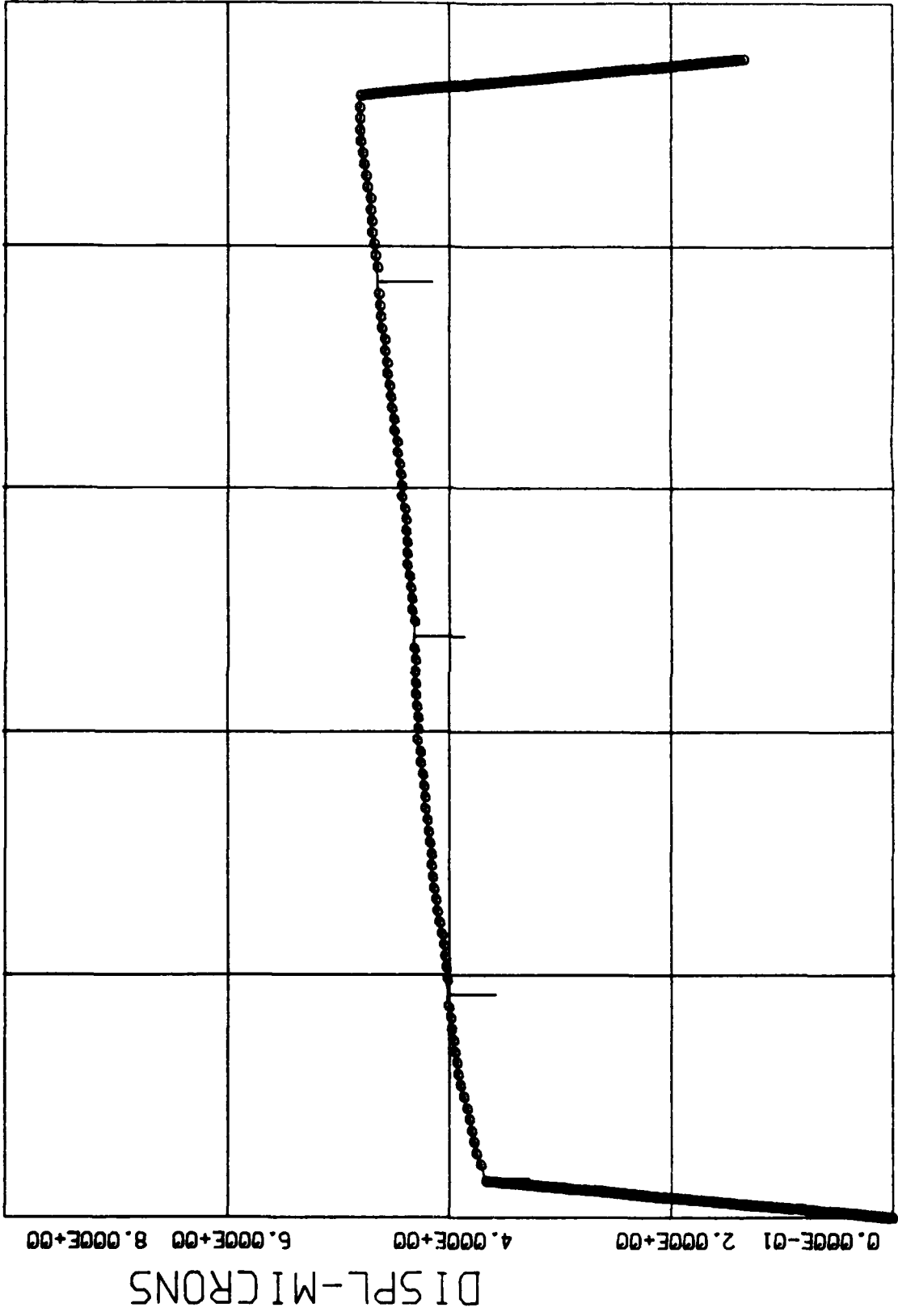
NL





MICROCOPY RESOLUTION TEST CHART  
NATIONAL BUREAU OF STANDARDS-1963-A

A23092

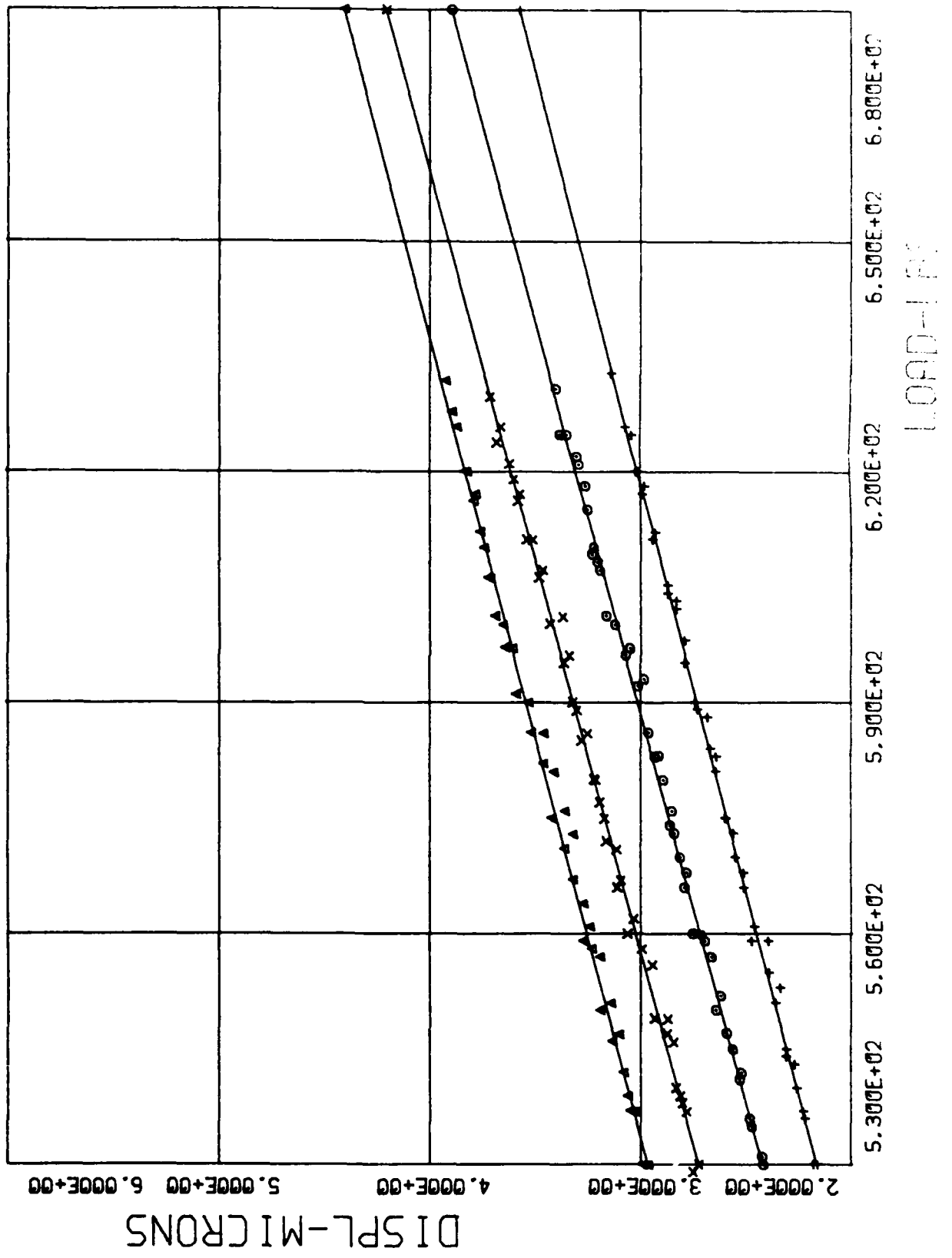


0.000E-01 4.400E+01 8.800E+01 1.320E+02 1.760E+03 2.200E+03

DISPL-MICRONS

TIME-SECONDS

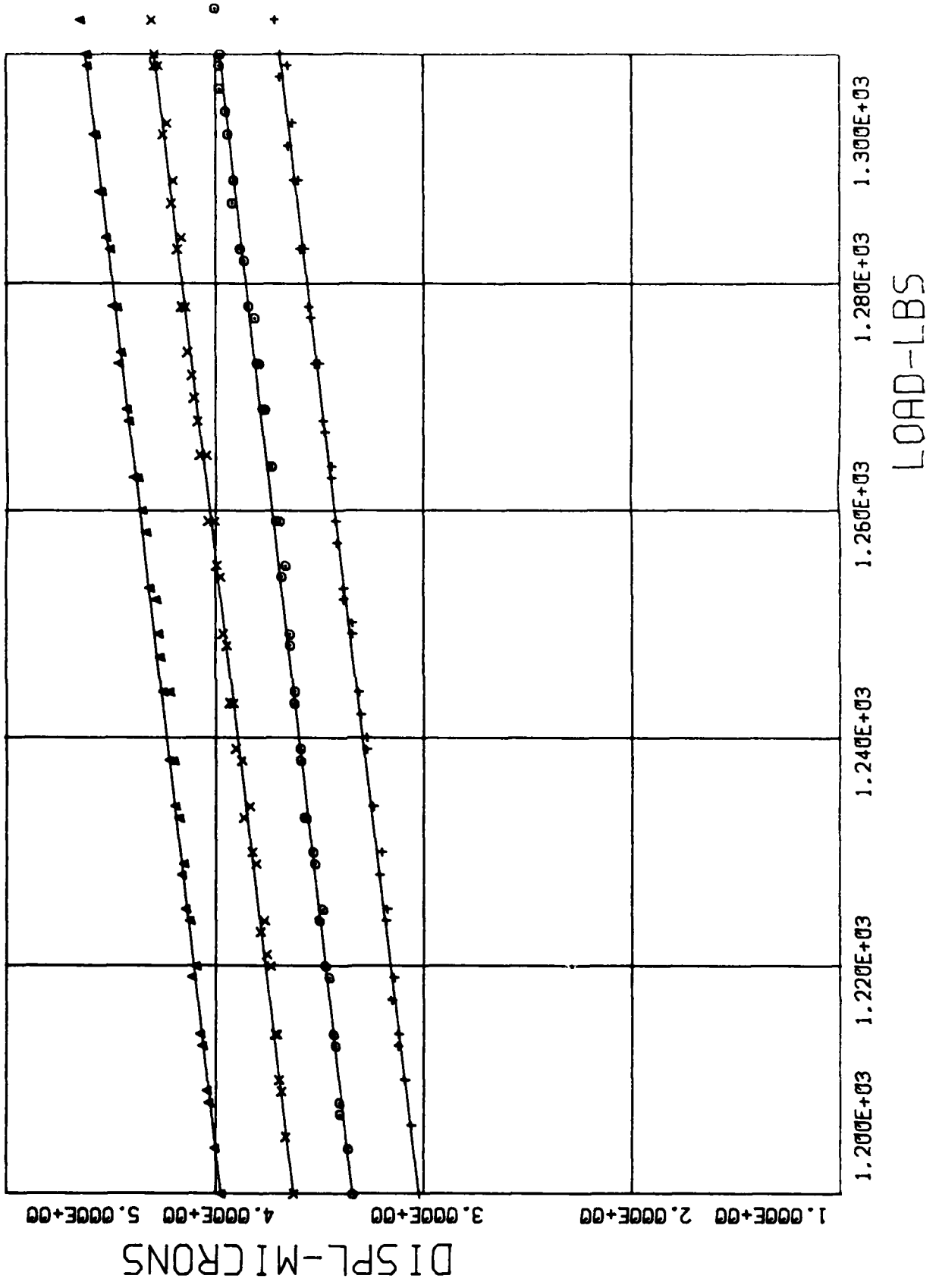
B22092



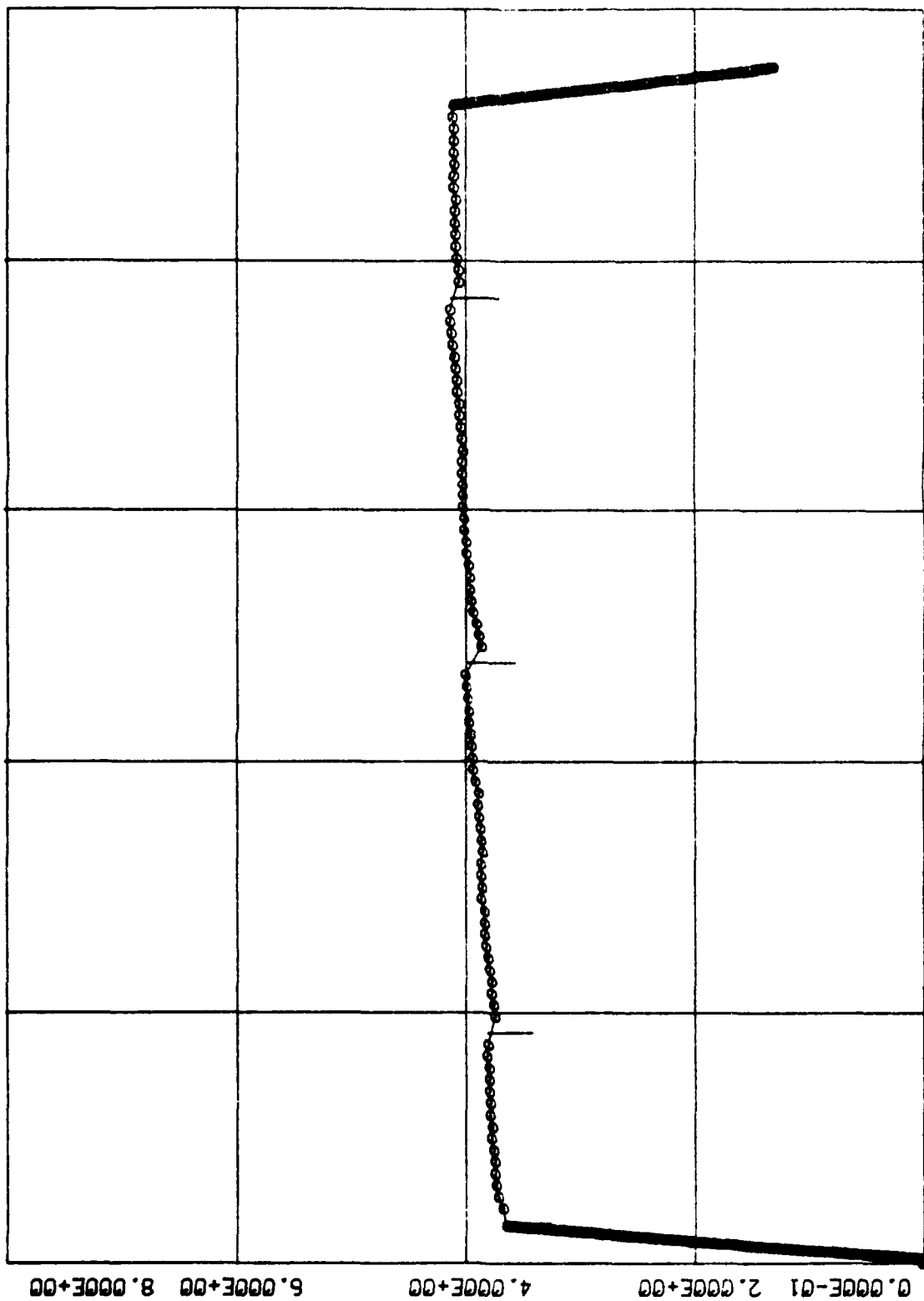
DISPL-MICRONS

LOAD-LBS

B23092



A24092



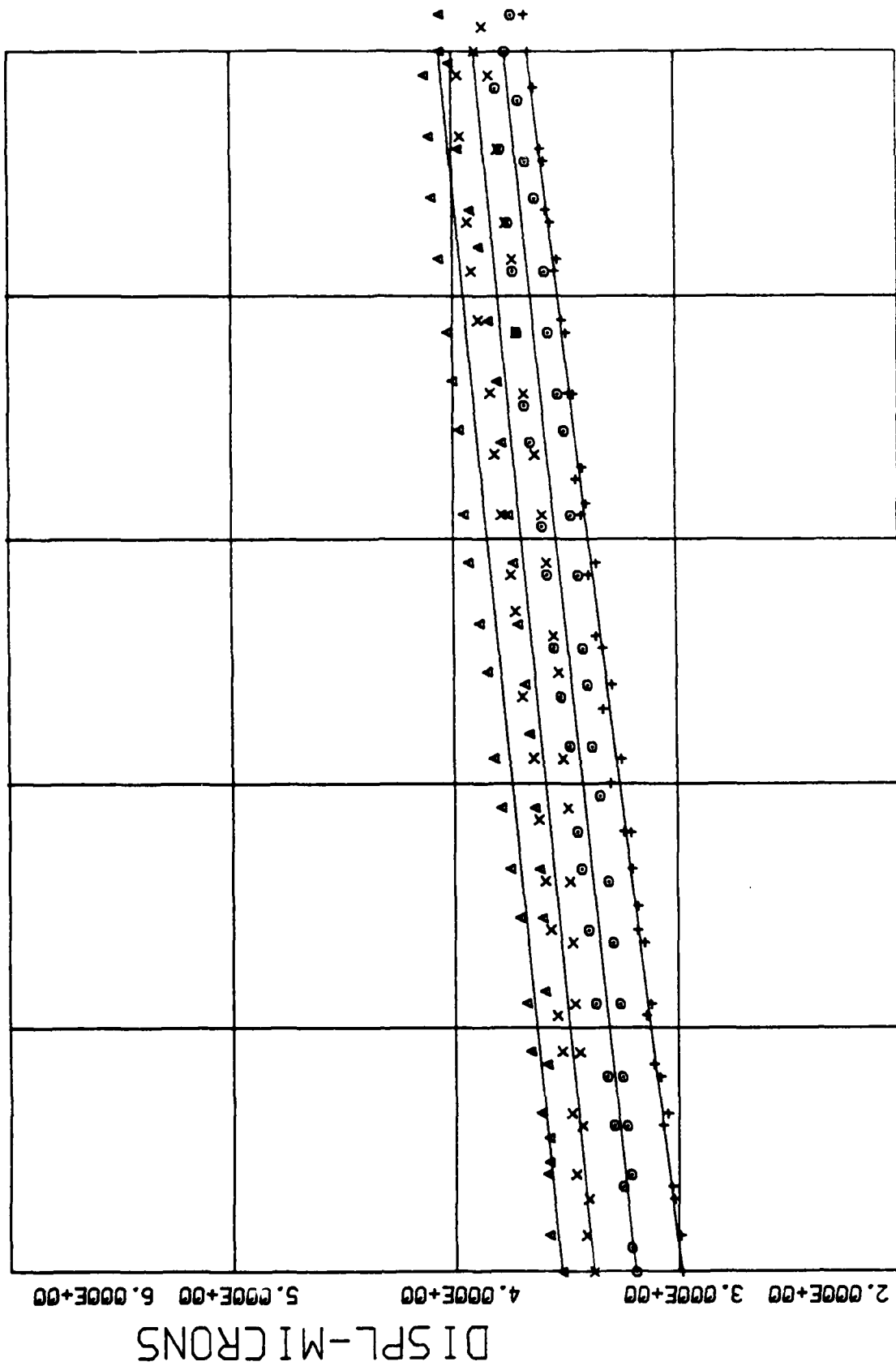
DISPL-MICRONS

0.000E-01 4.400E+02 8.800E+02 1.320E+03 1.760E+03 2.200E+03

TIME-SECONDS



B24092



7.000E+02 7.200E+02 7.400E+02 7.600E+02 7.800E+02 8.000E+02

LOAD-LBS

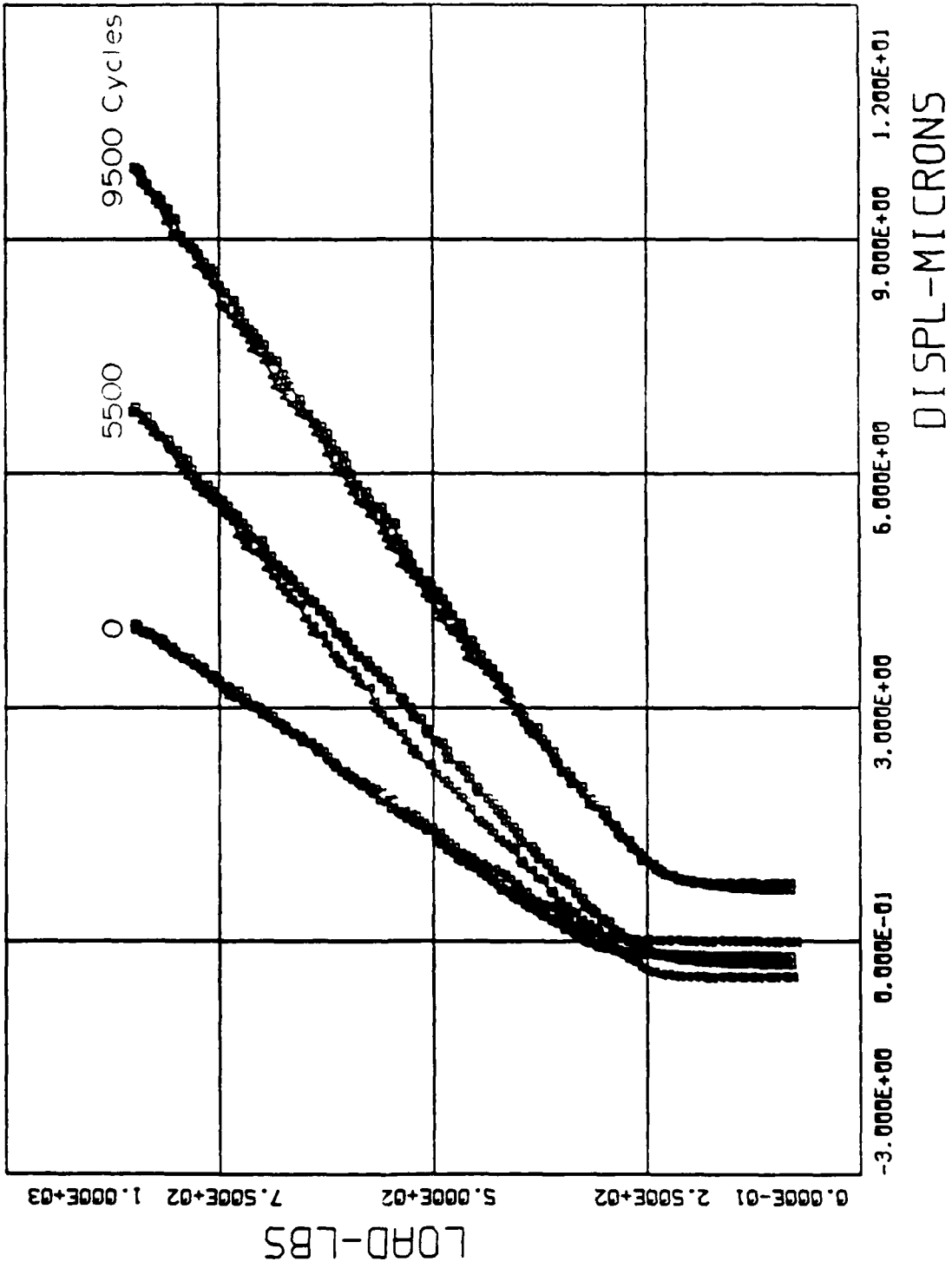
DISPL-MICRONS

2.000E+00 3.000E+00 4.000E+00 5.000E+00 6.000E+00

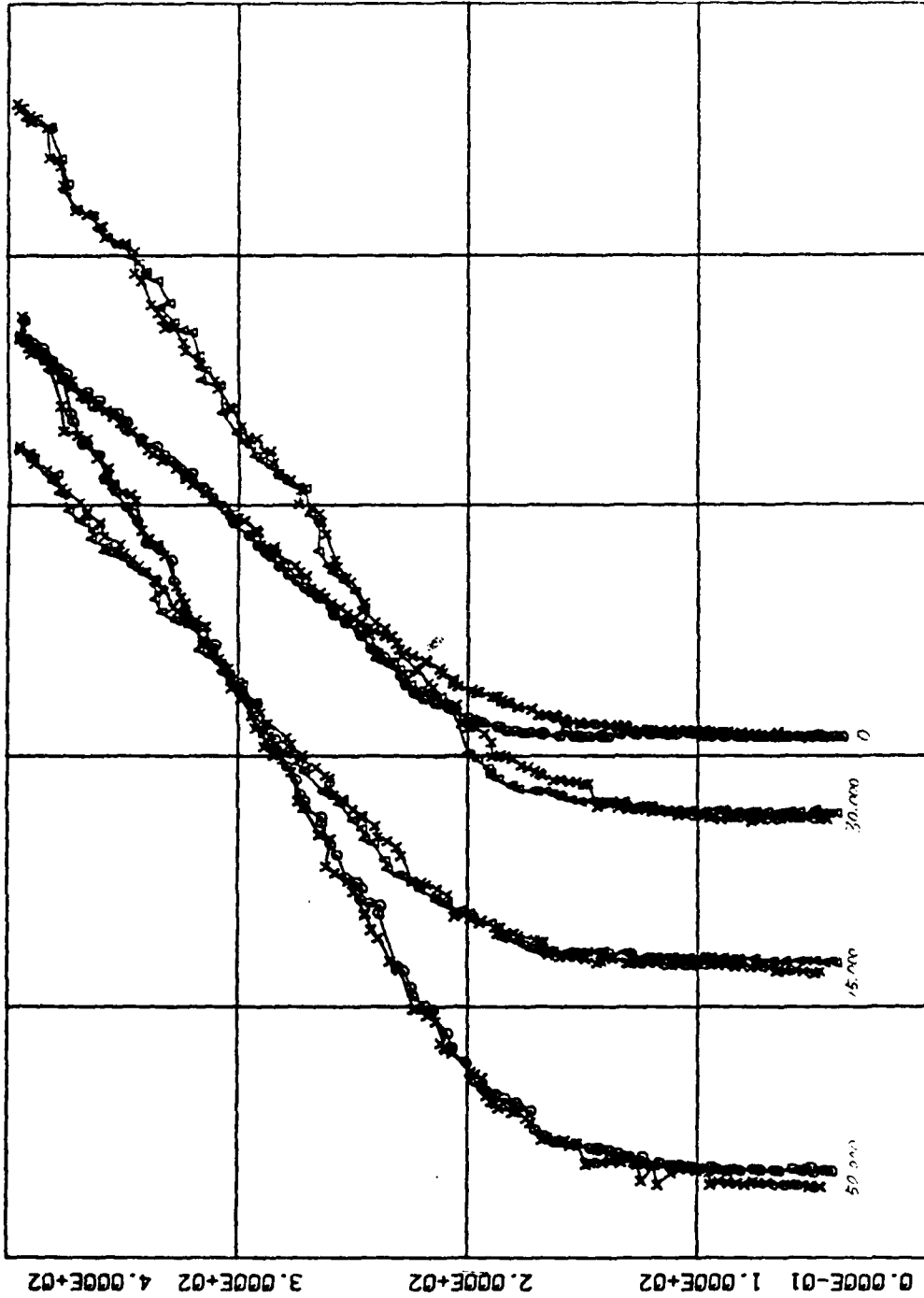
APPENDIX B  
FATIGUE TEST RESULTS

Load-displacement plots for selected cycles of the fatigue tests.  
See Table 6, page 46, for details on loading, crack lengths, and  
indentations.

B08083



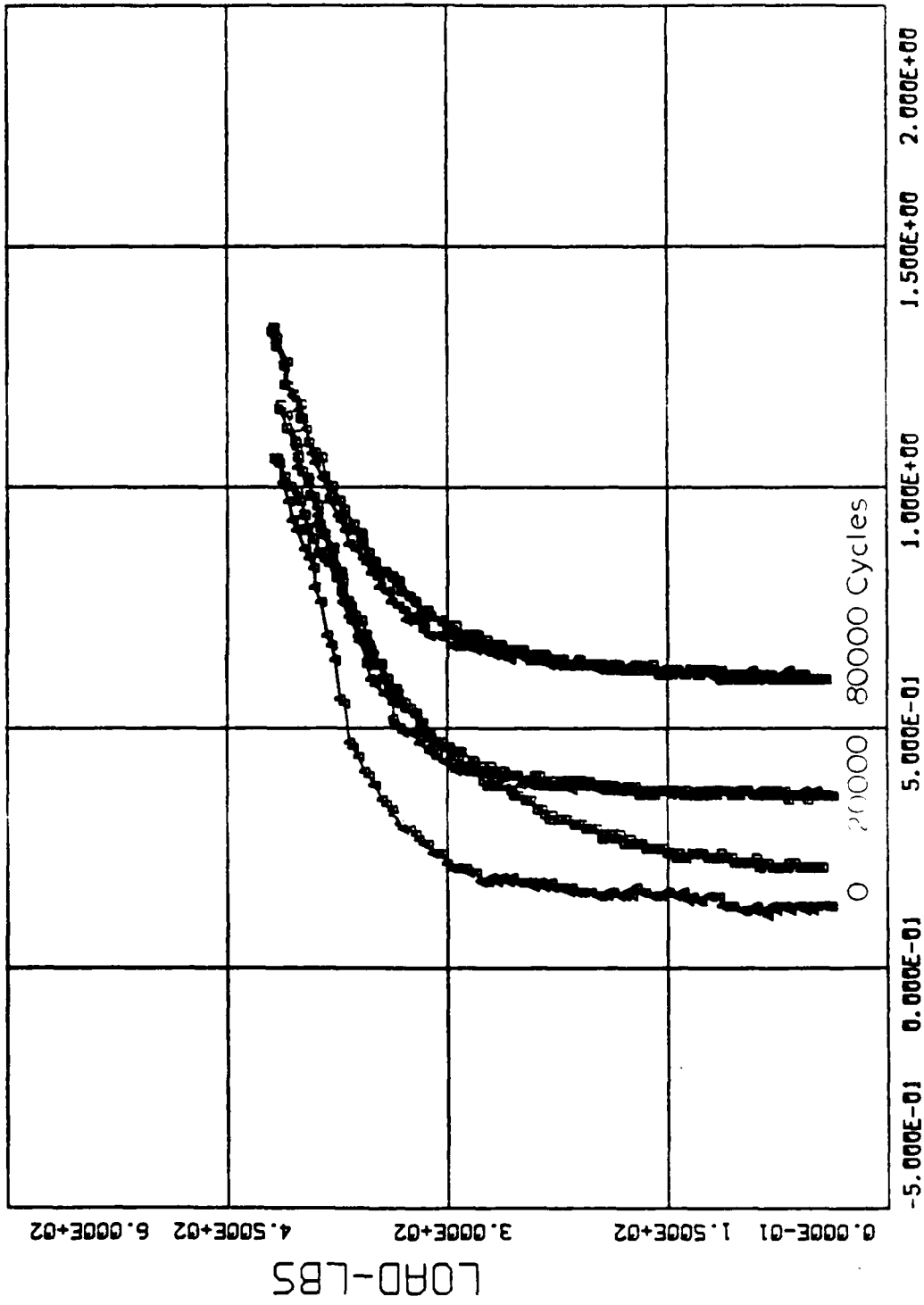
A11083



-2.400E+00 -1.200E+00 2.384E-07 1.200E+00 2.400E+00 3.600E+00

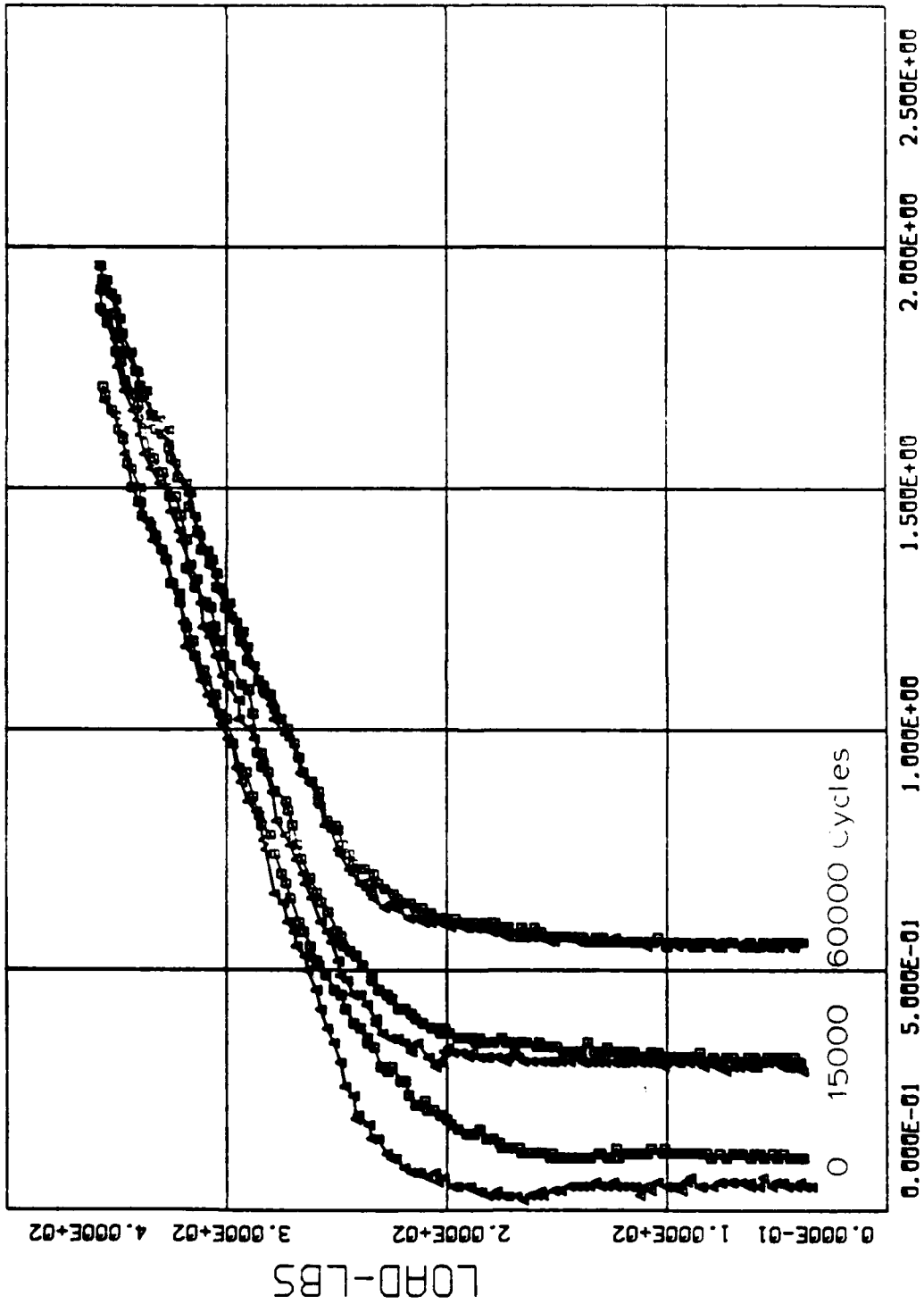
DISPL-MICRONS

A12083



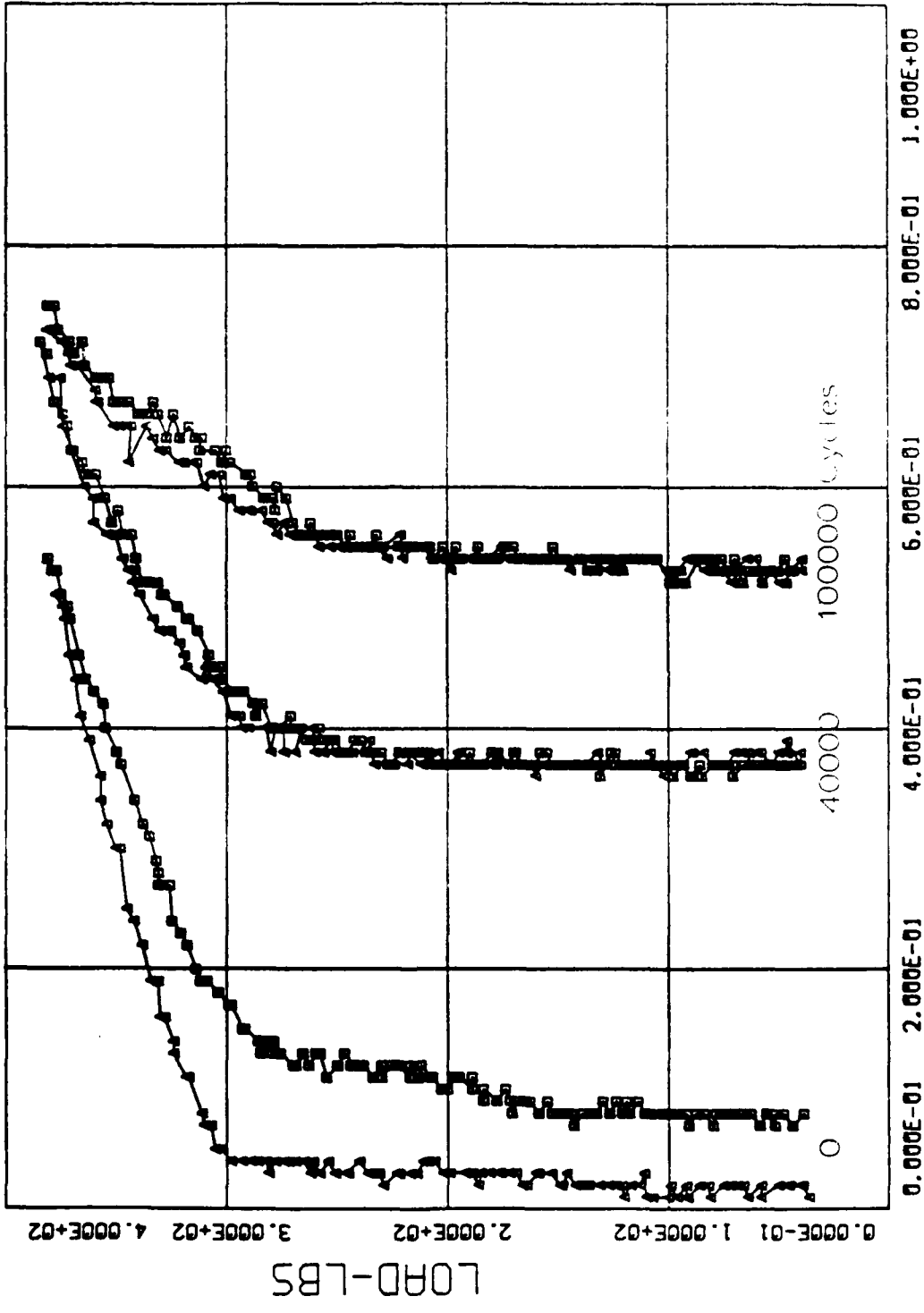
DISPL-MICRONS

A16083

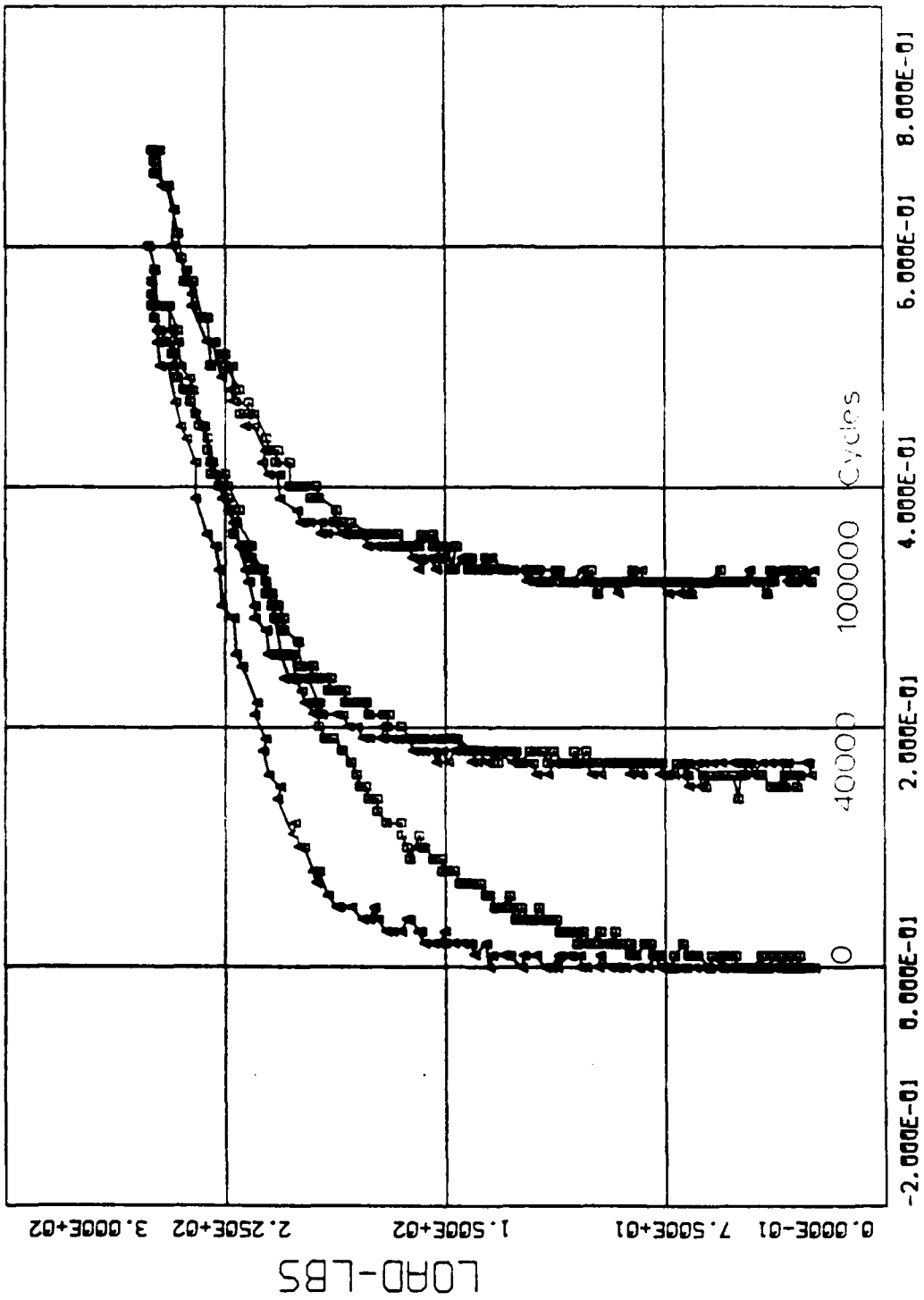


DISPL-MICRONS

A09083



B17083





## REFERENCES

1. R. C. Donath, "Crack Growth Behavior of Alloy IN-100 under Sustained Load at 730C," AFWAL-TR-80-4131, Air Force Wright Aeronautical Laboratories, Wright-Patterson Air Force Base, Ohio, 343 pgs., April 1981.
2. T. R. Hsu, R. Lewak, and B. J. S. Wilkins, "Measurements of Crack Growth in a Solid at Elevated Temperatures by Holographic Interferometry", *Experimental Mechanics*, Vol. 18, pp. 297-302, 1978.
3. J. G. Kaufman, K. O. Bogardus, D. A. Mauney, and R. C. Malcolm, "Creep Cracking in 2219-T851 Plate at Elevated Temperatures," *Mechanics of Crack Growth*, ASTM STP 590, pp. 149-168, 1976.
4. J. D. Landes, and J. A. Begley, "A Fracture Mechanics Approach to Creep Crack Growth," *Mechanics of Crack Growth*, ASTM STP 590, pp. 128-148, 1976.
5. J. R. Haigh, "The Mechanisms of Macroscopic High Temperature Crack Growth", *Materials Science and Engineering* Vol. 20, pp. 213-223, 1975.
6. P. A. Domas, W. N. Sharpe, M. Ward, and J. Yau, "Benchmark Notch Test for Life Prediction", NASA CR-1655571, NASA-Lewis Research Center, Cleveland, Ohio, 220 pgs., June, 1982.
7. W. N. Sharpe, Jr., and M. Ward, "Benchmark Cyclic Plastic Notch Strain Measurements", *Journal of Engineering Materials and Technology*, Vol. 105, pp. 235-241, 1983.
8. M. W. Guillot, and W. N. Sharpe, Jr., "A Technique for Cyclic-Plastic Notch Strain Measurement", *Experimental Mechanics*, Vol. 23, pp. 354-360, 1983.
9. W. N. Sharpe, Jr., and J. J. Shen, "A New Method for Determining Threshold Values of Creep Crack Growth", presented at 1983 ASME Failure Prevention and Reliability Conference, to be published.
10. W. N. Sharpe, Jr., "Applications of the Interferometric Strain/Displacement Gage", *Optical Engineering*, Vol. 21, pp. 483-488, 1982.
11. W. N. Sharpe, Jr., "Interferometric Surface Frame Measurement", *International Journal of Nondestructive*

- Testing, Vol. 3 pp. 59-76, 1971.
12. A. Saxena, and S. J. Hudak, Jr., "Review and Extension of Compliance Information for Common Crack Growth Specimens", International Journal of Fracture, Vol. 14, pp. 453-468, 1978.
  13. G. J. Groendyke, and W. N. Sharpe, Jr., "An Interferometric Technique for Constant Strain-Rate Testing at High Temperatures", Novel Techniques in Metal Deformation Testing, The Metallurgical Society of AIME, pp. 175-187, 1983.
  14. W. N. Sharpe, Jr., "Creep Crack-Opening Displacement Measurements in IN-100 at 732C", AFWAL-TR-83-4005, Air Force Wright Aeronautical Laboratories, 46 pgs., 1983.
  15. A. S. Kobayashi, "Experimental Techniques in Fracture Mechanics", Iowa State University Press, p. 15, 1973.
  16. D. E. Macha, W. N. Sharpe, Jr., and A. F. Grandt, Jr., "A Laser Interferometry Method for Experimental Stress Intensity Factor Calibration", ASTM STP661, American Society for Testing and Materials: pp. 449-465, 1976.
  17. K. Sanada, and P. Shahinian, "Creep Crack Growth in Alloy 718", Metallurgical Transactions A, Vol. 7A, pp. 439-449, 1977.
  18. J. W. Jones, D. E. Macha, and D. M. Corbly, "Observations on Fatigue Crack Opening Load Determinations", International Journal of Fracture, Vol. 14, pp. R25-R30, 1978.

REPROD

FILMED

8